Aus der Neurochirurgischen Klinik und Poliklinik

der Ludwig-Maximilians-Universität München

Direktor: Prof. Dr. med. Jörg-Christian Tonn

Studies on the two secretory peptides Apelin and Humanin to target the tumor microenvironment for glioblastoma therapy

Dissertation

zum Erwerb des Doktorgrades der Medizin

an der Medizinischen Fakultät der

Ludwig-Maximilians-Universität zu München

vorgelegt von

Min Li

aus

Hunan, P.R. China

2020

Mit Genehmigung der Medizinischen Fakultät

der Universität München

Berichterstatter:	Prof. Dr. rer. nat. Rainer Glaß
Mitberichterstatter:	Prof. Dr. Antje Grosche
	Prof. Dr. Jochen Herms
	Prof. Dr. Christian Ries
Mitbetreuung durch den promovierten Mitarbeiter:	Dr. sc. nat. Roland Kälin
Dekan:	Prof. Dr. med. dent. Reinhard Hickel

Tag der mündlichen Prüfung: 19.03.2020

Eidesstattliche Versicherung

Li, Min
Name, Vorname

Ich erkläre hiermit an Eides statt,

dass ich die vorliegende Dissertation mit dem Thema

Studies on the two secretory peptides Apelin and Humanin to target the tumor microenvironment for glioblastoma therapy

selbständig verfasst, mich außer der angegebenen keiner weiteren Hilfsmittel bedient und alle Erkenntnisse, die aus dem Schrifttum ganz oder annähernd übernommen sind, als solche kenntlich gemacht und nach ihrer Herkunft unter Bezeichnung der Fundstelle einzeln nachgewiesen habe.

Ich erkläre des Weiteren, dass die hier vorgelegte Dissertation nicht in gleicher oder in ähnlicher Form bei einer anderen Stelle zur Erlangung eines akademischen Grades eingereicht wurde.

Munich Gemany, 19.03.2020
Ort, Datum

Min Li
Unterschrift Doktorandin/Doktorand

I. Contents

II. List of figures

III. List of tables

IV. Abbreviations

Ab42	42 amino acid form of the b-amyloid peptide
aCSF	Artificial cerebrospinal fluid
AKD	APLN-Knockdown
Ang-II	Angiotensin II
Apelin-F13A	Mutant APLNR ligand
APLN	Apelin gene
APLNR/APJ	Apelin receptor
AT1R	Angiotensin II receptor type 1
BBB	Blood brain barrier
bFGF	Basic Fibroblast growth factor
BSA	Bull Serum Albumin
CDKN2A	Cyclin-dependent kinase Inhibitor 2A
CNTFR	Ciliary neurotrophic factor receptor
CPEO	Chronic progressive external ophthalmoplegia
DC101	VEGFR2-blocking antibody
EGFR	Epidermal growth factor receptor
FPRL1	Formyl-peptide receptor-like-1
GBM	Glioblastoma multiforme
GDNF	Growth factor glial cell-derived neurotrophic factor
gp130	Glycoprotein 130
GPCR	G protein-coupled receptor
GSCs	Glioblastoma stem cells
hEGF	Human epidermal growth factor
hFGF	Human fibroblast growth factor
HIF	Hypoxia-inducible factor
HN	Humanin
HNG	S14G Humanin
Iba1	Ionized calcium-binding adapter molecule 1

IDH	Isocitrate dehydrogenase
IGFBP-3	Insulin-like growth factor-binding protein-3
IL-27	Interleukin-27
MGMT	O6-methylguanine-DNA methyltransferase
NF1	Neurofibromatosis type 1
NPCs	Neural-precursor cells
NSC	Non-silencing control
NSCLC	Non-small cell lung cancer
PDGFRA	Platelet-derived growth factor receptor-α
PFA	Paraformaldehyde
PIGF	Placenta growth factor
PKB	Protein kinase B
PKC	Protein kinase C
PTEN	Phosphatase and tensin homolog
PVNS	Pigmented villonodular synovitis
STAT3	Signal transducer and activator of transcription 3
SVZ	Subventricular zone
TAMs	Tumor-associated myeloid cells
TCGA	The Cancer Genome Atlas
TKI	Tyrosine kinase inhibitor
TLR2	Toll-like receptor-2
TMZ	Temozolomide
TNF-α	Tumor necrosis factor-α
VEGF	Vascular endothelial growth factor
VLD	Vessel length density
vWF	von Willebrand factor
WGA	Wheat germ agglutinin
WSX-1	Interleukin-27 receptor

1. Introduction

1.1 Glioblastoma

Gliomas are the most prevalent primary central nervous system (CNS) tumors and presumably are of glial origin [1-3]. Among all gliomas, glioblastoma, also called glioblastoma multiforme (GBM), is the most frequent and most devastating brain neoplasm. Those toward have the highest histological grade, namely grade IV, as classified by the World Health Organization (WHO) [4, 5]. GBM is characterized morphologically by hypercellularity, nuclear atypia, mitotic figures, high vascularization, necrosis and pseudopalisades [6]. The degree of these morphological features is positively correlated with the malignancy. Ninety percent of the GBM cases are primary or de novo glioblastoma, which are diagnosed in patients with no clinical history for brain tumors. Secondary glioblastoma account for the remaining 10% which often originates from the progression of a low-grade glioma like diffuse or anaplastic astrocytomas [7]. Primary glioblastomas are isocitrate dehydrogenase gene wild-type (IDH-WT) glioblastoma with a median overall survival of 9.9-15 months, and secondary glioblastomas are IDH-mutant glioblastoma with an average survival of 24-31 months [5].

1.1.1 Glioblastoma treatment

The complete surgical resection of GBM is virtually impossible because tumor cells extensively invade the surrounding brain tissue. As a consequence, for the newly diagnosed GBM, the treatment strategy always requires the combination of maximum

safe surgical debulking, radiotherapy, and chemotherapy [8-10]. The standard chemotherapy scheme for GBM is temozolomide (TMZ, an alkylating agent can induce the death of tumor cells by breaking the DNA double-strand) [9]. The treatment outcomes of patients who received the combined therapy of temozolomide and radiotherapy is significantly better than radiotherapy alone when the gene promoter of a DNA repair enzyme MGMT (O6-methylguanine-DNA methyltransferase) is methylated and epigenetically silenced [11]. Despite aggressive surgery, radiotherapy, and chemotherapy, the prognosis of GBM patients remains poor with a median survival of 14 to 16 months [12, 13]. Therefore, new treatment approaches for GBM are desperately needed.

1.1.2 Genetic subtypes of glioblastoma

To achieve a better patient stratification, researchers have investigated genomic expression alteration from the Cancer Genome Atlas (TCGA) dataset and classified glioblastoma into four subtypes which were named classical, proneural, mesenchymal and neural [14]. The neural subtype is less well defined and more inclined to be considered as a potential artifact now [15]. The classical subtype is characterized by the upregulation of the *EGFR* (epidermal growth factor receptor) gene expression and the loss of *PTEN* (phosphatase and tensin homolog) and *CDKN2A* (cyclin-dependent kinase Inhibitor 2A) gene loci. Alterations in the *TP53* (one of the most frequently mutated genes in glioblastoma) are nearly absent in this genetic subtype [14, 16]. Unlike the classical GBM, the proneural tumors are marked by mutations in the *TP53*

(54%) and *IDH1* (isocitrate dehydrogenase 1; 30%) genes, and by overexpression of the *PDGFRA* (platelet-derived growth factor receptor-α) gene [14, 16]. The mesenchymal GBM subtype has frequent inactivation of three tumor suppressor genes: the *NF1* (Neurofibromatosis type 1; 37%), *TP53* (32%), and *PTEN* (32%) genes [14, 16]. The genetic stratification of glioblastoma provides the possibility to establish more personalized therapies and improve the clinical efficacy.

Glioblastoma stem cells (GSCs) are a subset of cells with the ability of self-renewal and multi-lineage differentiation in the tumor microenvironment and are also the main cause of the chemoradiotherapy resistance and tumor recurrence [17, 18]. Isolation and purification of GSCs from GBM patients are important to investigate more specific targeting therapies for these cells [19, 20]. Furthermore, the neural precursor cells (NPCs) in the subventricular zone (SVZ) of mice can be isolated and manipulated to model different genetic subtypes of GSCs by altering genomic expression in these cells: for instance, the mouse glioblastoma cell line $p53^{KO}$PDGFB GSC is a good model of the proneural GBM subtype by knocking out *TP53* and overexpression of *PDGFB* in mouse NPCs [21].

1.1.3 Anti-angiogenic therapy for glioblastoma

Judah Folkman first proposed the hypothesis in the early 1970s that angiogenesis is required for the expansion of tumor spheroids beyond a diameter of 2-3 mm at which point the oxygen/nutrient supplies and waste products removal become difficult without the vasculature [22]. Since then tumor angiogenesis has been studied

intensively and is now known as one of the hallmarks of cancer [23, 24]. The development of the vasculature is a vital process during embryogenesis including vasculogenesis (the generation of new endothelial cells from progenitor cells and tube formation by these endothelial cells) and angiogenesis (the process of new vessels sprouting from existing ones) [25-27]. Once established, the vasculature becomes quiescent. In the adult, angiogenesis is controlled by pro-angiogenic and anti-angiogenic regulators in dynamic homeostasis and only transiently turned on during physiological processes such as wound healing and the female reproductive cycle. However, during tumor progression, the homeostasis is disrupted and an "angiogenic switch" is turned on activating continuous sprouting of new vessels to support expanding neoplastic growth [24-26]. The most studied angiogenic inducer is vascular endothelial growth factor (VEGF) which is highly expressed by cancer cells in hypoxic condition together with hypoxia-inducible factor (HIF) to trigger tumor angiogenesis [28-30]. Three subtypes of VEGF receptor (VEGFR1, VEGFR2, and VEGFR3) have been identified [31]. Among them, VEGFR2 is the major one expressed on endothelial cells for the angiogenic response [32]. Consequently, VEGF or VEGFR targeting is considered a promising therapy for the cancer treatment, and inhibitors of VEGF or VEGFR have been included as the potential anti-cancer agent in clinical trials [33, 34]. Bevacizumab (a humanized antibody targeting VEGFA) has become the first anti-angiogenic agent granted the approval of United States Food and Drug Administration (FDA) in 2004 for the treatment of colorectal cancer [35].

GBM is a highly vascularized brain tumor with VEGF abundantly expressed around

the hypoxic or necrotic area [36, 37]. This prompted the development of anti-VEGF or anti-VEGFR therapies for GBM [37-40]. Bevacizumab was approved by FDA recently (full approval in 2017) for the treatment of recurrent glioblastoma but failed to get the approval of the European Medicines Agency (EMA) [41-43]. Different findings were displayed in various clinical studies for recurrent GBM. A phase II clinical trial (BELOB) showed that bevacizumab plus lomustine (an alkylating nitrosourea compound used in chemotherapy) could improve both the 6-month progression-free survival (PFS) and 9-month overall survival (OS) of recurrent GBM patients in comparison to either agent alone [44, 45]. Nevertheless, a subsequent phase III study published in 2017 (EORTC 26101) only validated the benefits of bevacizumab plus lomustine treatment on PFS but not on OS [46]. For newly diagnosed GBM patients, a phase II clinical trial and two randomized phase III clinical studies (AVAglio and RTOG 0825) reported that bevacizumab combined with temozolomide chemoradiotherapy did not show an improved OS in comparison to standard chemoradiotherapy, but only improved PFS [47-50]. Studies of other anti-angiogenic agents for glioblastoma such as cilengitide (a synthesized cyclic pentapeptide targeting α_v integrins) and cediranib (a tyrosine kinase inhibitor which blocks all VEGFRs) showed similar outcomes like the trials for bevacizumab [37, 51, 52].

While tumor biology of GBM underscores the potential of anti-angiogenic therapy, the results of prior studies remain disappointing and underscore the importance of investigating tumor resistance mechanisms to anti-VEGF/VEGFR agents. The

activation or upregulation of alternative pathways for angiogenesis could be one of the prime causes of the resistance to anti-VEGF/VEGFR therapies [53-55]. Besides VEGF, there are several additional regulatory factors such as basic fibroblast growth factor (bFGF), angiopoietin 2 (ang-2), placenta growth factor (PIGF), stromal cell-derived factor 1 (SDF-1/CXCL12), and also apelin that are participating in tumor angiogenesis and upregulated (as compared to the tumor-free brain) in glioblastoma [27, 53-56]. For instance, the upregulation of bFGF and CXCL12 was found in progressive GBM after treatment with a pan-VEGFR tyrosine kinase inhibitor (TKI) AZD2171 [57]. Another possibility for the resistance to antiangiogenesis is that the tumor invasiveness increases after anti-VEGF/VEGFR treatment [53-55]. Glioblastoma is highly invasive in the brain instead of metastasizing to other organs outside the central nervous system [58]. Invasive GBM cells can be found as dispersed cells throughout the brain. These invasive cells can also co-opt preexisting blood vessels [30, 53]. Kunkel and colleagues found a remarkable increase of tumor invasiveness in a glioblastoma mouse model after the treatment of a monoclonal antibody (DC101) against VEGFR2 [59]. However, stratification of patients that may be resistant or sensitive to anti-angiogenic therapy [60-62], e.g. by post-hoc analysis of a clinical trial (AVAglio), suggests that IDH1 wild-type GBM patients of proneural subtype can profit from bevacizumab treatment [63]. Erdem-Eraslan et al. reported that the classical subtype showed a better response in recurrent GBM patients treated with bevacizumab and lomustine [64].

1.2 Apelin/APLNR signaling

O'Dowd et al. cloned a gene encoding a protein with strong homology to angiotensin II (Ang-II) receptor type 1 (AT1R) in 1993, and named this new receptor the angiotensin II receptor-like 1 or APJ [65]. The gene encoding human APJ was found on the long arm of chromosome 11. The receptor APJ is a seven-transmembrane G protein-coupled receptor (GPCR) consisting of 377 amino acids, which remained orphan until Tatemoto and coworkers identified its endogenous ligand (a bioactive peptide) from bovine stomach extract in 1998 [66]. Thus, this newly discovered bioactive peptide was named apelin (APJ Endogenous Ligand), and thereafter the APJ gene was renamed as apelin receptor (APLNR) gene. Despite the remarkable sequence similarity between AT1R and APLNR, Ang-II does not bind to APLNR, nor does apelin bind to AT1R [67]. The human apelin gene (*APLN*) encodes a 77 amino acid-long pro-apelin peptide (apelin-77) and is located on the long arm of the X chromosome. A pro-apelin peptide is proteolytically cleaved to several shorter biologically active isoforms, including apelin-36, apelin-17, apelin-16, apelin-13, and apelin-12 (Table 1.2) [68, 69]. A post-translational modification of apelin-13 (pyroglutamylated apelin-13, Pyr1-apelin-13) improves resistance to enzymatic degradation. This represents the major apelin isoform found in human blood plasma [70]. Functionally, the 12 C-terminal amino acids of apelin-77 are important for the biological activity, and apelin-13, together with Pyr1-apelin-13, is considered to be the pharmacologically most active isoform [71].

Apelin-F13A is a mutant ligand for APLNR created in the first apelin structure studies

by replacing C-terminal phenylalanine (F) residue of Pyr1-apelin-13 with alanine (A) (Table 1.2). This peptide was first reported as an antagonist for apelin-13 due to the lower binding efficiency to APLNR and lower potency to trigger downstream effects of APLNR [72]. However, some studies found that apelin-F13A showed similar binding activity and internalization responses to those of Pyr1-apelin-13 for human APLNR *in vitro* [73]. Also, apelin-F13A competed with apelin-13 binding in human heart tissue and showed bioactivity in endothelium-denuded saphenous vein [74]. Therefore, it seems more appropriate to consider apelin-F13A as a competitive agonist for natural APLNR ligands [74, 75].

Table 1.2 Sequence of apelin peptides and analogues.

Peptide (Human)	Amino acid sequence
Apelin-36	LVQPRGSRNGPGPWQGGRRKFRRQRPRLSHKGPMPF
Apelin-17	KFRRQRPRLSHKGPMPF
Apelin-16	FRRQRPRLSHKGPMPF
Apelin-13	QRPRLSHKGPMPF
Apelin-12	RPRLSHKGPMPF
Pyr1-apelin-13	Pyr-RPRLSHKGPMPF-OH
Apelin-F13A	Pyr-RPRLSHKGPMPA-OH

1.2.1 The physiological role of apelin/APLNR signaling

Both in human and rodents, apelin and APLNR are expressed extensively in the CNS and peripheral tissues including brain, spinal cord, heart, lung, liver, kidney, ovary,

adipose tissues, etc. [68, 71]. Because of the structural similarity between APLNR and AT1R, it was investigated if apelin may regulate cardiovascular functions. Indeed, apelin has been shown to play a role in the cardiovascular system by increasing cardiac contractility and enhancing vasodilatation [68, 69]. The potent inotropic effect of apelin appears to be associated with PKC (Protein kinase C) activation and the increase of intracellular Ca^{2+} levels, while the vasodilatation seems to be the result of the activation of endothelial nitric oxide synthase (eNOS) depending on PI3K-Akt signaling induced by apelin and APLNR binding [67-69].

As the expression of apelin and APLNR was found in the paraventricular and supraoptic nucleus of the hypothalamus, studies also explored the effect of apelin/APLNR signaling on food intake and body fluid homeostasis [68]. However, the results are inconsistent: Taheri et al. found that central administration of apelin-13 increases water intake in rats [76]; while some reported no change or a decrease of water intake after the treatment of apelin-13 by central injection [77, 78].

More importantly, many studies have determined a vital role of apelin/APLNR signaling in angiogenesis and embryonic development. APLNR is highly expressed on endothelial precursor cells in mouse and frog embryos [56, 79]. *In vitro*, apelin could increase the proliferation, migration and tube formation of human umbilical vein endothelial cells (HUVECs) [80] and retinal endothelial cell line (RF/6A) [81], and also promote the growth of mouse brain microvasculature-derived endothelial cells [79]. In the chick chorioallantoic membrane (CAM) assay, apelin stimulation showed a potent angiogenic effect with approximately equivalent vascular branch

points to VEGF treatment [79]. Kälin et al. found that apelin is essential for the angiogenic sprouting of intersomitic blood vessels of *Xenopus* tadpoles by conducting loss-of-function experiments [56]. Apelin knockout in the mouse resulted in decreased blood vessel diameter but did not cause obvious fatal defects in embryonic development [68]. An impaired myocardial contractility was observed exclusively in aging apelin knockout mice [82]. However, APLNR knockout led to vasculature malformations in mouse embryos resulting in augmented lethality. The discrepancy displayed in apelin knockout mice and APLNR knockout mice may be due to the effect of a second ligand that was identified recently and named apela (also called elabela or toddler) [68]. As an early endogenous ligand of the apelin receptor, apela may compensate for the loss of apelin in embryos of apelin knockout mice. This hypothesis is supported by the findings that severe heart developmental defects in zebrafish embryos caused by apela mutation are similar to those in APLNR knockout mice, which can be rescued by early ectopic expression of apelin [83, 84].

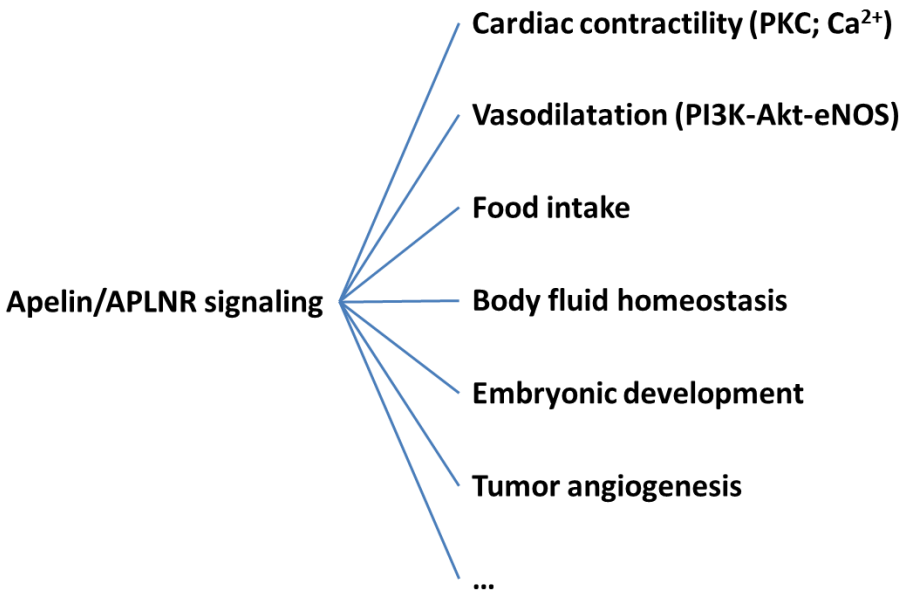

Figure 1.2.1 The physiological and pathophysiological role of apelin/APLNR signaling.

1.2.2 Apelin/APLNR in cancer

Since tumor angiogenesis is a hallmark of cancer and apelin/APLNR signaling is important for angiogenesis, it is not surprising that investigators have reported that 39% of solid tumor samples (60/154) analyzed by RNA hybridization technology showed the upregulation of apelin at least 2-fold in comparison to matched non-tumor controls [85]. The overexpression pattern of apelin has been detected in cancers including hepatocellular carcinoma, lung cancer, colon cancer, oral squamous cell carcinoma, brain tumor, etc. [86, 87]. Lacquaniti et al. also reported significantly increased apelin levels in the serum of cancer patients relative to healthy controls [88]. In human non-small cell lung cancer (NSCLC), patients showed a significantly worse survival where apelin expression levels were high as compared to patients with low apelin

levels [89]. In animal experiments, overexpression of apelin enhanced tumor vessel formation and tumor growth [90]. In brain tumors, Kälin and colleagues found apelin and APLNR to be upregulated in the neovascular areas of GBM but no apelin and low levels of APLNR expression in the normal non-tumor brain [56]. They confirmed the overexpression pattern of apelin in GBM by interrogating the TCGA data set of GBM, and also found that *APLN* is co-expressed with other genes inducing angiogenesis [68]. Altogether, these findings suggest that apelin/APLNR signaling could be a promising target for the cancer treatment.

1.2.3 Apelin/APLNR in pathological/tumor angiogenesis

Apart from physiological processes, apelin is involved in pathological angiogenesis of many diseases like ischemic stroke, retinal angiogenesis diseases, myocardial infarction, and tumor. [91]. In particular, accumulating evidence suggests that apelin could be an essential regulator of tumor angiogenesis. Studies have found hypoxia-responsive elements in the apelin gene (*APLN*) sequence which allows *APLN* to be activated by HIF [79, 92-94]. And *APLN* was identified as a tumor-endothelial specific gene by comparing gene expression profiles in tumors and normal endothelium [95]. Also, Masiero et al. identified the APLNR gene as one of the genes belonging to a tumor angiogenesis core signature [96]. In the analysis of specimens from NSCLC patients, apelin expression was positively correlated to the density of microvessel [89]. In a subcutaneous xenograft mouse model for hepatocellular carcinoma, the treatment of apelin-F13A, a mutant ligand for APLNR, decreased the

tumor vessel density and inhibited tumor growth [97]. With regards to GBM, *APLN* was not only highly upregulated but also found to be co-expressed with VEGF in the hypoxic area, indicating that there may be a collaborative function of these two angiogenic factors [68]. As described above (section 1.1.3), the upregulation of alternative pathways of angiogenesis may be one of the leading causes of the unsatisfactory results in anti-VEGF/VEGFR therapy. Therefore, apelin/APLNR signaling could be an important angiogenic pathway resulting in the resistance to anti-VEGF/VEGFR treatment in GBM.

1.3 Glioblastoma-associated myeloid cells and humanin peptide

1.3.1 Glioblastoma-associated microglia/macrophages

One major caveat for current GBM therapies is the strong support of tumor growth by the GBM microenvironment. The tumor stromal niche consists of parenchymal cells of the brain like astrocytes, endothelial cells, pericytes, microglia, and macrophages. [98]. Among them, microglia and macrophages accumulate abundantly in the tumor area, accounting for 30% of the total number of cells in the GBM tumor mass, whereas microglia account for only 5%-10% of the cells in normal brain tissue [99], indicating that the tumor-associated myeloid cells (TAMs) may play an important role in GBM. In fact, the infiltrating TAMs are manipulated by tumor cells in order to support the maintenance and progression of glioblastoma based on the results of recent studies [99-101].

Microglial cells are the major innate immune cells in the CNS and can secrete

inflammatory cytokines to coordinate immune responses against infection [102, 103]. They also engulf and digest pathogens and cellular debris by phagocytosis [104]. Upon loss of the blood brain barrier (BBB), monocytes can migrate into the brain, differentiate into macrophages and accumulate in the tumor area [101]. Glioblastoma cells first recruit microglia and macrophages by releasing plenty of chemoattractants (Figure 1.3.1) such as the macrophage colony-stimulating factor (M-CSF), monocyte chemoattractant protein-1 (MCP-1), and glial cell-derived neurotrophic factor (GDNF) [99, 101]. Then the accumulated TAMs can interact with glioblastoma cells to enhance tumor cell invasiveness and tumor angiogenesis [99]. Glioblastoma cells can, for example, produce a molecule called versican which triggers the increase of Toll-like receptor-2 (TLR2) expression in TAMs [105]. TLR2 upregulates the membrane type 1-matrix metalloproteinase (MT1-MMP), and then MT1-MMP cleaves the pro-form of matrix metalloprotease-2 (MMP2) and activates this enzyme to hydrolyze the extracellular matrix, increasing the invasion of glioblastoma cells (Figure 1.3.1) [99, 101]. TAMs can promote the tumor angiogenesis as well by synthesizing and releasing pro-angiogenic molecules (e.g. MMP-9 and tumor necrosis factor-α, TNF-α) [99]. Thus, TAMs, as the important cellular component of the tumor microenvironment, provide a promising therapeutic intervention option in glioblastoma that has attracted ongoing research attention.

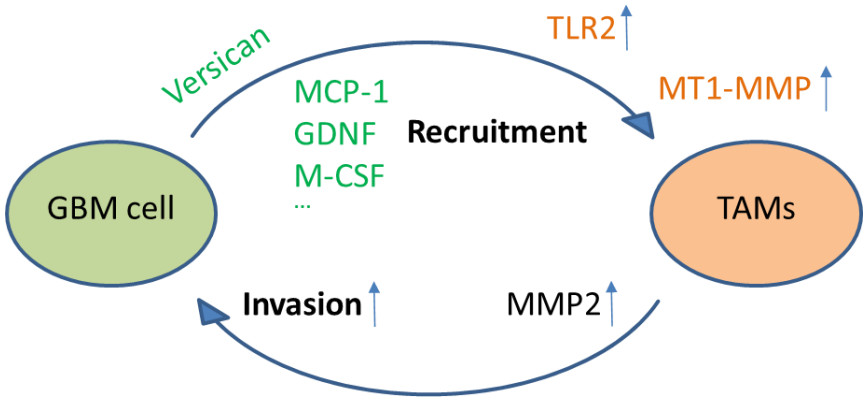

Figure 1.3.1 The interactions between glioblastoma cells and tumor-associated myeloid cells.

1.3.2 Humanin

Humanin (HN) is a peptide identified by Hashimoto and colleagues in 2001 through functional expression screens of a cDNA library obtained from the intact brain region of an Alzheimer's disease (AD) patient [106]. The researchers found that all the cDNA clones that could rescue the neuronal cells from three AD-related insults (mutant amyloid precursor protein, presenilin 1 and 2) shared a small (75 base-pair) open reading frame (sORF) encoding a 24 amino acid peptide. And overexpression of this sORF in neuronal cells also protected them from those AD-relevant toxicities. As this short peptide holds the potential for restoring the humanity of AD patient, it was named humanin [106, 107]. The HN ORF shows high identity with a portion of the mitochondrial 16S rRNA encoding region (*MT-RNR2*), suggesting the mitochondrial origin of this peptide (Figure 1.3.2) [108]. Guo et al. also cloned HN as a binding partner of Bax (a pro-apoptotic protein) by a yeast two-hybrid screen. The initiation of the apoptosis signal by the translocation of Bax from cytoplasm to mitochondria was

inhibited after HN bound to Bax [109]. Similarly, a third group cloned HN in the process of searching interactive proteins of the insulin-like growth factor-binding protein-3 (IGFBP-3) from another yeast two-hybrid screen. These researchers found that HN can also suppress apoptosis induced by IGFBP-3 [110].

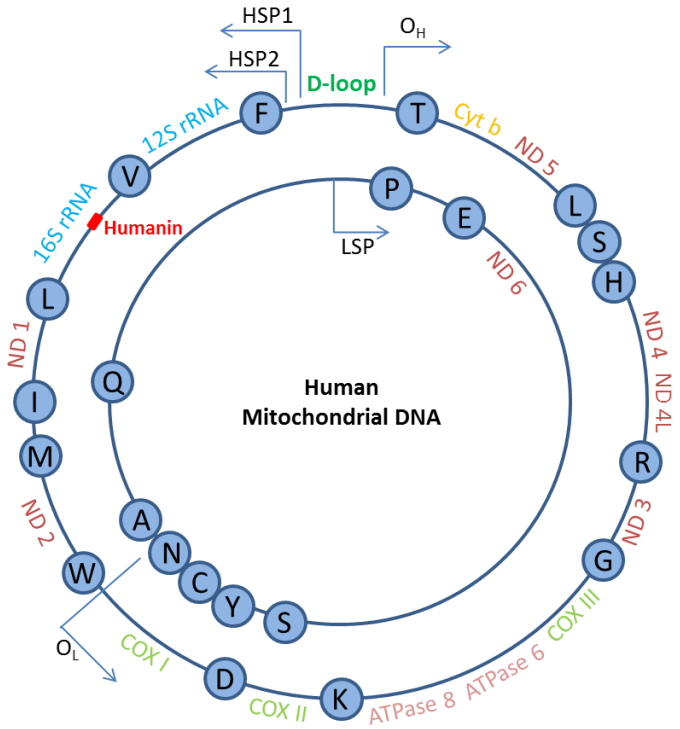

Figure 1.3.2 Schematic diagram of the circular, double-stranded human mitochondrial DNA and the location of the humanin open reading frame. There are 22 tRNA-coding genes (circles), 2 rRNA-coding genes (blue), and 13 canonical protein-coding genes (other colors) in the human mitochondrial genome. The HN ORF (red) is located in the 16S rRNA gene. Adapted from Xiao et al. (2016) [111].

Besides the identity found between HN ORF and a part of mitochondrial 16S rRNA gene, the HN ORF also showed varying degrees of homology with several nuclear

genomic regions [106, 112]. HN is a 24 amino acid peptide if synthesized in the cytoplasm while it is a 21 amino acid peptide if synthesized in mitochondria due to the difference of codon usage pattern (Table 1.3.2), but both are biologically effective [109]. Hence, the origin and translational site of HN remain unclear despite of more evidence suggesting the mitochondrial origin [108]. To investigate the relationship of structure and function, researchers have performed a substitution study on each amino acid residue of HN. Residues 3, 7-9, 11-13, and 19 are essential for the ability of apoptosis protection by HN. Replacement of serine at position 14 with glycine can yield a potent HN analogue S14G HN or HNG, which increases the biologic potency by approximately 1000-fold. Phe6 and Cys8 are important for the IGFBP-3 and Bax binding ability respectively. As for the secretion of HN, Leu9-11, Pro19 and Val20 are required [111].

Table 1.3.2 Sequence of humanin peptides and analogues.

Peptide (Human)	**Amino acid sequence**
Humanin (HN, cytoplasm)	MAPRGFSCLLLLT**S**E**I**DLPVKRRA
HN (mitochondria)	MAPRGFSCLLLLTSE**M**DLPVK
HNG	MAPRGFSCLLLLT**G**EIDLPVKRRA

1.3.3 The functions of humanin

HN can be secreted by cells and is detectable in plasma [106, 113], thus its actions were considered to be mediated by specific receptors. Ying et al. identified

formyl-peptide receptor-like-1 (FPRL1; a seven-transmembrane G protein-coupled receptor) as the first HN receptor [114]. HN can compete with the 42 amino acid form of the b-amyloid peptide (Ab42) for binding to FPRL1 and abolish the cytotoxicity of Ab42 in neuroblasts. This cytoprotective effect may be accomplished by activation of ERK1/2 signaling after HN binds to FPRL1 as an agonist [114]. Another study found that HN can activate both FPRL1 and FPRL2 in Chinese hamster ovary (CHO) cells [115]. In addition, Nishimoto et al. demonstrated that the STAT3 (signal transducer and activator of transcription 3) activation is essential for the process of neuroprotection by HN. Thus it is possible that another type of HN receptor belongs to the cytokine receptor family [116]. Subsequently, they discovered a tripartite receptor involving gp130 (glycoprotein 130), CNTFR (ciliary neurotrophic factor receptor), and WSX-1 (interleukin 27 receptor, alpha subunit) as a second HN receptor [117]. As mentioned above, HN also interacts with intracellular molecules such as Bax and IGFBP-3 in addition to its functions mediated by membrane receptors. Within cells, HN inhibits apoptosis by interacting with these two proteins (Figure 1.3.3).

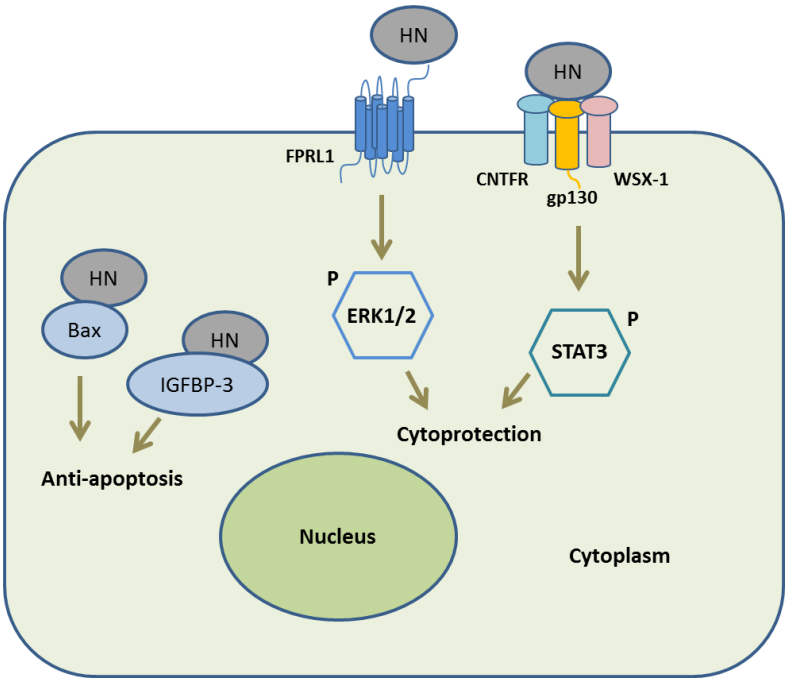

Figure 1.3.3 Humanin intracellular binding partners, membrane receptors and associated signaling pathways. Adapted from Lee et al. (2013) [108]. There are two types of humanin receptor on the cell membrane: FPRL1 and gp130/CNTFR/WSX-1 trimetric receptor with the ERK1/2 and STAT3 signaling pathway as the downstream respectively. Humanin can also act in the cytoplasm by interacting with pro-apoptotic proteins like Bax and IGFBP-3. P, phosphorylation.

HN is associated with a number of diseases such as chronic progressive external ophthalmoplegia (CPEO), mitochondrial encephalomyopathy with lactic acidosis and stroke-like episodes (MELAS), and pigmented villonodular synovitis (PVNS). A remarkable increase of HN expression was found in these diseases, implying that HN may act as a protective factor to response to cellular stress [108, 111]. On the other hand, HN levels appear to be negative correlated with age in rodents and human [113]. Furthermore, studies have reported the neuroprotective effect of HN in AD (*in vitro*

and *in vivo*) as well as in ischemia and reperfusion (I/R) models [111]. A gene array profiling data performed by our research group revealed that HN is strongly overexpressed in glioblastoma-associated microglia/macrophages compared with microglia in tumor-free brain tissue taken from epilepsy patients. This finding suggests that HN may play an important role in GBM and therefore could be a candidate for the development of new GBM therapies.

1.4 Objective of the study

As described above, apelin/APLNR signaling and humanin could both be potential targets for the improvement of the treatment outcomes of glioblastoma. Thus, the first aim of this thesis was:

a) To investigate the impact of apelin/APLNR targeting for GBM therapy by assessing the survival benefit in novel GBM mouse models;
b) To test the effect of combining APLNR targeting with established anti-angiogenic VEGFR2 treatment;
c) To assess the mechanistic role of apelin/APLNR signaling in tumor angiogenesis, tumor cell proliferation and invasion.

The second aim of this thesis was the study of the effect of microglia-secreted peptide humanin on GBM cell survival and protection against chemotherapeutic agents.

2. Materials

2.1 Devices

Table 2.1 Devices

Equipment / Software	**Company**
Axiovision Rel. 4.8 / 4.9 software	Carl Zeiss
Balances-AG204	Mettler Toledo
Balances-MonoBloc	Mettler Toledo
Centrifuge	Thermo Fisher Scientific/Eppendorf
Clamp Mount Micromanipulators	ADInstruments
Countess II FL Automated Cell Counter	Thermo Fisher Scientific
Digital Vortex Mixer	VWR
Fridge (4 ℃, -20 ℃, -80 ℃)	LIEBHERR
Hera safe hood	Thermo Fisher Scientific
Incubator	Thermo Fisher Scientific
LAS X software	Leica Microsystems
Leica SP8X WLL upright confocal microscope	Leica Microsystems
Magnetic Hotplate Stirrer	VWR
Microliter syringe	Hamilton
Micropipette (10µl, 20µl, 100µl, 200µl, 1000µl)	Eppendorf
Microscope Axioskop 2	Carl Zeiss

Microscope Axiovert 25	Carl Zeiss
Microscope camera Axiocam MRm	Carl Zeiss
Microtome Slide 2003	PFM medical AG
Microwave	Siemens
Olympus-BX53-microscope	Olympus Europe
Perfusion system Dose IT P910	Integra Biosciences AG
pH meter WTW Multical bench	Sigma Aldrich
Pipette boy	Eppendorf
Shaker	Biozyme Scientific
StereoInvestigator Software 10.21.1	MicroBrightField Bioscience
Stereotactic Frame	Stereotactic Frame
Surgical instruments	Aesculap
Vibratomes VT 1200S	Leica
Water bath	Memmert

2.2 Consumables

Table 2.2 Consumables

Product	**Supplier**
8-well culture slide	Falcon
Alzet Brain Infusion Kit 3	ALZET
Alzet Osmotic Pump Model 1002	ALZET
Cell Culture Flask (T25, T75, T150)	TPP

Centrifuge tubes (0.5ml, 1ml, 2ml)	Eppendorf
Centrifuge tubes (15ml, 50ml)	TPP / Falcon
Cover slips	Gerhard Menzel
Culture Dish	TPP / B. Braun Melsungen AG
Culture insert (PICM03050)	Millipore
Ethibond excel (5-0) sutures	Ethicon
Microtome Blade A35	Feather
Pap-pen	Dako
Pipette tips (10µl, 100µl, 200µl, 1000µl)	Eppendorf
Plate (6wells, 12 wells, 24 wells)	TPP
Scalpel (#15, #23)	Feather
Slide for immunolabeling	Gerhard Menzel
Stripette™ Serological Pipets (5ml, 10ml, 25ml)	Corning
Syringe (1ml, 5ml, 10ml, 50ml)	B. Braun Melsungen AG
Syringe needle (20G, 21G, 27G, 30G)	B. Braun Melsungen AG
Tissue-Tek Cryomold (15mm ×15mm ×15mm)	Sakura Finetek

2.3 Cell culture materials

Table 2.3 Cell culture materials

Material	**Catalog Number**	**Supplier**
Accutase	A6964	Sigma Aldrich
B27	17504-044	Invitrogen
DMEM	FG0415	Biochrom
DMEM-F12	11320-074	Invitrogen
Fetal Bovine Serum	10270-106	Life Technologies
hEGF	236-EG	R&D systems
hFGF	100-18B	PeproTech
MEM non-essential amino acids	11140-035	Life Technologies
NeuroCult™ Basal Medium	5700	STEMCELL Technologies
NeuroCult™ Proliferation Supplement	5701	STEMCELL Technologies
Penicillin-streptomycin	15140-122	Life Technologies
Trypan Blue Solution 0.4%	T8154	Sigma Aldrich
Trypsin/EDTA	L2153	Merck Millipore

2.4 Reagents and Chemicals

Table 2.4 Reagents and Chemicals

Product	**Supplier**
2,2,4-Trimethylpentane	Thermo Fisher Scientific
Acetone 100%	Sigma Aldrich
Agarose	Sigma Aldrich
Aqua ad iniectabilia	B. Braun Melsungen AG
Aquatex mounting medium	Sigma Aldrich
Bepanthen	Bayer
Blue Alkaline Phosphatase Substrate Kit	Vector Laboratories
Bull Serum Albumin (BSA)	Sigma Aldrich
$CaCl_2 \cdot 2H_2O$	Sigma Aldrich
Citric acid monohydrate	Sigma Aldrich
Clodronate-Liposomes	Liposoma B.V.
Cryomatrix	Thermo Fisher Scientific
DAB-DC135c006	DCS Labline
DAB-substrate-PC136R100	DCS Labline
Dako Antibody Diluent	Dako
DAPI	Sigma Aldrich
DC101	Eli Lilly
Donkey serum	Jackson ImmunoResearch
Dual Endogenous Enzyme block	Dako

Dual Endogenous Enzyme Block	Dako
Entellan® mounting medium	Merck
Eosin G solution	Sigma Aldrich
Ethanol 100%	CLN GmbH
Ethanol 70%	CLN GmbH
Ethanol 96%	CLN GmbH
Ethylene glycol	Sigma Aldrich
Fluorescence Mounting Medium	Dako
Glucose 20%	B. Braun Melsungen AG
Glycerol	Sigma Aldrich
HBSS (Gibco™)	Life Technologies
HCl	Sigma Aldrich
Horse serum (Gibco™)	Life Technologies
Hygromycin B	Sigma Aldrich
Isopropanol	Sigma Aldrich
KCl	Sigma Aldrich
Ketamin 10%	Zoetis Deutschland GmbH
KH_2PO_4	Sigma Aldrich
Laminin	Sigma Aldrich
L-Glutamine (200mM, Gibco™)	Life Technologies
Lipofectamine 3000 reagent	Thermo Fisher Scientific
Mayer's Hematoxylin Solution	Carl Roth

MEM (Gibco™)	Life Technologies
$MgCl_2 \cdot 6H_2O$	Sigma Aldrich
$Na_2HPO_4 \cdot 7H_2O$	Sigma Aldrich
NaCl 0.9%	B. Braun Melsungen AG
NaCl	Merck Millipore
NaOH	Sigma Aldrich
$NaH_2PO_4 \cdot H_2O$	Sigma Aldrich
Paraformaldehyde (PFA)	Sigma Aldrich
PBS	Apotheke Klinikum der Universität München
PBS-Liposomes	Liposoma B.V.
pCEP4 plasmid Humanin ORF	Eurofins Genomics
Pentobarbital (Narcoren®)	Merial
Poly-D-Lysine	Thermo Fisher Scientific
Povidone iodine solution 7.5%	B. Braun Melsungen AG
Protein Block	Dako
Protein Block Serum-Free	Dako
Rompun 2%	Bayer
Roti® Histol	Carl Roth
Sucrose	Sigma Aldrich
Sudan black B	Sigma Aldrich
Temozolomide (TMZ)	Sigma Aldrich
Tri-Natriumcitrat-Dihydrat	Sigma Aldrich

Tris base	Sigma Aldrich
Triton X-100	Roche Diagnostics
Tween-20	Sigma Aldrich
WGA-594	Thermo Fisher Scientific

2.5 Peptides

Table 2.5 Peptides

Product	**Catalog Number**	**Supplier**
[Gly14]-Humanin (HNG)	H54838	Designer BioScience
(Ala13)apelin-13 (Apelin-F13A)	H-7752	Bachem
pyroglutamylated apelin-13	H-4568	Bachem

2.6 Primary Antibodies

Table 2.6 Primary Antibodies

Immunogen	**Host Species**	**Isotype**	**Dilution**	**Catalog number**	**Provider**
GFP	Goat	IgG	1:500	R1091P	Acris
Humanin	Rabbit	IgG	1:100	PA1-41325	Thermo Fisher
Iba1	Goat	IgG	1:400	ab5076	Abcam
Ki67	Rabbit	IgG	1:200	ab16667	Abcam
vWF	Rabbit	IgG	1:400	A0082	Dako

2.7 Secondary Antibodies

Table 2.7 Secondary Antibodies

Conjugation	Antigen	Host Species	Dilution	Catalog number	Provider
Alexa Fluor 488	Goat IgG	Donkey	1:500	705-545-147	Jackson ImmunoResearch
Alexa Fluor 594	Rabbit IgG	Donkey	1:500	711-585-152	Jackson ImmunoResearch
Alexa Fluor 647	Goat IgG	Donkey	1:500	705-605-147	Jackson ImmunoResearch
Biotinylated	Goat IgG	Horse	1:200	BA9500	Vector Laboratories
Biotinylated	Rabbit IgG	Donkey	1:200	711-065-152	Jackson ImmunoResearch

2.8 Streptavidin-conjugates

Table 2.8 Streptavidin-conjugates

Conjugation	Dilution	Catalog number	Provider
Alkaline phosphatase	1:200	SA-5100	Vector Laboratories
HRP	1:200	016-030-084	Jackson ImmunoResearch

3. Methods

3.1 Animal experiments

3.1.1 Animals

All the animal experiments in this study were approved by the local animal care committee of the Government of Oberbayern and performed according to the National Guidelines for Animal Protection, Germany. Animals were kept in the Walter-Brendel-Centre of Experimental Medicine in standard cages with *ad libitum* access to water and food. All mice had a C57BL/6J background and lived in the 12-h light/dark cycle. During the survival monitoring, mice were checked twice a day for collecting the dead mice or the sick mice at a humane end-point to be sacrificed.

3.1.2 Tumor implantation

Mice were anesthetized with 7 µl/g of body weight of anesthetic comprising 1.02 ml 10% ketamine, 0.36 ml 2% Rompun and 4.86 ml 0.9% NaCl (intraperitoneal injection). After anesthesia, mice were immobilized on the mouse stereotaxic instruments in flat-skull position and kept warm. A skin incision along the midline was made on the skull with a scalpel after disinfection of the skin with 7.5% povidone iodine solution. The cornea of both eyes were protected and kept moist with the Bepanthen cream. A round hole was drilled into the skull with a 21G needle tip according to the coordinate (1.0 mm anterior and 1.5 mm right of the bregma). Then 1µl of glioblastoma cell (1×10^5, *p53*^{KO}PDGFB GSCs, GFP-positive) in the supplement-free medium was implanted within 2 min by stereotactic injection with a

22G Hamilton syringe at a depth of 3 mm (the needle was inserted for 4 mm starting from the skull surface then retracted 1 mm). After the resting time of one minute, the needle was retreated at a speed of 1 mm/min. Finally, the wound was cleaned and confirmed no bleeding, and then the incision was sutured carefully.

3.1.3 Intracerebral drug application

One day before implantation, Alzet osmotic minipumps were prepared by filling with 30 μg of apelin-F13A (a mutant APLNR ligand, Bachem) or 0.8 mg of DC101 (VEGFR2-blocking antibody, as a model of ramucirumab treatment in humans, Eli Lilly) alone or combined for sustained delivery over 14 days (Model 1002; Alzet) in aCSF (artificial cerebrospinal fluid, as described by Alzet) or with aCSF alone as the control following priming overnight in aCSF at 37 ℃. The Alzet osmotic minipumps were implanted subcutaneously under anesthesia as previously described with the needle of the Alzet brain infusion kit 3 inserted into the hole originally prepared for orthotopic tumor implantation.

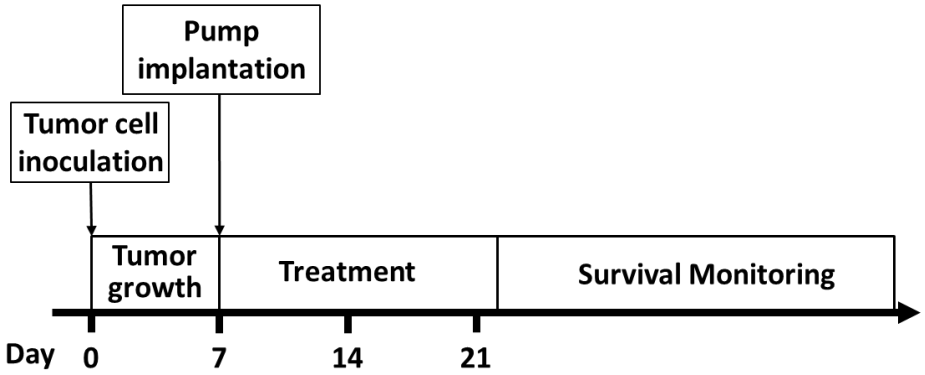

Figure 3.1.3 Time course of the experimental procedures in the survival study.

3.2 Histology

3.2.1 Perfusion and tissue preparation

Mice were anesthetized with Narcoren® and sacrificed by perfusion through ventriculus sinister with 0.01 M phosphate buffered saline (PBS) followed by paraformaldehyde solution (PFA, 4% w/v in 0.01 M PBS) at a humane end-point in the survival study. After successful perfusion, brains were extracted, post-fixed in 4% PFA at 4 ℃ for 48 hours, and immersed in sucrose (30% w/v in 0.01 M PBS). Then, brains were embedded in Cryomatrix and frozen in 2,2,4-Trimethylpentane with liquid nitrogen, and cut into 40-µm horizontal sections sequentially collected into a 24-well plate filled with about 1 ml cryoprotectant (Glycerol, Ethylene glycol and 0.01 M PB at a ratio of 1:1:2) in each well. The plates were stored in freezer (−20 ℃) and covered with aluminium foil.

3.2.2 H&E staining

To observe the tumor morphology and calculate the tumor volume, Hematoxylin and Eosin staining (H&E staining) was performed by the following steps: the floating sections were mounted on slides to air dry for 20 min; after dehydrated in 100% Ethanol for 30 seconds, sections were dyed in Mayer's Hematoxylin Solution for 2 min and rinsed in running tap water for 5 min; then sections were stained in 0.5% Eosin solution for 30 seconds and washed shortly in distilled water; dehydration was performed successively in ascending Ethanol series (70% Ethanol for 1 min, 96% Ethanol for 1 min, 100% Ethanol for 1 min); slides were covered with Entellan®

mounting medium. Pictures of the H&E staining were taken by Microscope Axioskop 2 with Axiocam MRm and Axiovision Rel. 4.9 software (Carl Zeiss).

3.2.3 Quantification of tumor volume and pseudopalisading area

Tumor volumes were obtained by measuring the area of the tumor region (marked by H&E staining or anti-GFP immunostaining) of every 12th mouse brain section with Axiovision Rel. 4.9 software or ImageJ software and then calculating with the Cavalieri Method (i.e. estimating the tumor volume $\hat{V}$ by summing the tumor areas A_i and multiplying by the mean section cutting thickness $\bar{t}$ and the section evaluation interval m': $\hat{V} = m' \cdot \bar{t} \cdot \sum A_i$) [118, 119]. The pseudopalisading area percentage in the tumor was estimated with ImageJ software by adjusting the threshold to identify the pseudopalisading necrosis.

3.3 Immunofluorescence staining and quantification

3.3.1 Immunofluorescence staining for mouse brain sections

Floating sections were transferred from the stored 24-well plate to a 12-well plate washing 5 min in PBT (0.1% Tween-20 in 1× PBS) for three times. Protein blocking was performed 1 hour for the sections at room temperature with blocking buffer (5% normal donkey serum and 0.3% Triton X-100 in 1× PBS). Then sections were incubated overnight at 4 ℃ in primary antibody solution. The primary antibodies used in this study and the corresponding dilutions were as follows: goat anti-GFP (1:500), rabbit anti-vWF (1:400), goat anti-iba1 (ionized calcium-binding adapter molecule 1;

1:400), and rabbit anti-Ki67 (1:200). On the second day, sections were incubated at room temperature for 2 hours with secondary antibody after washing with PBT for three times. The secondary antibodies were donkey anti-goat AF488 (1:500), donkey anti-rabbit AF594 (1:500) or donkey anti-goat AF647 (1:500). All antibodies were diluted in protein blocking buffer. After another round of PBT washing, nuclei were stained 2 min with DAPI (1:10,000). Then sections were mounted in Dako Fluorescent Mounting Medium after DAPI was washed away. Pictures were taken by the Axiovert25 microscope with Axiocam MRm and Axiovision Rel 4.8 software (Carl Zeiss) and quantified by ImageJ software.

3.3.2 Quantification of tumor microvasculature

A method of stereological analysis was used to quantify the microvasculature in the tumor area with green fluorescent tumor cells (GFP-positive) and red fluorescent blood vessels marked by von Willebrand factor (vWF) staining. Pictures were obtained by an Olympus-BX53-microscope with a motorized object table (MicroBrightField Bioscience). Every 12^{th} mouse brain section was examined and analyzed by the connected StereoInvestigator Software 10.21.1 (MicroBrightField Bioscience, Williston, VT, USA) using the function of space ball [120, 121]. Three parameters were generated after the measurement and analysis: vessel length density (VLD, the total vessel length per mm^3 of tumor), vessel length (the total vessel length in the whole tumor), and vascular network complexity (a ratio to estimate the complexity of vessel branching).

3.3.3 Assessment of *in vivo* tumor cell invasiveness

For the evaluation of the tumor cell invasiveness, three types of tumor volumes were determined from the GFP-stained tumor sections: 1) the overall tumor volume was calculated by the total tumor area including both the compact tumor regions and single invasive tumor cells (Cavalieri Method); 2) the compact tumor volume was obtained only by the area of compact tumor regions where tumor cells were in direct contact with each other; 3) the invasive tumor volume was calculated by subtracting the compact tumor volume from the overall tumor volume. And then tumor invasiveness was presented as the percentage of the invasive volume to the overall tumor volume. Photographs for the GFP-stained tumor were made by an Axiovert25 microscope (Objective 5×) with Axiocam MRm and Axiovision Rel 4.8 software (Carl Zeiss). Tumor area was measured by ImageJ software. The furthest distance of single tumor cells migrated from the compact tumor mass was measured as well (3 sections per mouse and 4 mice per group).

3.4 *In vitro* experiments

3.4.1 Cell culture

U87MG cell line was obtained from the American Type Culture Collection (ATCC) and cultured under adherent conditions in DMEM containing 1× MEM non-essential amino acids, 1% penicillin-streptomycin (i.e. 100 units/ml penicillin, 100 µg/ml streptomycin), and 10% fetal bovine serum. U87 *APLN*-Knockdown ($U87^{AKD}$) and non-silencing control cells ($U87^{NSC}$) had been previously obtained by transduction

with lentiviral vectors carrying the short-hairpin RNA (shRNA) of interest [122].

Human glioblastoma stem cells (GSCs: NCH644, GBM14, GBM5av, GBM2 and GBM11) were derived from glioblastoma patients biopsies (at the Medical Faculty Heidelberg or at the Charité Medical University of Berlin according to local ethical regulations) and were maintained under stem cell cultivation conditions in DMEM-F12 supplemented with 1 × B27, 1% penicillin-streptomycin, 10 ng/ml human epidermal growth factor (hEGF) and 10 ng/ml human fibroblast growth factor (hFGF) for NCH644, GBM14 or in Neural Stem Cell Medium (450ml) with Proliferation supplement (50ml), 1% penicillin-streptomycin, 10 ng/ml hEGF and 10 ng/ml hFGF for GBM5av, GBM2 and GBM11. $GBM14^{AKD}$ and $GBM14^{NSC}$ cells were obtained as the method for $U87^{AKD}$ and $U87^{NSC}$ cells [122].

Neural precursor cells (NPCs) had been previously isolated from the subventricular zone (SVZ) of the 5-day-old BL6/J mice with homozygous deletion of *TP53*. Isolated cells were cultured in spheroid conditions with DMEM-F12 medium supplemented with 1 × B27, 1% penicillin-streptomycin, 10 ng/ml hEGF and 10 ng/ml hFGF. Mouse transgenic glioblastoma cells as a model of the proneural GBM subtype ($p53^{KO}$PDGFB GSCs) had been previously generated by transduction of a single cell suspension of $p53^{KO}$ NPCs for 1 h with a multiplicity of infection (MOI) of 80 of VSV-G pseudotyped GFP-PDGFB retroviral particles. Human PDGFB cDNA was derived from the RCAS-pBIG plasmid. Transduction efficiency was verified by GFP immunofluorescence and was >99% [122].

All cells were maintained under the condition of 95% O_2 and 5% CO_2 humidified

atmosphere in a 37 ℃ incubator. The cell counting for GBM14 proliferation in apelin experiments or for GBM2 and GBM11 in humanin experiments was performed by Countess II FL with 0.4% Trypan Blue Solution identifying the alive and dead cells at a dilution of 1:2.

3.4.2 Wound healing assay

U87 or GBM14 cells were seeded in the 24-well plate (3 or 5 × 10^5 cells/well, respectively). After 24 hours incubation at 37 ℃, a scratch wound was created using a 1,000 µl (U87) or 200 µl (GBM14) micropipette tip and cellular debris was removed. Then 200 nM apelin-13 or apelin-F13A was added. Pictures were taken at 0 h and after 10 h (U87) or 24 h (GBM14) with an Axiovert25 microscope with Axiocam MRm and Axiovision Rel 4.8 software (Carl Zeiss). The cell covered area was measured by ImageJ software.

3.4.3 Fluorescent immunocytochemistry

An 8-well culture slide (Falcon®) was coated in 37°C incubator with 50 µg/ml poly-D-lysine overnight followed by 5 µg/ml laminin for 2 hours. Then cells were plated at the concentration of 50,000 cells per well and incubated in DMEM containing supplements for 24 hours. Culture medium was removed subsequently, and cells were washed with 1 × PBS once, continued with 10 min of fixation with 4% PFA at room temperature and 1× PBS washing for three times. After 1 hour of permeabilization at room temperature with blocking buffer (5% donkey serum and 0.3%

Triton-X in 1 × PBS containing), cells were incubated with rabbit anti-Ki67 (1:200) at 4 ℃ overnight. On the second day, cells were washed with 1 × PBS and incubated with the secondary antibody donkey anti-rabbit AF594 (1:500) at room temperature for 2 hours. All antibodies were diluted in blocking solution. After three times of 1 × PBS wash, nuclei were stained by DAPI (1:10,000) for 2min. The slides were covered by coverslips with Dako Fluorescent Mounting Medium. Fluorescent pictures were taken by Axiovert25 microscope with Axiocam MRm and Axiovision Rel 4.8 software (Carl Zeiss).

3.4.4 Specific GFP-apelin internalization

GBM14 cells were seeded in an 8-well culture slide (Falcon®; 10,000 cells/well) previously coated with 50 μg/ml poly-D-lysine in 37 ℃ incubator overnight followed by 2 hours of 5 μg/ml laminin and then incubated in DMEM for 24 h. After cells adhered to the slide, the medium was removed and replaced by 200μl of fresh DMEM with 2 μM the N-terminally GFP-conjugated Apelin-13, Apelin-F13A, Apelin-13scr (containing the scrambled amino acid sequence of Apelin-13) or GFP-linked oligomer 728 (positive control) continued by 120 min incubation at 37 ℃. In the competition experiment, before the addition of 2 μM GFP-apelin-13 or GFP-apelin-F13A, GBM14 cells were incubated with 2 nM, 20 nM, 200 nM, 2 μM, or 20 μM unlabeled apelin-13 or apelin-F13A for 30 min respectively. After all the treatments, fixation was performed with 4% PFA for 30 min followed by 10 min incubation of WGA-594 1:200 (cell membrane staining) and DAPI 1:10,000 (nucleus staining) in 1 × PBS at

room temperature. Then cells were washed with 1× PBS and the slides were covered by coverslips with Fluorescent Mounting Medium. Fluorescent photographs were taken by confocal microscope (the Leica SP8X WLL upright with the LAS X software) and analyzed by ImageJ software Fiji package. The quantification of the competition experiment was performed by measuring the number of cells containing GFP-conjugated peptides on the total number of cells in the picture. Six pictures were quantified for each condition.

3.4.5 Brain slice culture procedures

6-day old C57/BL6J mice were used to obtain the organotypic brain slice cultures under sterile conditions in this study. The brains were taken out after decapitation. A Leica vibratome was used to cut the whole brain hemispheres into 350 μm thick slices. Then brain slices were transferred onto the membrane (pore 0.4 μm) of a culture insert in the 6-well plate containing 1 ml of culture medium (25% HBSS, 44.75% MEM, 2 mM L-Glutamine, 25% heat inactivated horse serum, 1% penicillin-streptomycin, 6.5 mg/ml glucose) per well and 0.5 mg/ml Clodronate-liposomes (for microglia depletion) or PBS-liposomes (control). The slices were cultured in an incubator with 5% CO_2 and humidified atmosphere at 37℃ for 24 hours. After medium was removed, brain slices were washed with 1× PBS, cultured in fresh culture medium (without liposomes), and incubated for 3 days (waiting for microglia depletion in Clodronate-liposomes group). 0.5μl of 5,000 glioblastoma cells (GFP-positive NCH644 and GBM5av) was inoculated into brain

slices by a 1µl Hamilton syringe installed in a micromanipulator. The needle was inserted for 200 µm deep then retracted by 50 µm. A micro pump was used to inject the cell suspension slowly over 1 minute. For all brain slices, the fluorescent glioblastoma cells were injected in the same region. Fluorescence microscopy photographs were made to record the area of the all tumor cells in the slices at day 0 (immediately after injection), day 1, day 3, day 5 and day 7 by Axiovert25 microscope with Axiocam MRm and Axiovision Rel 4.8 software (Carl Zeiss). Photographs were analyzed and quantified as described in [123, 124] using ImageJ software. The distance between the center of the injection canal and the individual fluorescent tumor cells were measured, and the accumulated data were used to assemble the distance histograms.

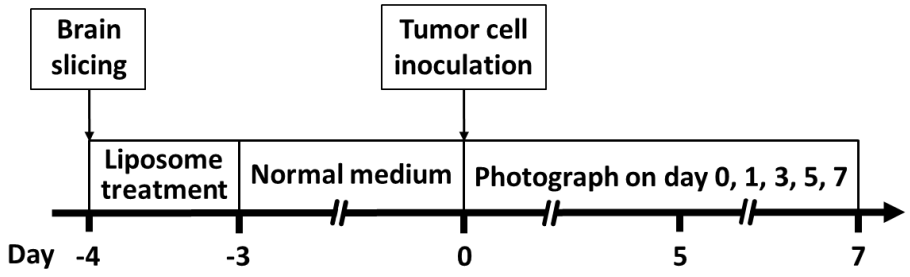

Figure 3.4.5 Time course of the experimental procedures in brain slice experiments.

3.5 Immunostaining of patient specimens

3.5.1 Immunohistochemistry (Paraffin-embedded human GBM sections)

Paraffin-embedded sections of human GBM specimen or epilepsy non-tumor control

were deparaffined twice in 60℃ isopropanol for 20 min. Slides were taken out for airdry and cool-down, and then fixed in -20℃ 70% acetone for 10 min. After 1× PBS washing for 5 min 3 times, slides were immersed in 0.01 M citrate buffer (18ml 0.1 M Citric acid monohydrate and 82ml 0.1 M Tri-Natriumcitrat-Dihydrat mixed in distilled water; 1L, pH 6.0) and cooked with the microwave for 20 min (antigen retrieval). After slides cooled down, 1× PBS washing was performed for 5 min 3 times followed by endogenous peroxidase blocking with Dako endogenous enzyme block for 20 min and another round of 1× PBS washing. Then sections were incubated 30 min with Dako protein blocking reagent (protein blocking) and continued with rabbit anti-humanin primary antibody (1:100) overnight at 4℃. On day 2, sections were incubated for 2 hours with the donkey anti rabbit biotinylated secondary antibody (1:200) at room temperature, and then incubated for 30 min with streptavidin conjugated HRP (1:200) at room temperature followed by DAB incubation under the microscope (PBS washing performed between each steps). Then distilled water was used to wash away DAB and 4% PFA was applied for fixation 10 min. After this step, washing was changed to Tris buffer (50mM Tris base and 0.3M NaCl, pH 7.0) 5min 3 times. Then sections were incubated for 30 min at room temperature with Dako protein blocking reagent continued by 4℃ overnight with goat anti-iba1 primary antibody (1:200). On day 3, horse anti goat biotinylated secondary antibody (1:200) was added onto sections and incubated at room temperature for 2 hours. Then streptavidin conjugated alkaline phosphatase was incubated for 30 min at room temperature. All antibodies were diluted in Dako Antibody Diluent. Subsequantly,

VECTOR Blue Alkaline Phosphatase Substrate Kit incubation was performed under the microscope (Tris buffer washing performed between each steps). Then sections were washed with distilled water and the coverslips were mounted with Aquatex mounting medium. Photographs were made by Microscope Axioskop 2 with Axiocam MRm and Axiovision Rel. 4.9 software (Carl Zeiss).

3.5.2 Immunofluorescence staining (Paraffin-embedded human GBM sections)

Paraffin-embedded sections of human GBM specimen or epilepsy non-tumor control were deparaffined twice in 60℃ isopropanol for 20 min. Slides were taken out for airdry and cool-down, and then fixed in -20℃ 70% acetone for 10 min. After 1× PBS washing for 5 min 3 times, slides were immersed in citrate buffer and cooked with the microwave for 20 min (antigen retrieval). After slides cooled down, 1× PBS washing was performed for 5 min 3 times followed by protein blocking for 30 min (5% donkey serum and 0.3% Triton-X in 1× PBS). Then the primary antibodies rabbit anti-humanin (1:100) and goat anti-iba1 (1:200) was added onto section and incubated overnight at 4℃. On day 2, sections were incubated at room temperature with the secondary antibodies donkey anti rabbit AF594 (1:200) and donkey anti goat AF488 (1:200) for 2 hours. All antibodies were diluted in blocking solution. Then sections were incubated for 20 min with Sudan black B solution (0.1% w/v in 70% Ethanol) to reduce the auto-fluorescence. DAPI 1:10,000 was used for nuclei staining (PBS washing performed between each steps). The slides were covered by coverslips with Fluorescent Mounting Medium. Fluorescence microscopy photographs were made by

Axiovert25 microscope with Axiocam MRm and Axiovision Rel 4.8 software (Carl Zeiss).

3.6 Cell counting experiments

3.6.1 Cell counting experiments for cells treated with HNG

Cells were distributed to 5 groups: 1) culture medium with EGF&FGF and addition of 10 mg/ml BSA (vehicle for HNG); 2) medium without EGF&FGF and addition of BSA; 3) medium without EGF&FGF and addition of 2 μM HNG dissolved in 10 mg/ml BSA; 4) medium without EGF&FGF and addition of 10 μM HNG; 5) medium without EGF&FGF and addition of 20 μM HNG. Each condition was in triplicate.

On day 0, cells (GBM2 and GBM11) were plated in the 6-well plate (100,000 cells per well) and treated with BSA or HNG. Medium were changed every 24 hours with BSA or HNG of the same concentration for the next 4 days. On day 7, day 14 and day 21, the Countess II FL Automated Cell Counter was used to count the cell number of each well. And 100,000 cells were replated in each well for all groups with medium containing BSA or HNG after cell counting on day 7 and day 14.

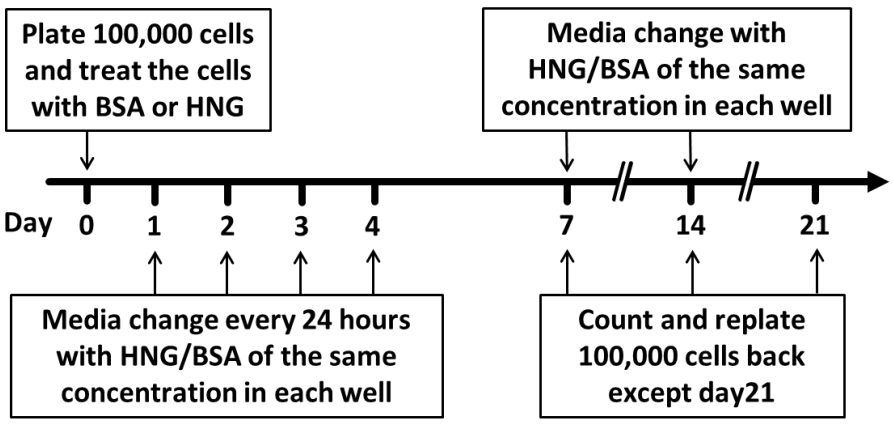

Figure 3.6.1 Cell counting experiments for cells treated with HNG.

3.6.2 Cell counting experiments for cells treated with HNG and TMZ

There were 3 basic conditions: 1) culture medium with EGF&FGF and addition of 10 mg/ml BSA (vehicle); 2) medium without EGF&FGF and addition of BSA; 3) medium without EGF&FGF and addition of 20 μM HNG. On each condition, cells were also treated with TMZ of 0 μM, 100 μM or 300 μM respectively. Each condition was in triplicate.

On day 0, cells (GBM2 and GBM11) were plated in the 6-well plate (100,000 cells per well) and treated with BSA or HNG. Cells were treated with TMZ from day 0 to day2 and also treated with BSA or HNG of the same concentration every other day. The cell number of each well was counted by Automated Cell Counter on day 7, day 14. And 100,000 cells were replated in each well with medium containing BSA or HNG of the same concentration on day 7.

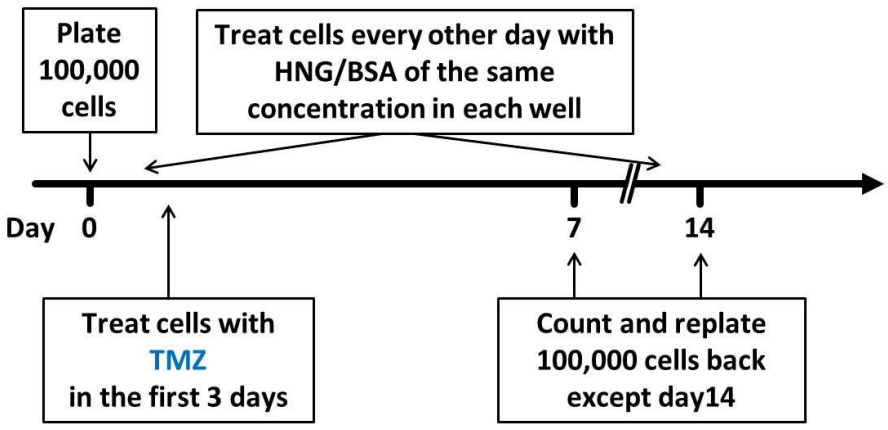

Figure 3.6.2 Cell counting experiments for cells treated with HNG and TMZ.

3.6.3 Cell counting experiments for HN overexpressing cells

GBM2 and GBM11 cell lines were transfected with pCEP4 plasmid containing the humanin (HN) open reading frame and hygromycin resistance gene or transfected with empty vector pCEP4 plasmid containing hygromycin resistance gene by Lipofectamine 3000 reagent for 2 days. Then transfected cells were transferred to fresh culture medium and selected for 4 weeks with 400 μg/ml of hygromycin B. After that, the selection was maintained using 200 μg/ml of hygromycin B.

Transfected cells (GBM2 HN, GBM2 pCEP4, GBM11 HN and GBM11 pCEP4) were plated in the 6-well plate (100,000 cells per well) on day 0 and treated with TMZ of 0 μM, 100 μM or 300 μM respectively from day 0 to day 2. The cell number of each well was counted by Automated Cell Counter on day 7, day 14. And 100,000 cells were replated in each well on day 7. Each condition was in triplicate.

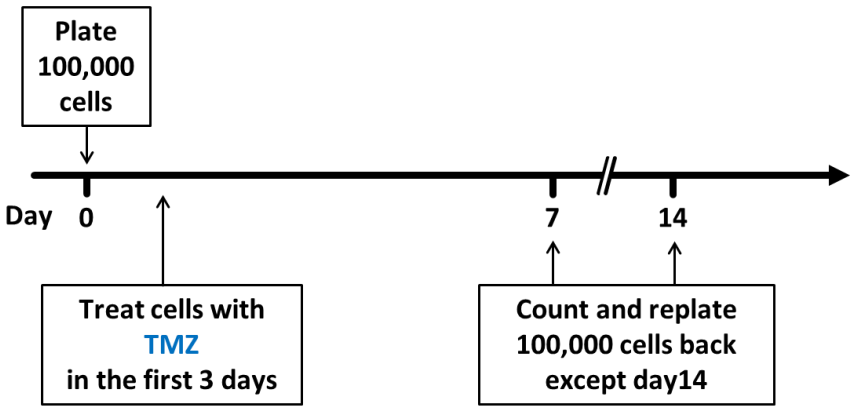

Figure 3.6.3 Cell counting experiments for HN overexpressing cells.

3.7 Statistics

Statistical analyses in this thesis were performed with the GraphPad Prism software. To determine statistical significance in the survival experiment, the Log-rank (Mantel-Cox) test was applied. For the comparison of two independent groups, the unpaired Student’s t-test was used. Differences among three or more groups were analyzed by One-way analysis of variance (one-way ANOVA) with Tukey's multiple comparisons test as the post hoc test. The statistical tests for each experiment are described in the figure legends. The criterion for the statistically significant difference was $p < 0.05$.

4. Results

4.1 Targeting apelin/APLNR reduces angiogenesis and tumor cell invasiveness in glioblastoma

4.1.1 Combination treatment targeting VEGFR2 and apelin/APLNR synergistically improves survival of glioblastoma-bearing mice

In animal models, systemic administration of VEGFR2-blocking antibody DC101 was shown to suppress the growth of various tumors, including glioblastoma (GBM) [125]. However, Kunkel et al. reported a side effect of DC101 with significant increase of tumor invasion (small satellite tumors) in addition to the inhibition of tumor growth and angiogenesis in a glioblastoma mouse model (intracerebral G55 xenografts, G55 is a human GBM cell line) [59]. Recently, our laboratory found that targeting apelin/APLNR by apelin-F13A (a mutant ligand for APLNR) decreased the tumor invasiveness in human primary GBM mouse models as well as transgenic mouse models ($p53^{KO}$PDGFB GSCs, generated from mouse neural precursor cells with *TP53* deletion and *PDGFB* overexpression; see Figure 5 in [122]). Also, one of the major suspected causes of the failure of anti-angiogenic treatment for glioblastoma by targeting VEGF/VEGFR2 signaling is the upregulation of alternative angiogenic factors. A previous study from our research group demonstrated that apelin/APLNR signaling plays an essential role in angiogenesis during embryonic development as well as in GBM pathology [56]. Hence, in the present study, I investigated whether the combination of anti-VEGFR2 therapy and targeting of apelin/APLNR signaling can achieve a better outcome than anti-VEGFR2 treatment alone. The $p53^{KO}$PDGFB

GSCs were orthotopically implanted in C57 BL6/J mice and allowed to expand for 7 days. Mice were divided into four groups and treated intracerebrally with apelin-F13A (n = 9), anti-VEGFR2 antibody (DC101; n = 7), apelin-F13A and anti-VEGFR2 antibody (n = 7), or with vehicle (artificial cerebrospinal fluid, aCSF) alone as a control (n = 10).

The median survival in the control group (aCSF treated mice) was 52 days. In the group of DC101 administration, the median survival increased to 67 days that was 28% longer than the control mice (p = 0.0145). A similar increase of median survival was achieved in apelin-F13A treated mice (63 days; 21% increase; p = 0.0139) in comparison with control mice. Notably, the mice with DC101 and apelin-F13A coadministration showed a significant increase in the survival (86 days; 65% increase vs. control mice; p = 0.0016). And the median survival of the co-treated group was also significantly longer compared with the administration of apelin-F13A (p = 0.0327) or DC101 (p = 0.0385) alone (Figure 4.1.1).

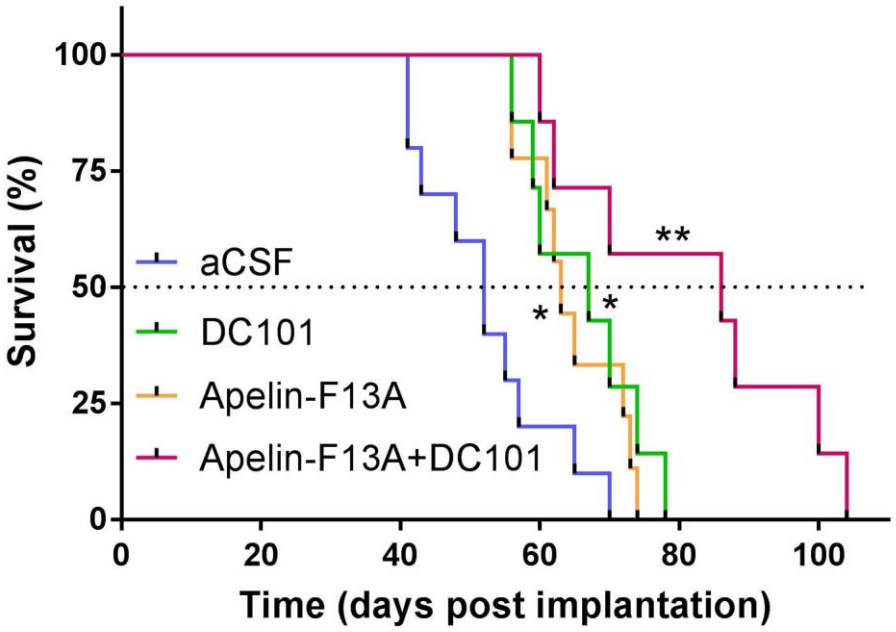

Figure 4.1.1 Survival of C57 BL6/J mice bearing *p53*^{KO}PDGFB GSCs. Mice were intracerebrally treated with vehicle (artificial cerebrospinal fluid, aCSF; n = 10), anti-VEGFR2 antibody (DC101, n = 7), apelin-F13A (a mutant ligand for APLNR, n = 9), or apelin-F13A combined with DC101 (n = 7) respectively. The median survival of DC101, apelin-F13A and the coadministration group significantly increased to 67 days (p = 0.0145), 63 days (p = 0.0139) and 86 days (p = 0.0016) respectively compared to the aCSF group (52 days). Log-rank (Mantel-Cox) test was used to determine statistical significance, *$p < 0.05$, **$p < 0.005$ compared to aCSF control group.

4.1.2 Tumor morphology and tumor volume in the survival study

In order to investigate histopathological changes in the experimental groups that might explain differences in survival, brains were collected from mice sacrificed at humane end-point. In all groups, big tumor masses were observed in the corpus striatum and cortex of the right hemisphere. The cerebral midline shifted to the left because of the extending tumor mass and single invading tumor cells were found in the left brain hemisphere of some animals. The tumors of the four treatment groups

showed typical glioblastoma morphology [6] (Figure 4.1.2a) characterized by large areas with high cell density, hyperangiogenesis with malformed blood vessels (examples shown as asterisks in Figure 4.1.2a A'&B'), local bleeding (arrows, Figure 4.1.2a A', the color of erythrocytes) and necrotic foci (cross, Figure 4.1.2a C'&D'), which were accompanied by pseudopalisades (white lines, Figure 4.1.2a C'). In the tumor necrotic foci (cross, Figure 4.1.2a C'), cell death with pyknotic nuclei (arrowhead) was surrounded by pseudopalisades (white lines).

The tumor volume calculated after Hematoxylin and Eosin staining (H&E staining) is shown in Figure 4.1.2b A. Because all the tumors were collected after the tumor-bearing animals entered the terminal stage and had to be sacrificed at humane end-point, there was a similar median of the tumor volume in aCSF control (142.5 mm^3), DC101 (138 mm^3), apelin-F13A (136.3 mm^3) and apelin-F13A + DC101 group (133.5 mm^3). However, these volumes were reached at different time points: 50 days in aCSF, 67 days in DC101, 62 days in apelin-F13A and 86 days in apelin-F13A + DC101 group (Figure 4.1.2b B). Two or three mice of every group showed a small tumor which might be due to the invasive glioblastoma cells growing into the ventricle and possibly blocking the circulation of CSF before a big tumor mass could be formed in the brain parenchyma.

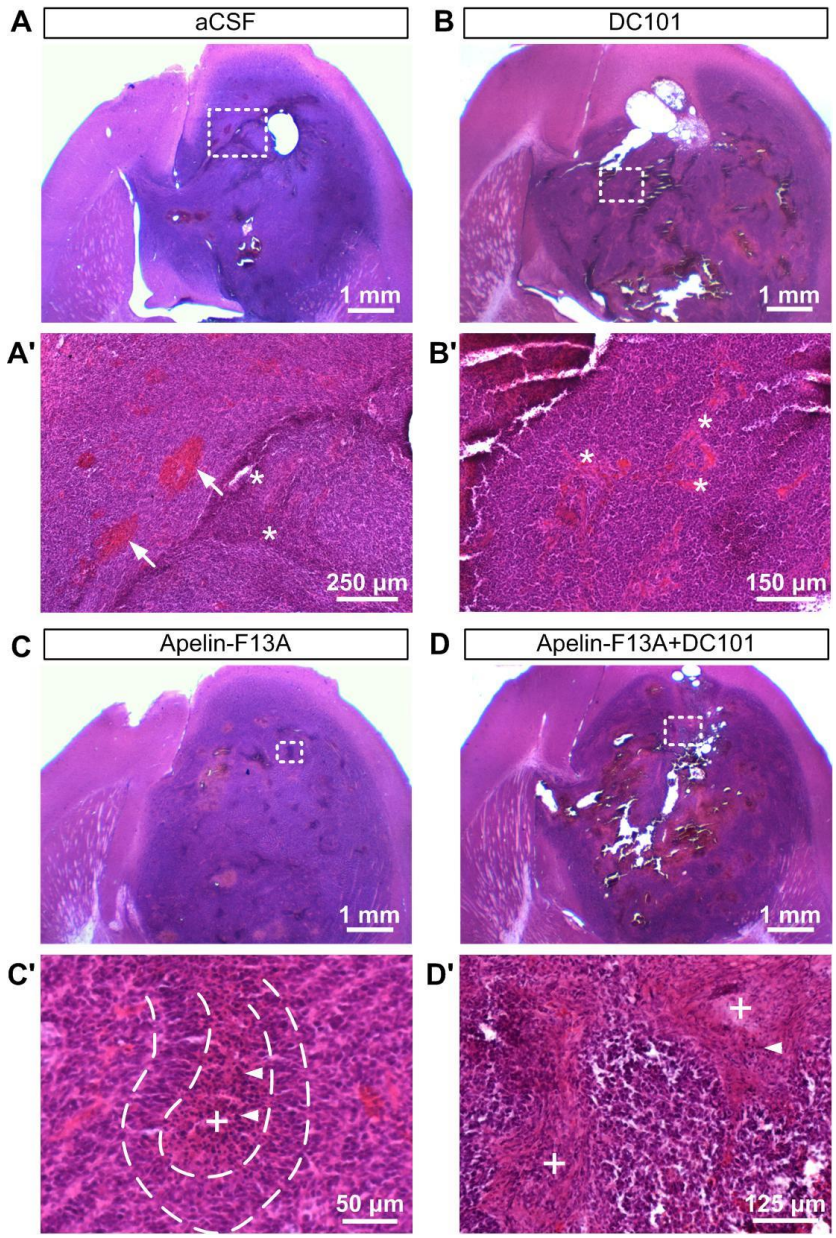

Figure 4.1.2a Tumor morphology at experimental end-point. (A-D) Hematoxylin and Eosin staining (H&E staining) shows examples of a big tumor on brain sections from four treatment groups. All tumors showed large area of dense cells with darkly stained nuclei, hyperangiogenesis with malformed blood vessels and bleeding area, and necrotic foci accompanied by pseudopalisades. No obvious difference of these morphological features was found among groups in H&E staining. (A') In the close-up image of aCSF control tumor, asterisks and arrows indicate the example of malformed blood vessels and bleeding respectively; (B') In the close-up image of DC101 treated tumor, asterisks indicate the example of blood vessels in the tumor. (C') Picture in higher magnification of apelin-F13A treated tumor shows the tumor necrotic foci (cross), dead cells with pyknotic nuclei (arrowhead), and pseudopalisading area (white lines). (D') Higher magnification images of apelin-F13A plus DC101 treated tumor show the tumor necrotic foci (cross), dead cells with pyknotic nuclei (arrowhead).

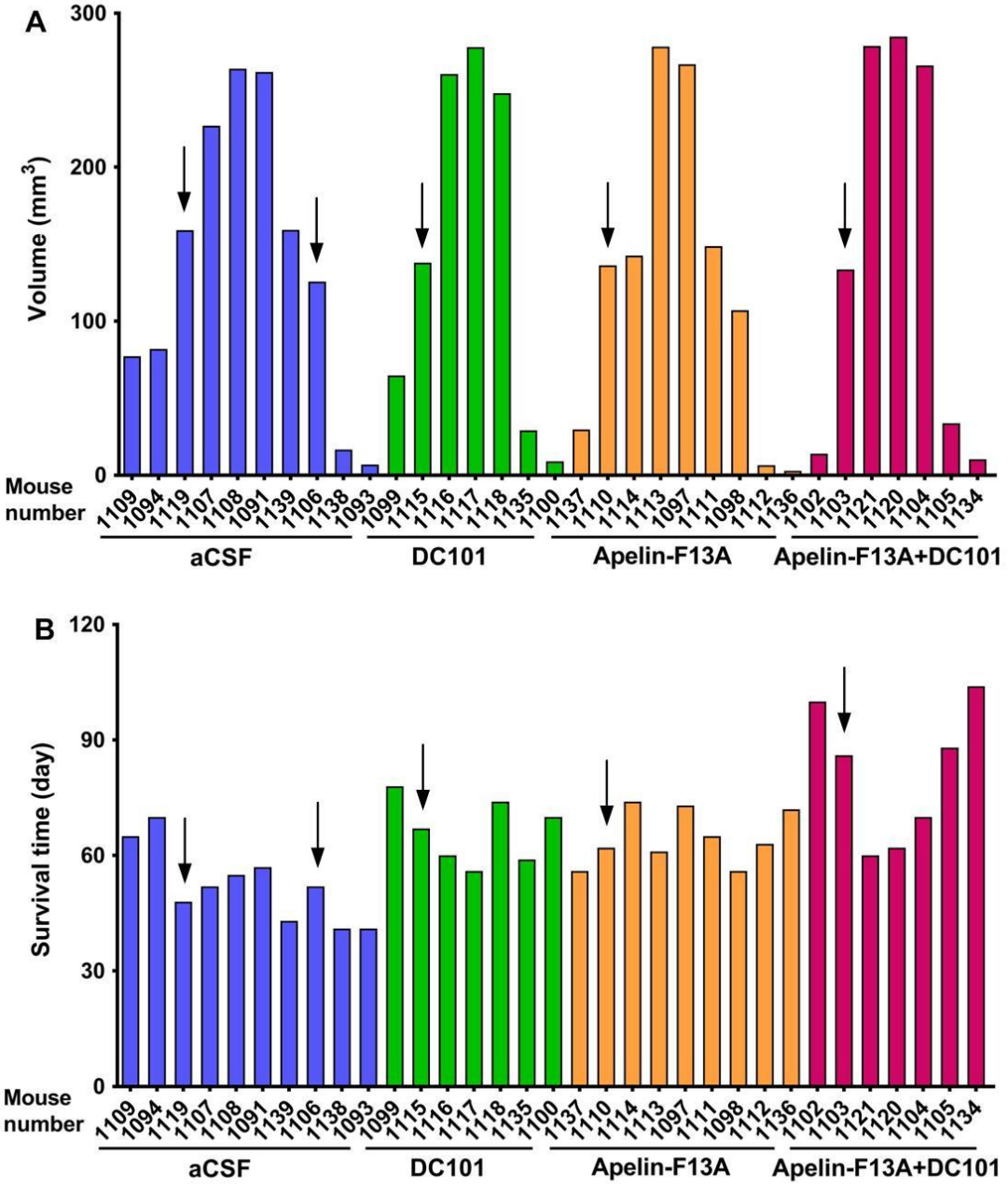

Figure 4.1.2b Tumor volume and survival time at experimental end-point. (A) Tumor volume of each mouse was estimated from the tumor area in H&E staining. The medians of the tumor volume (arrow) in four groups were: 142.5 mm^3 in aCSF, 138 mm^3 in DC101, 136.3 mm^3 in apelin-F13A and 133.5 mm^3 in apelin-F13A + DC101 group. No significant difference of tumor volume was found among groups assessed by Kruskal-Wallis test (p = 0.954). (B) Individual survival time for all samples. The survival time of mouse with a median tumor volume (arrow) was: 50 days in aCSF, 67 days in DC101, 62 days in apelin-F13A and 86 days in apelin-F13A + DC101 group.

4.1.3 Pseudopalisading area of the tumor

Pseudopalisades were observed in the H&E staining of murine *p*53^{KO}PDGFB GBM. To investigate whether there are differences in pseudopalisades in different treated groups, I quantified the pseudopalisades in tumors by measuring the percentage of pseudopalisading area over the total tumor area in H&E images (3 mice with comparable tumor size from each group). No significant difference of pseudopalisades was found in different treated tumors. The pseudopalisading area percentage was around 55% in all groups (Figure 4.1.3 A). I also investigated pseudopalisades of GBM specimens from patients before and after bevacizumab treatment. Likewise, no significant difference of pseudopalisades was detected in the GBM tissue before and after bevacizumab treatment (Figure 4.1.3 B).

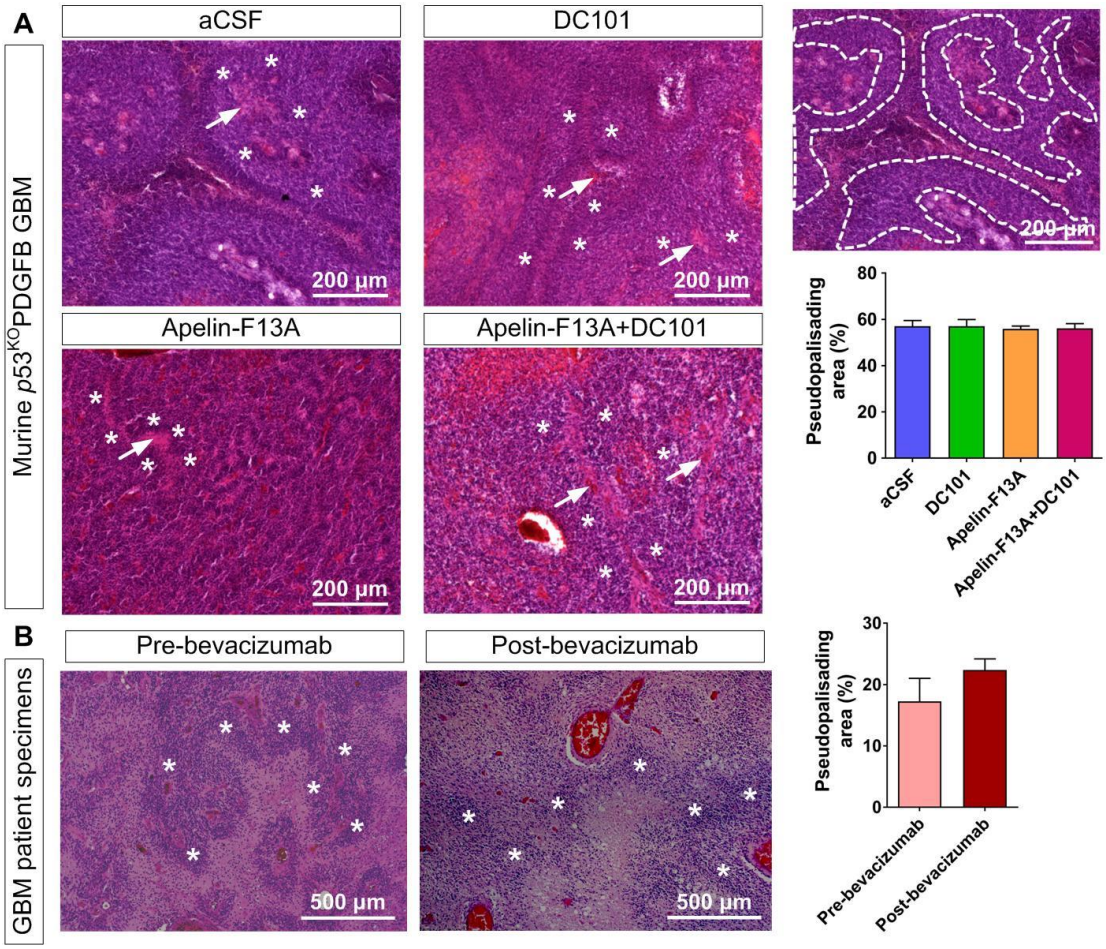

Figure 4.1.3 The extent of pseudopalisades is unchanged in murine *p*53^{KO}PDGFB GBM and human GBM specimens after different treatments. (A) Histopathological calculation of pseudopalisades in murine tumors at humane end-point. Asterisks indicate the pseudopalisading areas. Arrows indicate the necrotic foci surrounded by pseudopalisades. The image in the top right illustrates procedures for measuring the pseudopalisading area. Values are reported as the mean ± SEM (standard error of the mean). One-way ANOVA was used to determine statistical significance (p = 0.893). (B) H&E pictures and quantification of pseudopalisades in GBM specimens from patients pre- and post-bevacizumab treatment. Asterisks indicate the pseudopalisades. Values are reported as the mean ± SEM. Student's t-test was used to determine statistical significance (p = 0.226).

4.1.4 Apelin-F13A and DC101 inhibit tumor angiogenesis in murine glioblastoma

An Olympus-BX53-microscope with the connected StereoInvestigator Software (MicroBrightField Bioscience, Williston, VT, USA) was used to analyze the tumor angiogenesis in murine glioblastoma. Sections with comparable tumor size were stained for von Willebrand factor (vWF) to identify vessels. By using the function of space ball, three parameters were generated after the measurement and analysis: vessel length density (VLD, the total vessel length per mm^3 of tumor), vessel length (the total vessel length in the whole tumor), and vascular network complexity (a ratio to estimate the complexity of vessel branching) [120, 121]. After DC101 treatment, the VLD markedly decreased to 440 mm/mm^3 compared to 613 mm/mm^3 in controls (p = 0.035). Similarly, apelin-F13A treatment significantly decreased VLD to 357 mm/mm^3 (p = 0.004). Coadministration of DC101 and apelin-F13A further reduced VLD to 243 mm/mm^3 (p = 0.003), which was also much lower than that in DC101-treated tumors (p = 0.033; Figure 4.1.4 B). Similar results were found by assessing vascular network complexity (Figure 4.1.4 C). Total vessel length of the tumor also decreased remarkably in the apelin-F13A treated group and apelin-F13A + DC101 coadministration group as compared to controls (Figure 4.1.4 D). These data indicate that administration of DC101 or apelin-F13A alone can significantly suppress angiogenesis in glioma mouse models. Most importantly, combined administration of DC101 and apelin-F13A improved antiangiogenesis over all other experimental groups in this preclinical model.

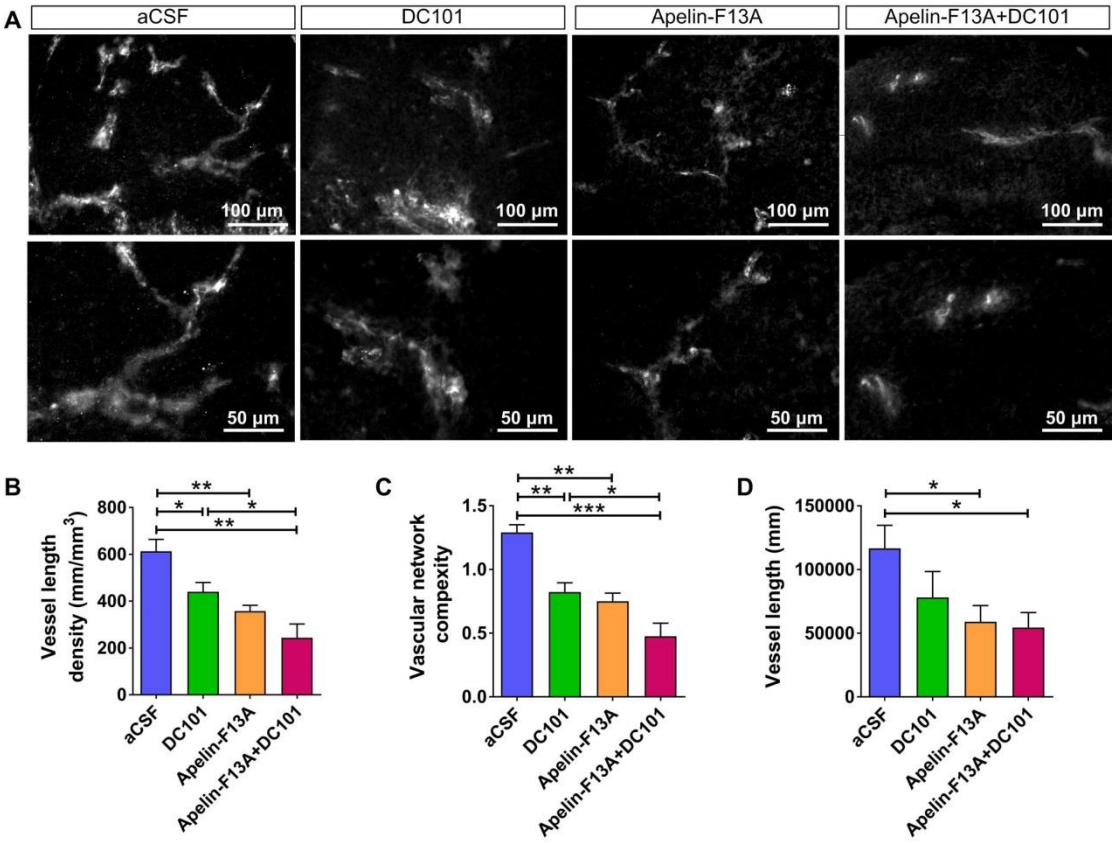

Figure 4.1.4 Tumor microvasculature at experimental end-point. (A) Immunofluorescence staining of von Willebrand factor (vWF) shows the vessels in the tumor of the four treatment groups. (B) Quantification of vessel length density (VLD) in the tumor area by stereomorphology (n = 4 per group). The VLD decreased significantly in DC101 (p = 0.035), apelin-F13A (p = 0.004) and apelin-F13A + DC101 group (p = 0.003) compared to aCSF controls. Also, the VLD in the apelin-F13A + DC101 group was significantly lower than that in DC101-treated tumors (p = 0.033). (C) The vascular network complexity was remarkably lower in DC101 (p = 0.003), apelin-F13A (p = 0.001) and apelin-F13A + DC101 group (p = 0.0005) than that in controls. The vascular network complexity in apelin-F13A + DC101 group was also significantly lower than that in DC101 group (p = 0.033). (D) The total vessel length decreased dramatically in the apelin-F13A group (p = 0.04) and apelin-F13A + DC101 group (p = 0.028) in comparison to aCSF controls. Values are reported as the mean ± SEM. Student's t-test was used to determine statistical significance, *p < 0.05, **p < 0.005, ***p < 0.0005.

4.1.5 VEGFR2-blockade increases but apelin-F13A decreases the invasiveness of glioblastoma cells

Next, GBM cell invasiveness was investigated in the *p*53^{KO}PDGFB GBM models. The *p*53^{KO}PDGFB GSCs (including the single invasive tumor cells) could be identified on histological brain sections by green fluorescent protein (GFP) expression and immunostaining for GFP, which facilitates the analysis of glioblastoma cell invasiveness. The tumor invasiveness was determined as the percentage of invasive tumor volume over the total tumor volume (invasive tumor volume plus compact tumor volume, Figure 4.1.5 C&D). Tumors with comparable size were analyzed. Invasiveness was inspected at 10× and 20× objectives and invasive area was measured on composite images of lower (5× objective) magnification. In the composite pictures, the blue line indicates the compact tumor border and the red line indicates the invasive tumor front (Figure 4.1.5 A). The invasive glioblastoma volume was 30% in control tumors. Administration of DC101 alone (as expected; [59]) had a pro-invasive effect. The invasive volume significantly increased to 55% in DC101 treated tumors. On the contrary, an anti-invasive effect was found in apelin-F13A treatment which reduced the invasive glioblastoma volume robustly to 8%. The percentage of invasive volume in mice co-treated with DC101 and apelin-F13A (18%) was between that in the DC101 treated group (55%) and apelin-F13A treated group (8%; Figure 4.1.5 B). The invasion trajectories from the dense tumor core were also quantified by measuring the distance of single tumor cells migrated away from the compact tumor mass. Similar results were found for the invasive distance (Figure

4.1.5 E). In the close-up photographs, the differences of invasiveness could be observed more clearly: massive invasion of single cells was visible in DC101 treated tumors; however, only a few individual cells invaded into the peritumoral brain tissue in apelin-F13A treated tumors (Figure 4.1.5 A). These results suggest that apelin/APLNR targeting has an anti-invasive effect on glioblastoma cells, decreasing the pathological side effects of established anti-angiogenic regimen such as anti-VEGFR2 therapy, offering one potential mechanism that explains improved survival after apelin-F13A coadministration in our preclinical study.

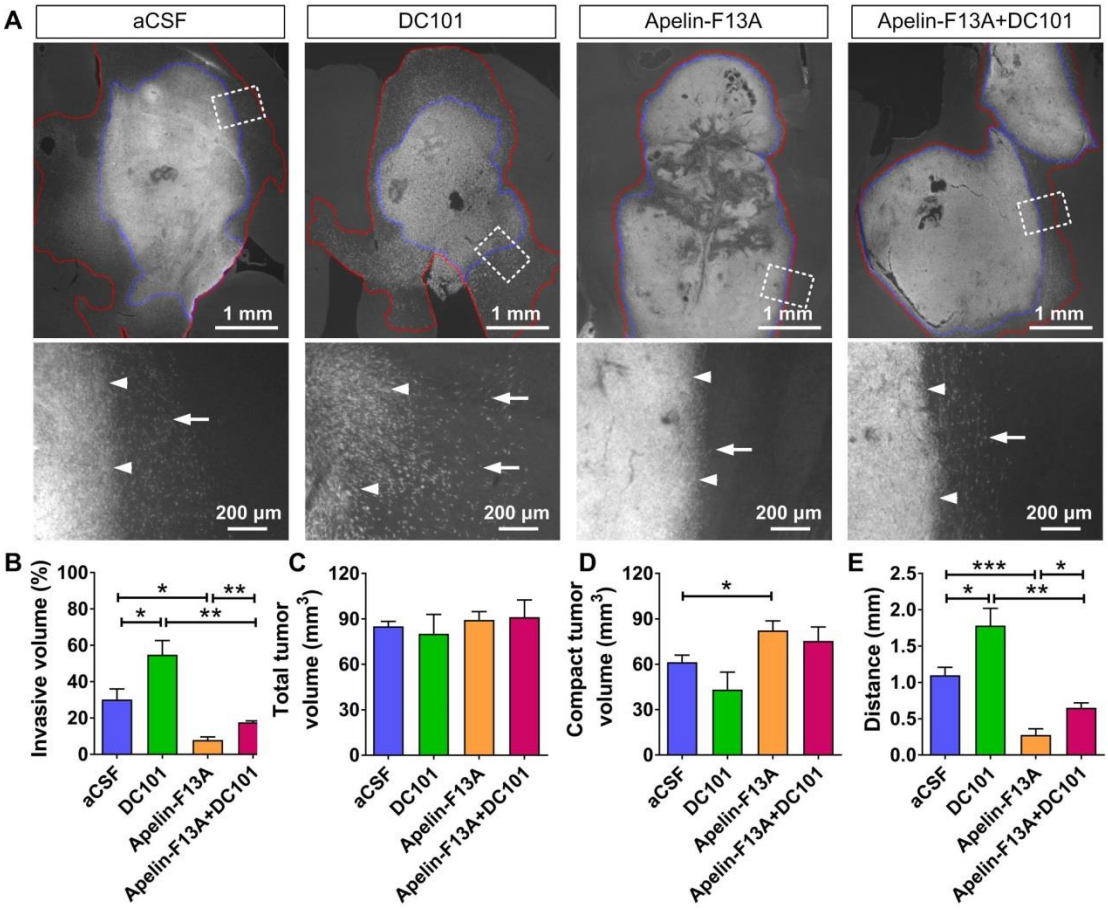

Figure 4.1.5 The invasiveness of glioblastoma cells at experimental end-point. (A) The upper panel gives an overview on tumors (composite images of 5× objective) with gliomas visualized by immunostaining for GFP. The blue line indicates the compact tumor border and the red line indicates the invasive tumor front. The lower panel shows higher magnification images of the compact tumor border (arrowhead) and invasive tumor cells (arrow). (B) Quantification of the percentage of the invasive tumor volume over the total tumor volume. The percentage of invasive tumor volume increased significantly in DC101 treated tumors (55%, n = 4, $p = 0.037$) but decreased remarkably in apelin-F13A treated tumors (8%, n = 4, $p = 0.014$) compared to aCSF controls (30%, n = 5). The percentage of invasive tumor volume in apelin-F13A + DC101 treated group (18%, n = 4) was between that in DC101 treated group and apelin-F13A treated group. (C) Quantification of the total tumor volume of the four treatment groups. No significant difference of the total tumor volume was found among groups. (D) Quantification of the compact tumor volume in the four experimental groups. There was a significant difference of the compact tumor volume between control and apelin-F13A treated group ($p = 0.029$). (E) The distance of invasion trajectories from the dense tumor core (3 sections per mouse and 4 mice per group). The invasive distance increased to 1.78 mm in DC101 group ($p = 0.04$) but decreased to 0.28 mm in apelin-F13A group ($p = 0.001$) compared to 1.10 mm in controls. The invasive distance in apelin-F13A + DC101 treated group was 0.65 mm. Values are reported as the mean ± SEM. Student's t-test was used to determine statistical significance, *$p < 0.05$, **$p < 0.005$, ***$p < 0.005$.

4.1.6 The APLNR ligand apelin-F13A reduces the number of iba1 positive cells in *p*53^{KO}PDGFB GBM

The immune state in the glioblastoma may be different after various treatments in the survival experiment and may also affect the tumor growth or glioblastoma cell migration and invasion. Microglia are the major innate immune cells in the CNS. Therefore, I quantified the tumor-associated myeloid cells in the tumor area marked by ionized calcium-binding adapter molecule 1 (iba1) staining [126, 127], and found that the number of iba1 positive cells in apelin-F13A treated group was less than that in other groups (Figure 4.1.6). In consideration of the pro-invasive and pro-angiogenic effect of glioblastoma-associated microglia/macrophage as reported by previous studies [123, 128-130], we hypothesize that there may be some interactions of apelin/APLNR signaling (glioblastoma cell) and tumor-associated microglia/macrophage in terms of glioblastoma cell invasiveness and angiogenesis, which warrants further investigation.

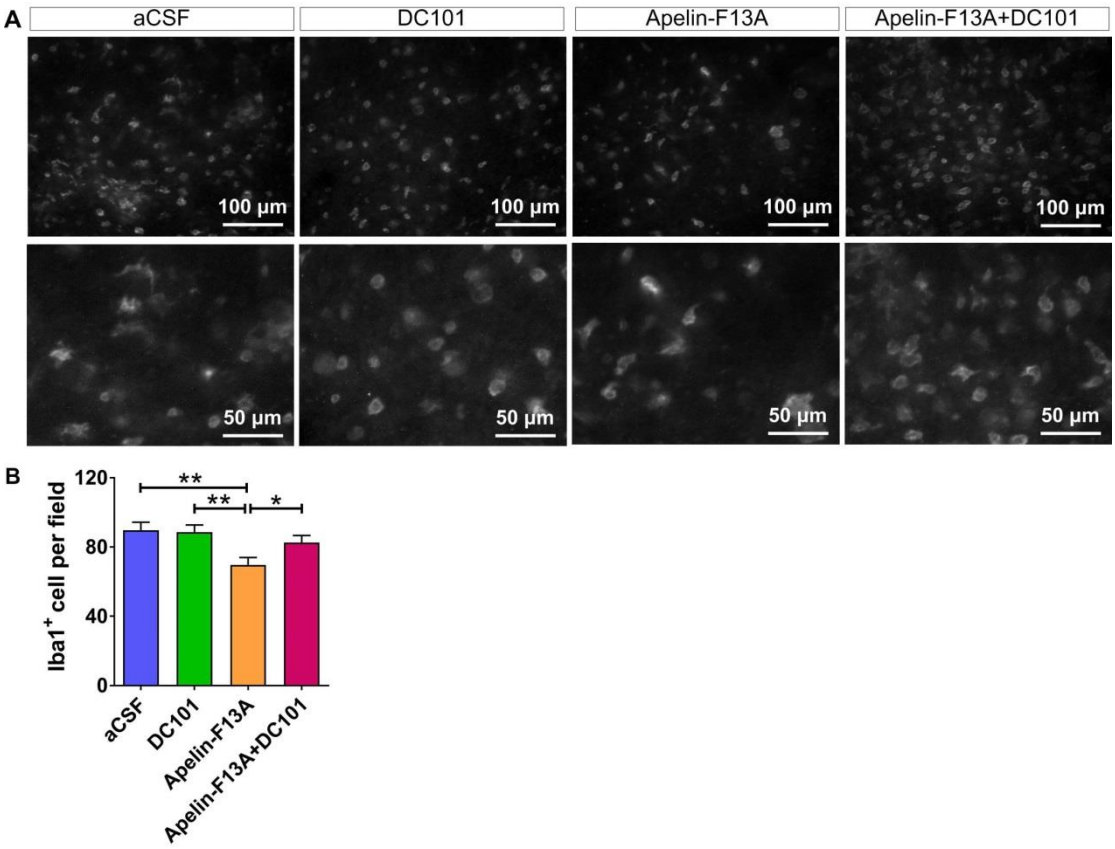

Figure 4.1.6 Iba1 positive cells in gliomas at experimental end-point. (A) Representative photographs of iba1 positive cells in the tumor area of four groups. (B) Quantification of iba1 staining in the tumor area. The number of iba1 positive cells in apelin-F13A group was significantly lower than aCSF ($p = 0.002$), DC101 ($p = 0.003$), and apelin-F13A + DC101 group ($p = 0.03$). Values are reported as the mean ± SEM (3 mice per group). Student's t-test was used to determine statistical significance, *$p < 0.05$, **$p < 0.005$.

4.2 The relationship of apelin/APLNR signaling and glioblastoma invasiveness

4.2.1 The APLNR ligand apelin-13 and apelin-F13A both inhibit tumor cell migration in a wound healing assay

To study the direct impact of apelin on APLNR expressing GBM cells, I performed a wound healing assay by using two cell lines (U87 and GBM14) of which the relatively high levels of apelin expression had been knocked down [122] ($U87^{AKD}$ and $GBM14^{AKD}$; with the non-silencing control cells as control, NSC). The tumor cell migration was assessed for 24 hours because the GBM14 cells (which grow as spheres) would detach from the culture-plate at later time-points. For U87 cells, the gap area would be completely closed by the migrating cells after 24 hours. Therefore, the cell covered area for U87 cells was measured 10 hours after the gap was formed. I found that the cell covered area increased faster in apelin knockdown cells compared to that in the non-silencing control cells for both cell lines, indicating that the invasiveness of glioblastoma cells increased significantly after endogenous apelin knockdown. Moreover, the increased migration in apelin knockdown cells could be diminished by exogenous addition of apelin-13 or apelin-F13A (Figure 4.2.1), which supports my finding that the invasiveness of glioblastoma cells *in vivo* could be inhibited by the stimulation of APLNR on glioblastoma cells with apelin-F13A.

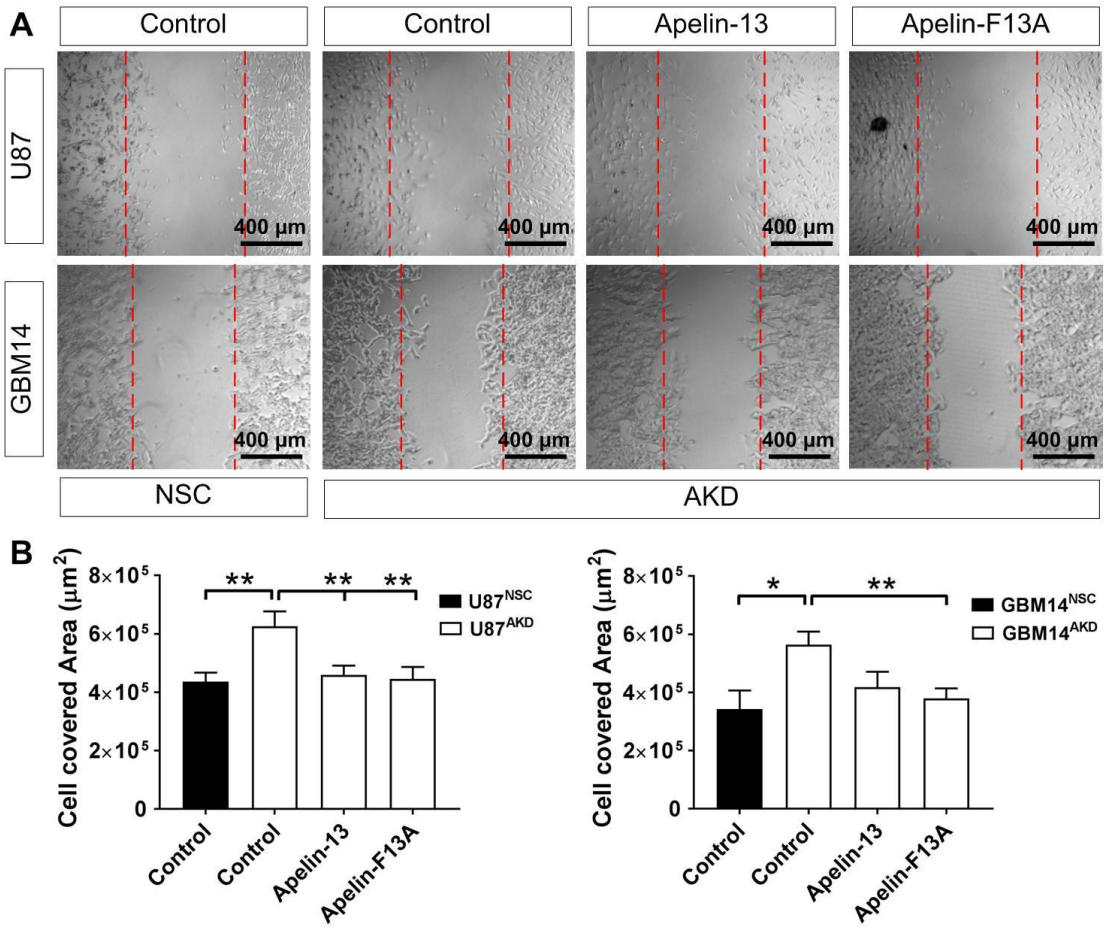

Figure 4.2.1 Glioblastoma cell migration in a wound healing assay. (A) Representative pictures for U87 cells and GBM14 cells are shown. The quantification of cell migration was performed by measuring the cell-covered area 10 hours (U87) or 24 hours (GBM14) after the gap was induced. The red lines indicate the edge of tumor cells at the starting time point. (B) Quantification of glioblastoma cell migration. Compared to apelin knockdown U87 ($U87^{AKD}$) control group, the cell covered area increased more slowly in $U87^{NSC}$ control group (NSC: non-silencing control; p = 0.003), $U87^{AKD}$ apelin-13 group (p = 0.009), and $U87^{AKD}$ apelin-F13A group (p = 0.009). Compared to $GBM14^{AKD}$ control group, the slower cell migration reached significance in $GBM14^{NSC}$ control group (p = 0.01) and $GBM14^{AKD}$ apelin-F13A group (p = 0.005), and reached marginal significance in $GBM14^{AKD}$ apelin-13 group (p = 0.05). Values obtained from three independent experiments are reported as the mean ± SEM. Student's t-test was used to determine statistical significance, *$p < 0.05$, **$p < 0.005$.

4.2.2 The invasiveness of glioblastoma cells in brain slices increases after apelin knockdown

In another approach to investigate apelin-modulated glioblastoma cell-invasion, I inoculated human primary glioblastoma cells (NCH644 and GBM5av) into murine orthotopic brain slice culture (Figure 4.2.2 A, F). The invasiveness of glioblastoma cells within organotypic brain slice cultures was measured by determining the number of single invasive cells migrating a certain distance away from the injection site (Figure 4.2.2 B). The quantified data were presented as the cell percentage distribution of the migration distances. The migration distance at day 7 for GBM5av showed that a significantly higher percentage of apelin depleted GBM5av^{AKD} cells reached farther migration distance compared to control GBM5av^{NSC} cells with migration radii > 900 μm (Figure 4.2.2 E). Significant difference were also observed when comparing the NCH644^{AKD} cells and NCH644^{NSC} cells (Figure 4.2.2 G), which demonstrates again that glioblastoma cells without the endogenous apelin stimulation become more invasive.

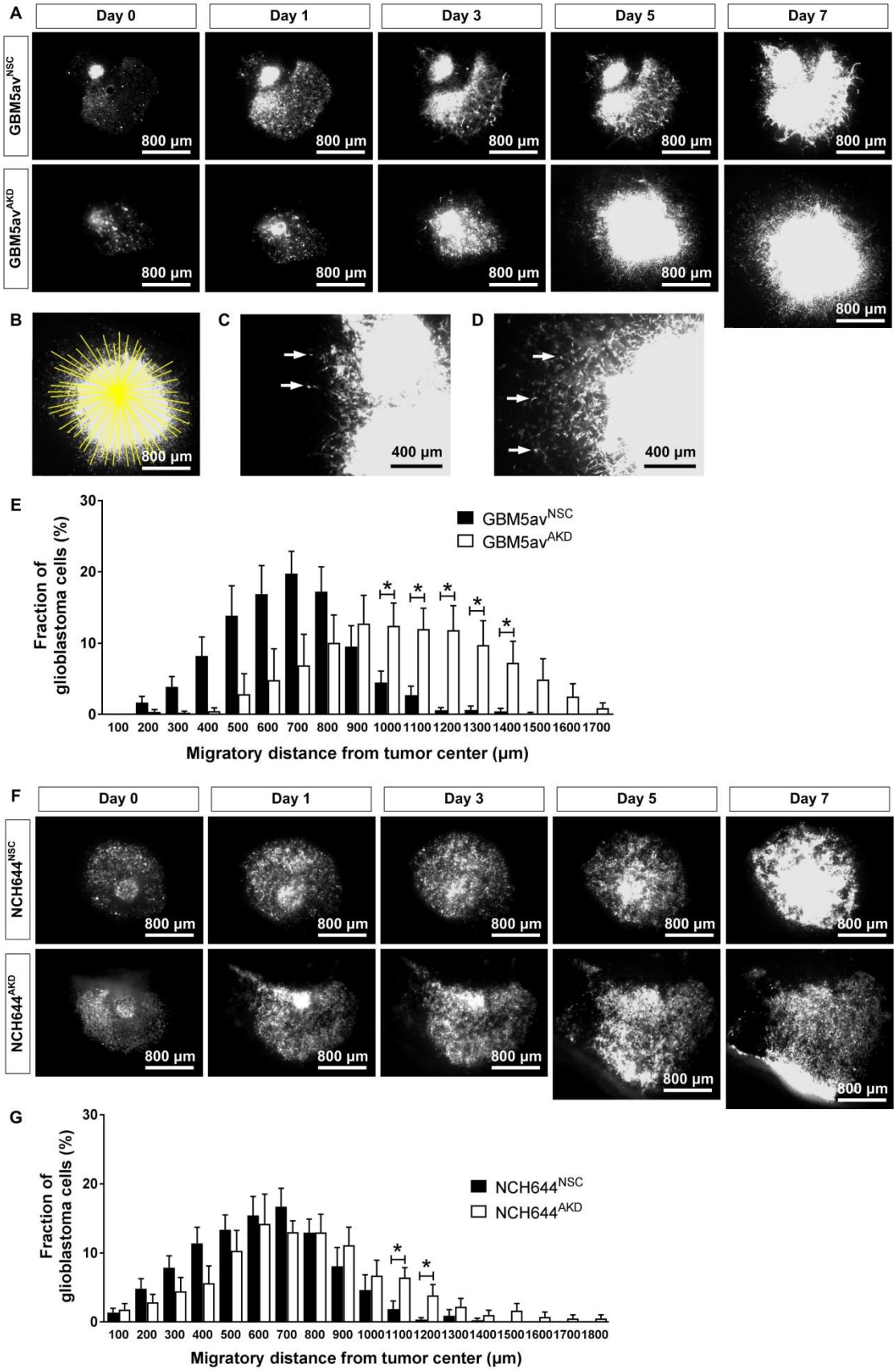

Figure 4.2.2 The invasiveness of glioblastoma cells in the brain slice increases after apelin knockdown. (A) Representative microscopy image for GBM5av^{NSC} and

GBM5av^{AKD} tumor cells in the brain slice on day 0, day 1, day 3, day 5 and day 7. (B) An example shows the method of measuring the migrating distance of single invasive cells from the injection site. (C, D) The close-up images show the single invasive GBM5av^{NSC} (C) and GBM5av^{AKD} cells (D) in the brain slice. Arrows indicate the invasive cells. (E) Cell percentage distribution histogram of the migrating distances for GBM5av^{NSC} and GBM5av^{AKD} tumor cells in brain slices. There was a significant difference between two groups in the distance of 1000-1400 μm. (F) Representative microscopy image for NCH644^{NSC} and NCH644^{AKD} tumor cells in the brain slice on day 0, day 1, day 3, day 5 and day 7. (G). Cell percentage distribution histogram of the migrating distances for NCH644^{NSC} and NCH644^{AKD} tumor cells in brain slices. There was a significant difference between two groups in the distance of 1100 μm and 1200 μm. 5-7 brain slices per group were used for the quantification. Values are reported as the mean ± SEM. Student's t-test was used to determine statistical significance, $*p < 0.05$.

4.2.3 The increased cell invasiveness in apelin knockdown GBM cells is lost upon microglia depletion

Microglia can be efficiently eliminated in brain slice cultures by administration of clodronate-liposomes (using PBS-liposomes as control) [123]. With this method, we could further explore the relationship of apelin/APLNR signaling and microglia in tumor invasiveness. Apelin knockdown cells and non-silencing control cells of GBM5av or NCH644 were inoculated in the microglia-depleted brain slice respectively and the invasion of glioblastoma was determined as mentioned above. Interestingly, no difference of invasiveness was found between apelin knockdown cells and non-silencing control cells after microglia were depleted in the brain slice (Figure 4.2.3 B, F). These findings suggest that microglia in the brain slice is required for the increase of invasiveness in the apelin knockdown cells (here GBM5av^{AKD} and NCH644^{AKD}). By comparing the invasiveness of apelin knockdown GBM cells in

microglia-intact and microglia-depleted brain slices, we found that these cells were more invasive in microglia-intact brain slices (Figure 4.2.3 C, G). Therefore, the pro-invasive effect of tumor-associated myeloid cells (also reported by previous studies [123, 128]) was not influenced by apelin knockdown in GBM cells.

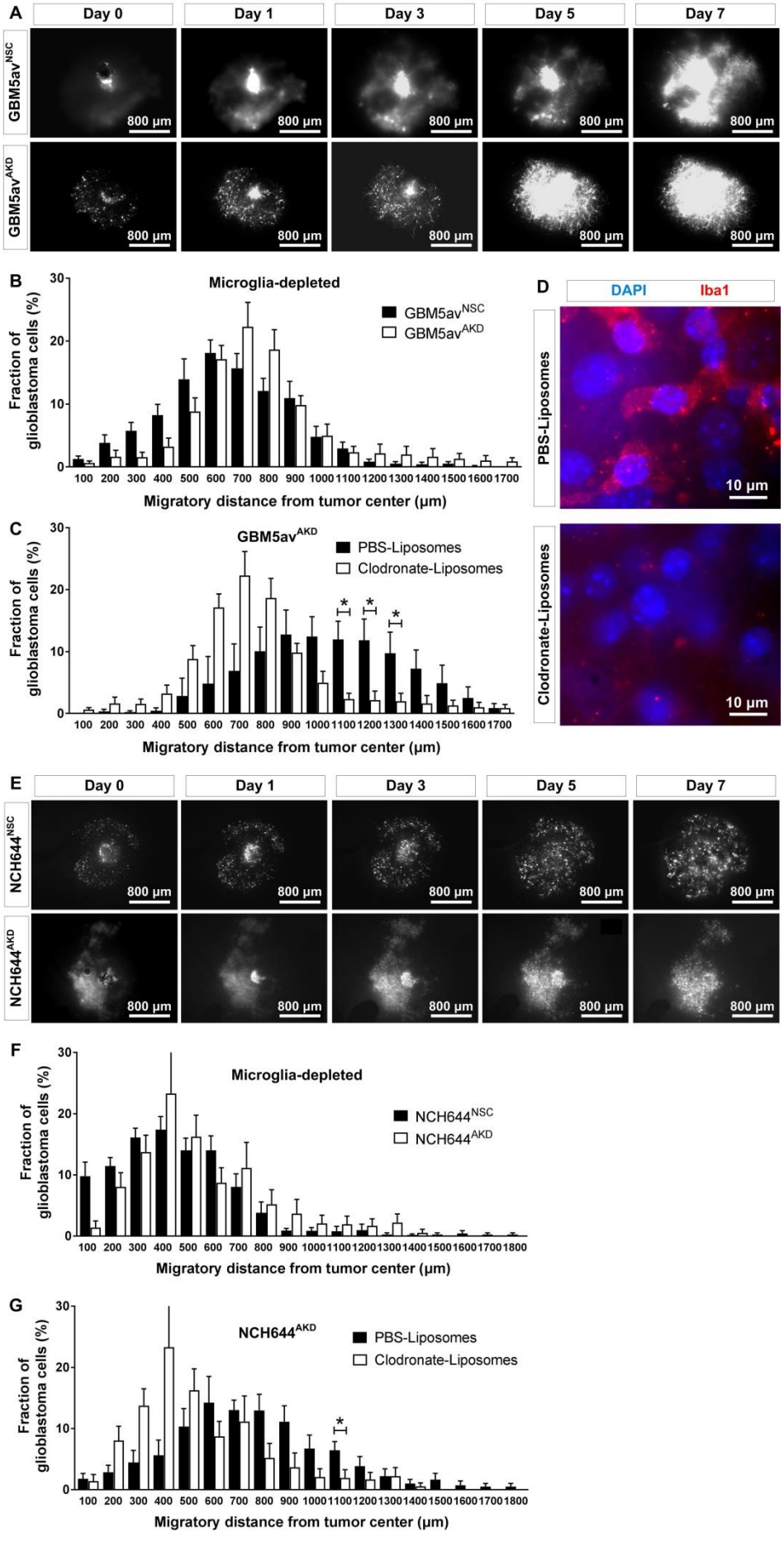
A
Day 0
Day 1
Day 3
Day 5
Day 7
GBM5av^NSC
GBM5av^AKD
800 µm
B
Microglia-depleted
GBM5av^NSC
GBM5av^AKD
Fraction of glioblastoma cells (%)
Migratory distance from tumor center (µm)
C
GBM5av^AKD
PBS-Liposomes
Clodronate-Liposomes
D
DAPI
Iba1
PBS-Liposomes
Clodronate-Liposomes
10 µm
E
NCH644^NSC
NCH644^AKD
F
Microglia-depleted
NCH644^NSC
NCH644^AKD
G
NCH644^AKD
PBS-Liposomes
Clodronate-Liposomes

Figure 4.2.3 Increased cell invasiveness in apelin knockdown GBM cells is lost upon microglia depletion. (A) Representative microscopy image for GBM5av^{NSC} and GBM5av^{AKD} tumor cells in microglia-depleted brain slice on day 0, day 1, day 3, day 5 and day 7. (B) Cell percentage distribution histogram of the migrating distances for GBM5av^{NSC} and GBM5av^{AKD} tumor cells in microglia-depleted brain slices. No significant difference was found between two groups. (C) Cell percentage distribution histogram of the migrating distances for GBM5av^{AKD} cells in microglia-intact and microglia-depleted brain slices. There was a significant difference between two groups in the distance of 1100-1300 μm. (D) Iba1 staining for brain slices verified the efficiency of microglia depletion after clodronate-liposomes treatment. (E) Representative microscopy image for NCH644^{NSC} and NCH644^{AKD} tumor cells in microglia-depleted brain slice on day 0, day 1, day 3, day 5 and day 7. (F) Cell percentage distribution histogram of the migrating distances for NCH644^{NSC} and NCH644^{AKD} tumor cells in microglia-depleted brain slices. No significant difference was found between two groups. (G) Cell percentage distribution histogram of the migrating distances for NCH644^{AKD} cells in microglia-intact and microglia-depleted brain slices. There was a significant difference between two groups in the distance of 1100 μm. 6-8 brain slices per group were used for the quantification. Values are reported as the mean ± SEM. Student's t-test was used to determine statistical significance.

4.2.4 The proliferation in apelin knockdown GBM14 cells is unchanged compared to non-silencing control GBM14 cells

To exclude the possibility that the increase of invasion in apelin knockdown cells was a result of enhanced *in vitro* proliferation after endogenous apelin depletion, I checked the cell proliferation of GBM14^{NSC} and GBM14^{AKD} cells. Thus, 100,000 cells of GBM14^{NSC} or GBM14^{AKD} were plated on day 0 and the cell numbers were counted on day 7 and day 14. The cell numbers did not show a difference between GBM14^{NSC} and GBM14^{AKD} (Figure 4.2.4 A). In addition, to assess the proliferative state of GBM14^{NSC} and GBM14^{AKD} cells, the Ki67 status [131] was examined by immunofluorescence staining in 40× objective for both cell lines *in vitro* as well as *in*

vivo in the tumor area (the mouse brain tumor tissue was obtained from my colleague Mengzhuo Hou's previous experiments). Similarly, no significant difference was detected (Figure 4.2.4 B, C).

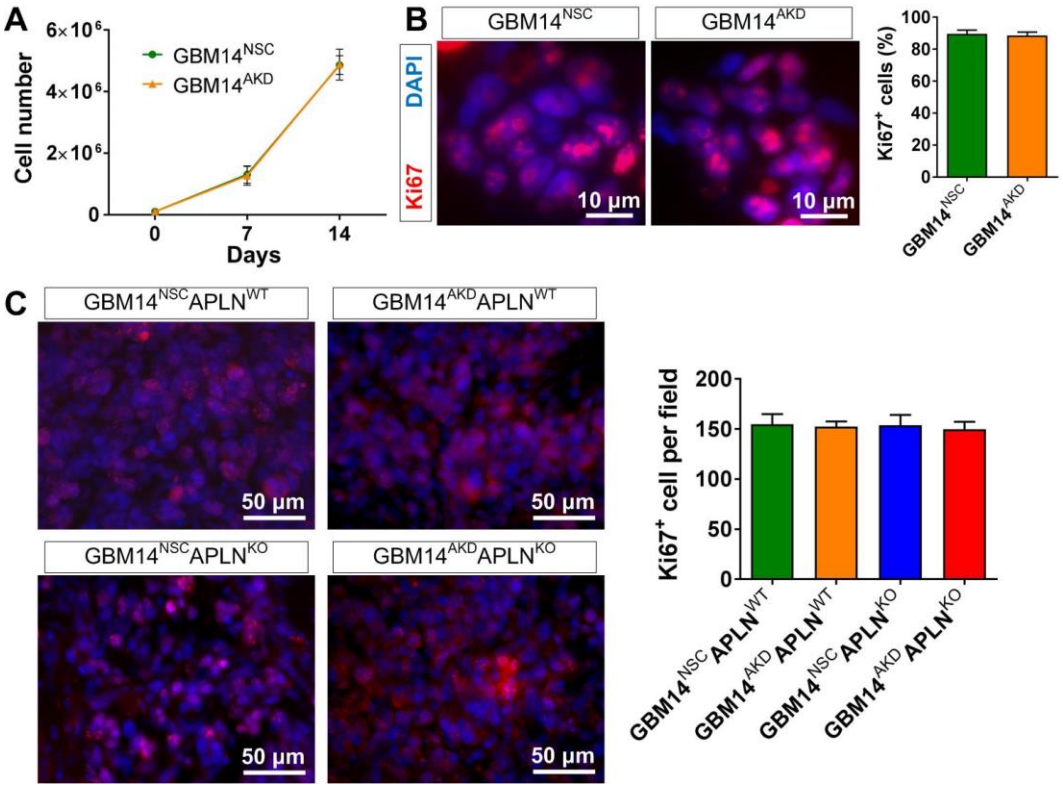

Figure 4.2.4 Cell proliferation of GBM14^{NSC} and GBM14^{AKD} *in vitro* and *in vivo*. (A) Proliferation examined by cell counting for GBM14^{NSC} and GBM14^{AKD} cells *in vitro*. 100,000 cells of GBM14^{NSC} or GBM14^{AKD} were plated on day 0 and the cell numbers were counted on day 7 and day 14 by Countess II FL with 0.4% Trypan Blue Solution identifying the alive and dead cells at a dilution of 1:2. 100,000 cells were replated after the cell counting on day 7. Three independent experiments were performed in triplicate. Values are reported as the mean ± SEM. Student's t-test was used to determine statistical significance. No significant difference was found between two groups. (B) Representative photographs and quantification of Ki67 staining for GBM14^{NSC} and GBM14^{AKD} cells *in vitro*. Nine pictures were used to quantify the percentage of Ki67 positive cells. Values are reported as the mean ± SEM. Student's t-test was used to determine statistical significance. No significant difference was found between two groups. (C) Representative pictures and quantification of Ki67 staining for GBM14^{NSC} or GBM14^{AKD} tumor in *APLN* gene wild-type (*APLN*^{WT}) or *APLN* gene knockout (*APLN*^{KO}) mouse brain (tissue from my colleague's previous experiments, the number of Ki67 positive cells per field in the tumor area was quantified for 3 mice per group). Values are reported as the mean ± SEM. One-way ANOVA was used to determine statistical significance. No significant difference was found among groups.

4.2.5 Apelin peptides activate GPCR internalization on APLNR expressing GBM cells

G-protein coupled receptors (GPCRs) get internalized upon ligand binding for signal desensitization [132]. To follow apelin-binding, apelin peptides were linked to a GFP-tag in the N-terminus (obtained from Sören Reinhard and Prof. Ernst Wagner, Department of Pharmacy, LMU Munich, Germany). I administered GFP-linked apelin peptides to GBM14 cells and found that both apelin-13 and apelin-F13A were internalized by GBM14 cells, while a scrambled apelin-13scr peptide (containing the scrambled amino acid sequence of Apelin-13) was not (Figure 4.2.5 A), which suggests that both apelin-13 and apelin-F13A can bind to APLNR and cause the internalization of the APLNR. Additionally, the specificity of peptide uptake was confirmed by a dose escalated competition assay with unlabeled peptide. The internalization of GFP-labeled apelin-13 and apelin-F13A was competitively blocked by unlabeled apelin-13 and apelin-F13A respectively, and the level of inhibition increased as the concentration of unlabeled peptides went higher (Figure 4.2.5 B).

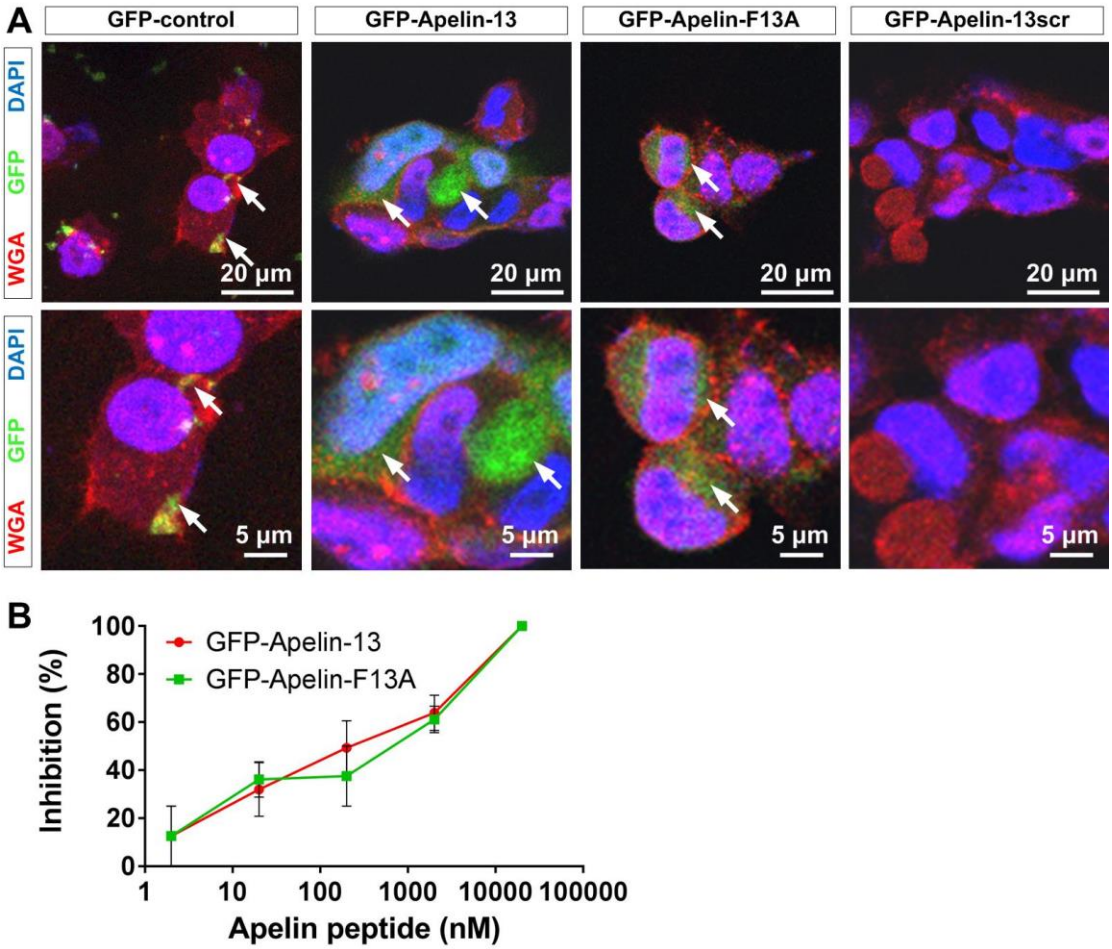

Figure 4.2.5 Specific internalization of GFP-labeled apelin-13 and GFP-labeled apelin-F13A by GBM14 cells. (A) Confocal microscopy images show the internalization of GFP-linked cationic lipo-oligomer 728 (unspecific positive control), GFP-Apelin-13 and GFP-Apelin-F13A, but no internalization of GFP-Apelin-13scr. The cell membrane and nuclei were stained by wheat germ agglutinin (WGA-Alexa Fluor 594) in red and DAPI in blue respectively. The arrows indicate the internalized GFP-labeled peptides. (B) Competitive inhibition of GFP-labeled apelin-13 or apelin-F13A (2 µM) uptake by unlabeled apelin-13 or apelin-F13A (2 nM, 20 nM, 200 nM, 2 µM, or 20 µM). The quantification was performed by measuring the number of cells containing GFP-conjugated peptides on the total number of cells in the picture. Six pictures were quantified for each condition. Values are reported as the mean ± SEM.

4.3 Microglia-associated peptide Humanin protects glioblastoma cells from stress

4.3.1 Humanin expression in human GBM specimens

In this second part of my thesis, I investigated another peptide humanin (HN) that our research group identified to be overexpressed in microglia from GBM patients. To study the local expression of HN in GBM, I examined paraffin-embedded human GBM sections by immunohistochemistry and immunofluorescence staining. Figure 4.3.1 A shows the single staining of the HN (brown) or iba1 (blue) in GBM tissue. Figure 4.3.1 B shows the double staining of the HN (brown) and iba1 (blue) in GBM tissue and tumor-free epilepsy tissue. The brown arrow indicates HN positive cells, the blue arrow indicates iba1 positive microglia/macrophage, and the red arrow points to the double stained cell in the picture of immunohistochemistry (Figure 4.3.1 B). Quantification showed that both HN positive cells and iba1 positive cells in the GBM tissue (n = 11 patients) were significantly more than those in tumor-free tissue (n = 5 patients). Moreover, about half the HN positive cells were also iba1 positive (Figure 4.3.1 C). In the immunofluorescence staining, the red cells are HN positive cells and the green cells are iba1 positive cells. GBM tissue showed more co-localization of iba1 and HN than tumor-free tissue (Figure 4.3.1 D). These results of staining indicate that HN is highly expressed in GBM compared to tumor-free tissue and that microglia could be the major source of HN in the microenvironment of GBM.

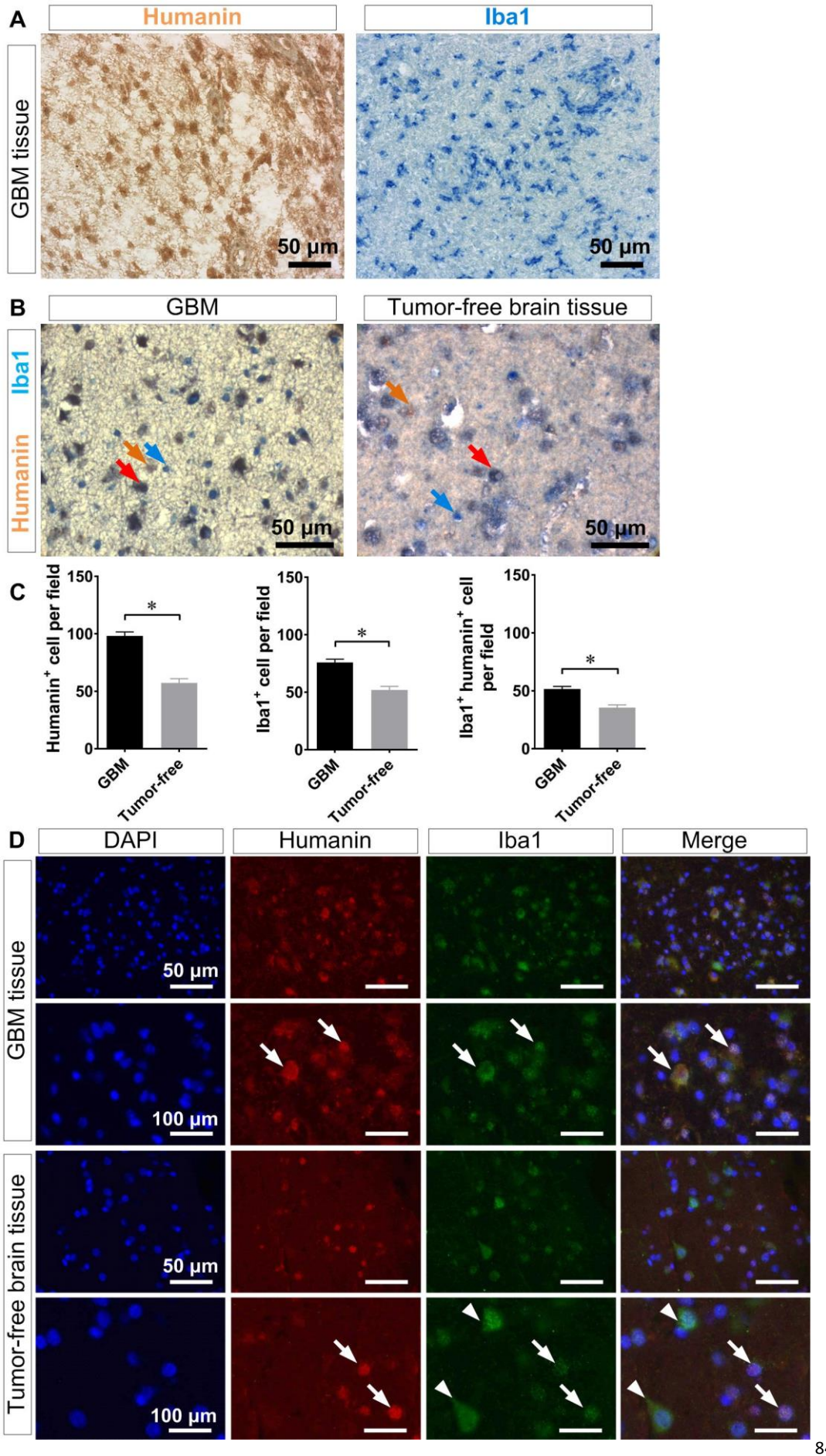
A
Humanin
Iba1
GBM tissue
50 μm
50 μm
B
GBM
Tumor-free brain tissue
Humanin
Iba1
50 μm
50 μm
C
Humanin+ cell per field
Iba1+ cell per field
Iba1+ humanin+ cell per field
150
100
50
0
*
GBM
Tumor-free
D
DAPI
Humanin
Iba1
Merge
GBM tissue
Tumor-free brain tissue
50 μm
100 μm
50 μm
100 μm

Figure 4.3.1 Humanin expression in human GBM specimens. (A) Immunohistochemistry for humanin (brown) or iba1 (blue) single staining in GBM tissue. (B) Immunohistochemistry for humanin and iba1 double staining in GBM tissue and tumor-free epilepsy tissue. The brown, blue, and red arrows indicate humanin positive cells, iba1 positive myeloid cells, and the double stained cells respectively. (C) The number of humanin positive, iba1 positive and double positive cells in GBM tissue (n = 11 patients) was significantly higher than in tumor-free tissue (n = 5 patients). Values are reported as the mean ± SEM. Student's t-test was used to determine statistical significance, $*p < 0.05$. (D) Co-immunofluorescence staining of humanin and iba1 for GBM tissue and tumor-free tissue. Most of the iba1-positive cells in GBM tissue were also humanin positive (arrows). In the tumor-free tissue, some iba1-positive but humanin-negative cells (arrowheads) were also found besides the double positive cells (arrows).

4.3.2 The cytoprotective effect of HNG for glioblastoma cells under growth factor-deprived conditions *in vitro*

The immunostaining showed high expression of HN in GBM; hence we asked if HN plays an important role in GBM. To test whether HN has a cytoprotective effect on tumor cells, I looked at two primary GBM cell cultures (GBM2 and GBM11) under stress condition. Towards this aim, cells were cultured in medium deprived for human epidermal growth factor (hEGF) and human fibroblast growth factor (hFGF; stress conditioned medium) and treated with a potent HN analogue (S14G HN or HNG, replacing serine at position 14 with glycine) [106, 133]. I found a dose dependent protective effect of HNG on GBM cells in EGF and FGF deprived medium (Figure 4.3.2 A, E). On day 7, the cell number in 2 μM HNG group was similar to that in growth factor-deprived control. However, in the groups treated with higher HNG concentrations (10 μM and 20 μM), cell numbers were significantly higher than that in growth factor-deprived control (Figure 4.3.2 B, F). In the first week, cells were

treated with HNG every day from day 0 to day 4. In the second and third week, cells were only treated with HNG on day 7 and day 14. I found that the protective effect of HNG decreased in the second week and disappeared on day 21 (Figure 4.3.2 D, H), implying that the rescued GBM cell growth under stress was largely depended on the continuous HNG support.

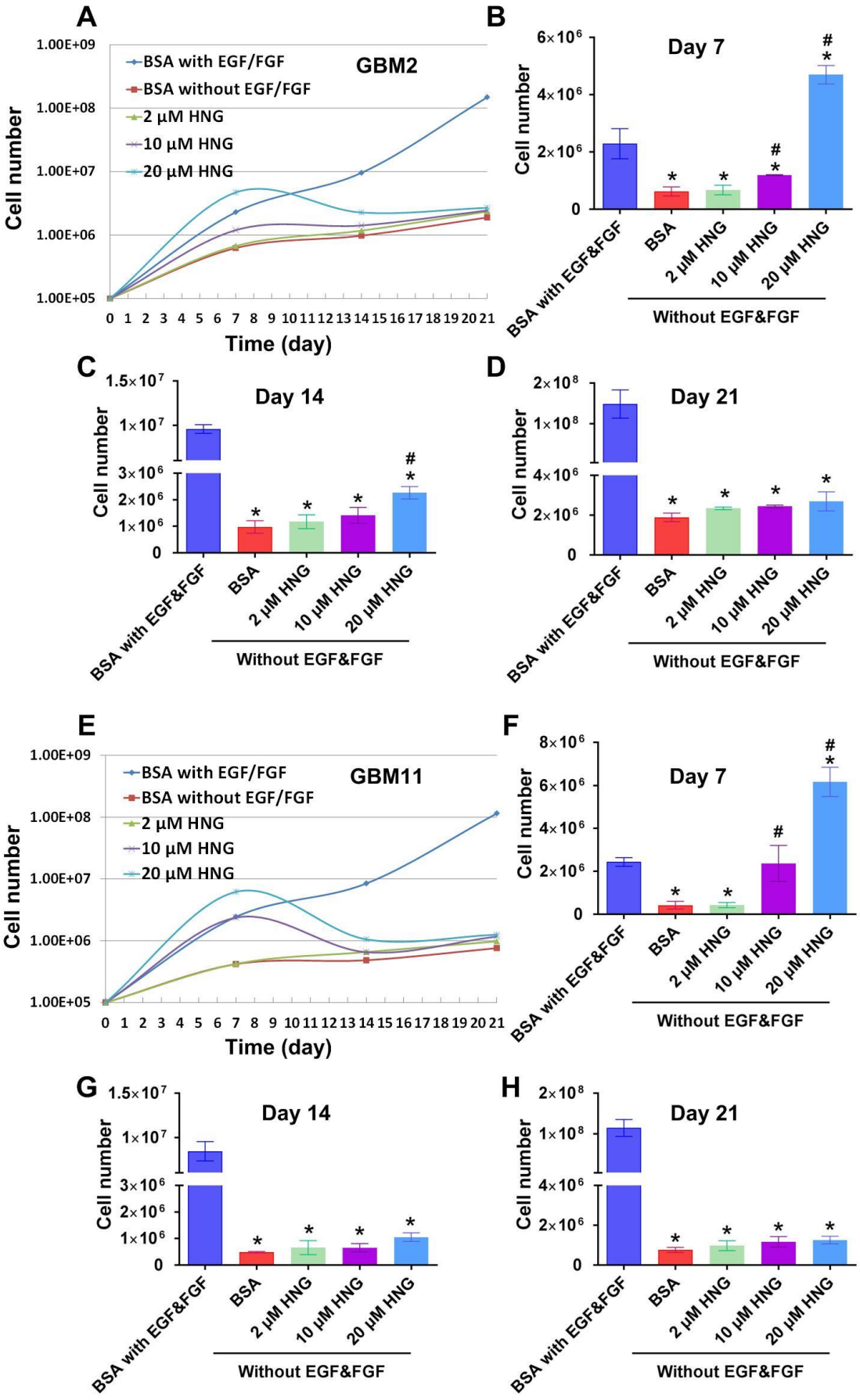
A
GBM2
BSA with EGF/FGF
BSA without EGF/FGF
2 μM HNG
10 μM HNG
20 μM HNG
Cell number
Time (day)
B
Day 7
C
Day 14
D
Day 21
BSA with EGF&FGF
BSA
2 μM HNG
10 μM HNG
20 μM HNG
Without EGF&FGF
E
GBM11
F
G
H

Figure 4.3.2 The cytoprotective effect of HNG for glioblastoma cells in growth factor-deprived condition. (A) Cell proliferation curves of GBM2 in different conditions. (B-D) Quantification of the cell counting for GBM2 in different conditions on day 7 (B), day 14 (C) and day 21 (D). (E) Cell proliferation curves of GBM11 in different conditions. (F-H) Quantification of the cell counting for GBM11 in different conditions on day 7 (F), day 14 (G) and day 21 (H). For the two cell lines, a dose dependent protective effect of HNG (a potent humanin analogue, replacing serine at position 14 with glycine) was found. On day 7, the cell number in 10 μM and 20 μM HNG group was significantly higher than in growth factor-deprived control group. Values are reported as the mean ± SEM. One-way ANOVA followed by Tukey's multiple comparisons test was used to determine statistical significance, $*p < 0.05$ compared to BSA with EGF&FGF, $^{\#}p < 0.05$ compared to BSA without EGF&FGF.

4.3.3 HNG protects glioblastoma cells from a chemotherapeutic agent temozolomide

To further investigate the cytoprotective effect of HNG for GBM cells, we created another clinically relevant stress condition for tumor cells by adding temozolomide (TMZ, an alkylating agent inducing the death of tumor cells by breaking the DNA double-strand) to the culture medium besides the stress of growth factors deprivation. 20 μM HNG was applied every other day in this experiment and the concentration of TMZ were applied at 0 μM, 100 μM and 300 μM. For both primary GBM cultures (GBM2 and GBM11) tested, the cell number of HNG treated cells in growth factor-deprived medium was similar to that of complete medium at every corresponding concentration of TMZ, but significantly higher than that of growth factor-deprived control at every corresponding concentration of TMZ (Figure 4.3.3). This indicates that HNG has a protective effect on GBM cells even under two types of stress (TMZ and growth factor deprivation). More specifically, in growth

factor-deprived culture condition, the cell number of HNG and 100 μM TMZ treated group was markedly higher than that of BSA treated control group on day 14 for both cell lines. The effect disappeared when the concentration of TMZ increased to 300 μM (Figure 4.3.3 B, D). These results demonstrate that HNG can protect glioblastoma cells from TMZ treatment *in vitro* (at least in 100 μM condition).

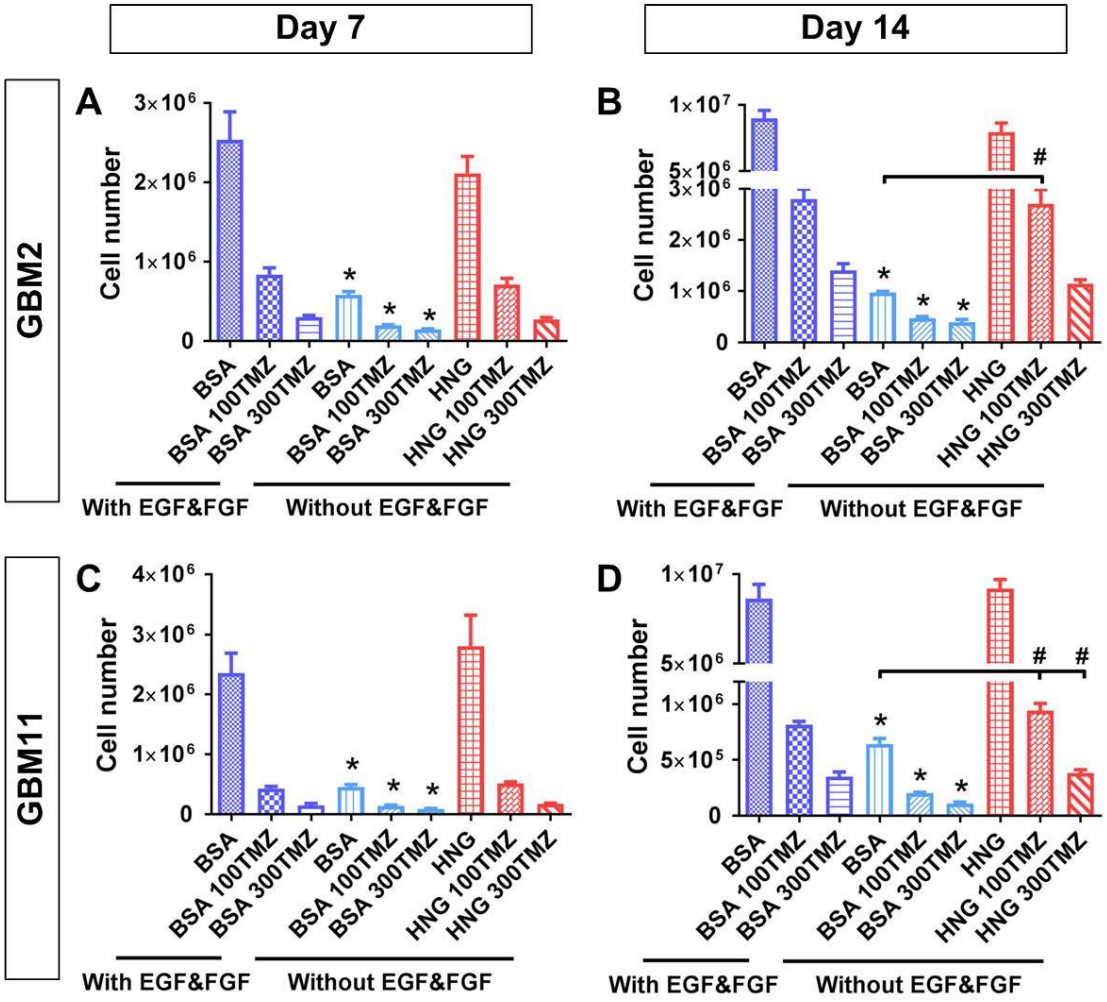

Figure 4.3.3 The cytoprotective effect of HNG for glioblastoma cells under treatment with temozolomide. (A, B) Quantification of GBM2 cells counted on day 7 and day 14 in different conditions. (C, D) Quantification of GBM11 cells counted on day 7 and day 14 in different conditions. For both cell lines, the cell number of HNG treated group and control group with complete medium was significantly higher than that of growth factor-deprived control group at every corresponding concentration of temozolomide (TMZ). Values are reported as the mean ± SEM.

One-way ANOVA followed by Tukey's multiple comparisons test was used to determine statistical significance, $*p < 0.05$ compared to BSA with EGF&FGF or HNG treatment at the corresponding concentration of TMZ, $^{\#}p < 0.05$ compared to BSA without EGF&FGF.

4.3.4 Humanin overexpression in the GBM cell fails to induce a cytoprotective effect

With the purpose of answering the question if the cytoprotective effect of HN can also be conferred by intracellular HN, I overexpressed HN in GBM2 and GBM11 cell by transfecting the cells with a plasmid containing the HN open reading frame (HN ORF) or an empty plasmid (pCEP4) as a control. Then both HN overexpressing cells and control cells were cultured in growth factor-deprived medium or complete medium additionally treated with TMZ at 0 μM, 100 μM and 300 μM respectively. Cell numbers were counted on day 7 and day 14 in all conditions. The dose dependent cytotoxic effect of TMZ was evident as the cell number decreased proportional to TMZ increase. The positive effect of EGF/FGF was observed as well when comparing the growth factor-deprived medium and complete medium conditions. However, the number of HN overexpressing cells and control cells in the corresponding medium was not different in all conditions (0 μM, 100 μM or 300 μM TMZ) (Figure 4.3.4), suggesting that HN overexpression inside the GBM cell cannot induce the cytoprotective effect.

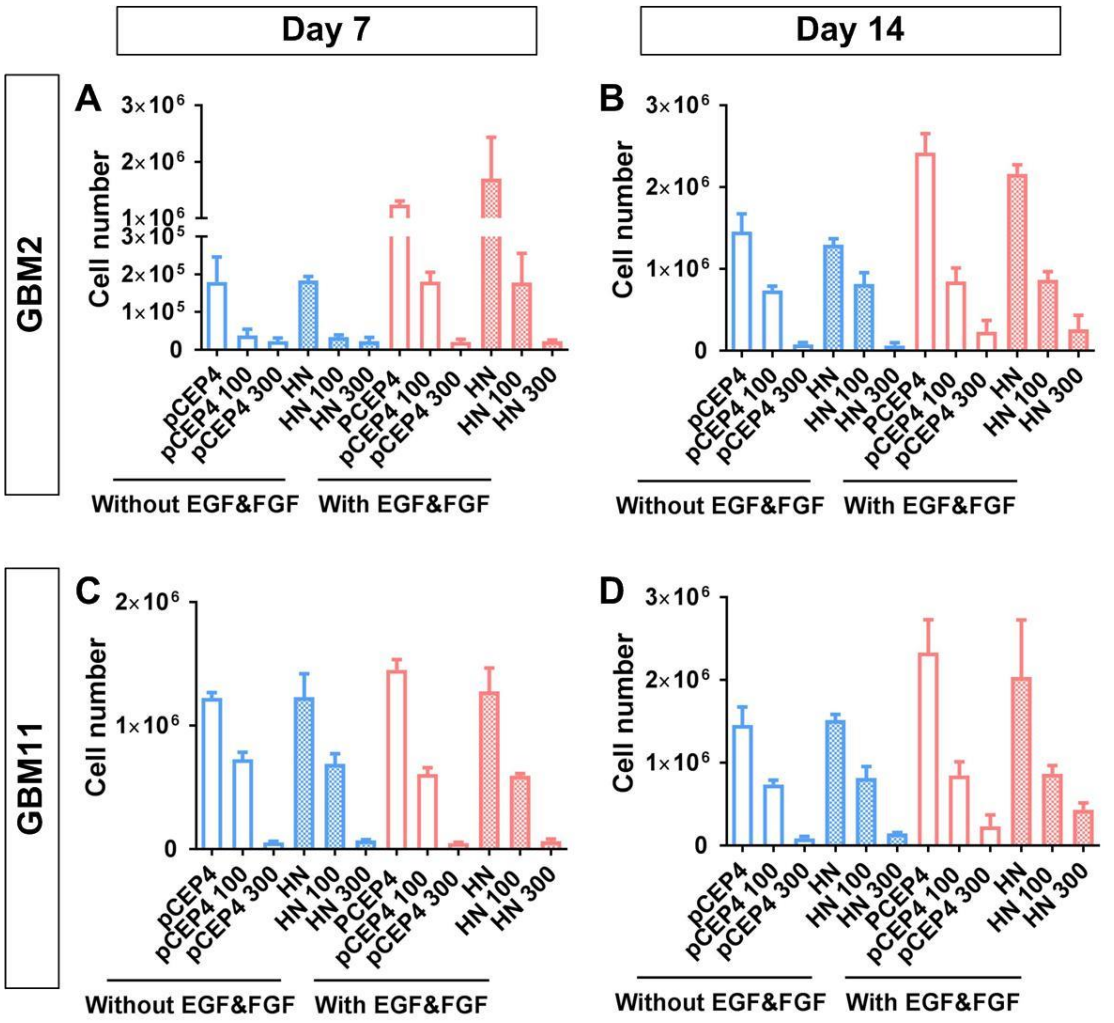

Figure 4.3.4 Overexpression of humanin in GBM2 and GBM11 fails to induce cytoprotective effects. (A, B) Quantification of cell numbers of HN overexpressing GBM2 cells (GBM2 HN) and control GBM2 cells (GBM2 pCEP4, an empty plasmid) counted on day 7 and day 14 in different conditions. (C, D) Quantification of GBM11 HN and GBM11 pCEP4 cell numbers counted on day 7 and day 14 in different conditions. No significant difference was found between HN overexpressing cells and control cells in the corresponding medium in all conditions (0 μM, 100 μM or 300 μM TMZ). Values are reported as the mean ± SEM. Student's t-test was used to determine statistical significance when comparing HN overexpressing cells and control cells in the same condition (for example, HN overexpressing cells vs. pCEP4 control cells in medium without EGF&FGF and treated with 100 μM TMZ).

5. Discussion

In the first part of my scientific project, I investigated the role of apelin/APLNR signaling in tumor angiogenesis and GBM cell invasiveness in an *in vivo* survival experiment, in an *in vitro* wound healing assay and in brain slice culture experiments. In the second part, I also investigated the effect of microglia-derived peptide humanin on the growth of primary GBM cell cultures.

5.1 Targeting apelin/APLNR inhibits both tumor angiogenesis and tumor cell invasion in glioblastoma

The *p*53^{KO}PDGFB GSCs that we used in the survival experiment generated a tumor in the mouse brain with typical glioblastoma morphology as assessed by histology. The cells were generated from mouse neural precursor cells (NPCs) with *TP53* deletion and *PDGFB* overexpression representing the proneural subtype of GBM [21]. Tumor volumes determined by H&E staining showed a comparable median volume in all four experimental groups because all the brains in the survival experiment were collected after the tumor-bearing mice entered the terminal stage and had to be sacrificed at humane end-point. Most of the mice had a big tumor in the brain, but a few mice in each group displayed a smaller tumor. One possible explanation is that the injection points in these mice are too close to the lateral ventricle, allowing tumor cells to grow into the ventricle early and block the circulation of cerebrospinal fluid before a large tumor mass can be formed.

Targeting apelin/APLNR signaling by apelin-F13A (a mutant ligand for APLNR) in

this glioblastoma mouse model prolonged the survival of animals compared to control treatment (aCSF, artificial cerebrospinal fluid). Coadministration of apelin-F13A and DC101 (anti-VEGFR2 antibody) further improved the survival when compared to mice with each single treatment. These effects probably result from the combined inhibition of tumor angiogenesis by apelin-F13A and DC101 and the anti-invasive effect of apelin-F13A. By examining the tumor on brain sections, we verified that blood vessel length density in the tumor area decreased after the treatment of apelin-F13A or DC101. And the vessel length density reached the lowest level in the combined treatment group. These results suggest that apelin/APLNR signaling indeed participates in the tumor angiogenesis of glioblastoma, and that apelin-F13A can enhance the repression of neoangiogenesis in DC101 treated tumor and may have synergistic effects with VEGFR2 inhibitors in antiangiogenesis.

On the other hand, we revealed a previously undiscovered role of apelin/APLNR signaling pathway in the invasiveness of glioblastoma cells. Although both apelin-F13A and DC101 can diminish tumor angiogenesis, their action on tumor cell invasion seems to be divergent. The glioblastoma cells became more invasive after the treatment of DC101, which is consistent with the previous findings that anti-VEGF/VEGFR therapy increases glioma cell invasion [53-55, 59]. Interestingly, apelin-F13A, on the contrary, inhibited the invasiveness of glioblastoma cells in comparison with aCSF controls. Moreover, apelin-F13A also counteracted the invasion-promoting adverse effect of DC101 in the APLNR and VEGFR2 co-targeting group. Hence, the anti-invasive effect of apelin-F13A may also be a

factor contributing to increased survival of apelin-F13A treated mice.

In line with the *in vivo* findings, my *in vitro* experiments provide additional evidence for the important role of apelin/APLNR signaling in the invasiveness of glioblastoma cells. By knocking down apelin in glioblastoma cells, we could investigate the function of tumor cell-derived apelin. The wound healing assay and brain slice experiment both showed an increase of cell migration/invasion after apelin knockdown in glioblastoma cells. Interestingly, the increased tumor cell migration of apelin knockdown cells was abolished after exogenous administration of apelin-13 or apelin-F13A in wound healing assays. Although a recent publication suggested that the apelin/APLNR signaling pathway plays a critical role in GSC maintenance [134], we did not find any difference in proliferation between apelin knockdown and non-silencing control cells examined by cell counting and Ki67 status, which rules out the possibility that the increased tumor cell invasion results from altered proliferation rates. Furthermore, APLNR belongs to G-protein coupled receptor family and APLNR internalization experiments confirmed the binding and uptake specificity of the apelin-13 and apelin-F13A by the glioblastoma cells.

Additional gene knockdown and knockout experiments performed previously by our research group [122] showed as well that apelin knockdown in the tumor cells or apelin knockout in the mice reduced the glioblastoma angiogenesis. Nevertheless, apelin knockdown in tumor cells or knockout in host mice increased the glioblastoma cell invasion [122], which implies that the apelin/APLNR signaling may have dichotomous roles in tumor angiogenesis and invasiveness in GBM. Taken together,

we speculate that apelin-F13A administrated in the survival experiment, on the one hand, modulates APLNR on glioblastoma cells to decrease tumor invasion; on the other hand, counteracts intratumoral apelin ligands, which can activate APLNR on endothelial cells and vascular sprouting. This could be supported by the pharmacological properties of apelin-F13A which is a partial agonist for APLNR with lower receptor binding capacity [72, 75] and a competitive agonist for natural APLNR ligands [75].

The extend of pseudopalisades in the *p*53^{KO}PDGFB GBM was not altered after administrated APNLR or VEGFR2 blocking, but the apelin mRNA expression in pseudopalisades decreased strongly and significantly within DC101-treated tumor (see Figure 1 in [122]). Therefore, the blocking of VEGFA/VEGFR2 signaling pathway by the anti-VEGFR2 antibody can reduce the apelin expression in glioblastoma and reduced VEGFR2-activation as well as apelin levels blunt glioma angiogenesis, but reduced apelin expression also disinhibits GBM cell invasion.

An important advantage of our novel GBM model (*p*53^{KO}PDGFB GSCs) is that we can investigate the immune compartment in fully immune competent mice. As microglia are the prime immune cells of the brain, I also analyzed the iba1 positive microglia/macrophages in the tumor area of this GBM model. Here I observed that the number of microglia/macrophages was reduced in apelin-F13A treated tumor in comparison to the controls. In brain slice experiments, the increased cell invasiveness in apelin knockdown GBM cells (compared to non-silencing control cells) is lost upon microglia depletion. These findings suggest that there may be some interactions of

apelin/APLNR signaling and tumor-associated microglia/macrophage in terms of glioblastoma cell invasiveness, which warrants further investigation.

A good approach to improve the treatment outcomes is the genetic stratification of glioblastoma, as different genetic subtypes may respond differently to one therapy. Recent studies have proposed that the proneural or classical subtypes of glioblastoma have a better therapeutic response to anti-VEGFA treatment [63, 64]. High apelin expression was also linked to angiogenesis only in the proneural or classical subtypes by gene ontology analysis, but not in mesenchymal glioblastoma [122]. Our research group previously found that apelin knockout in the host decreased tumor angiogenesis and increased tumor invasion in classical GBM mouse models [122]. The mouse cell line *p*53^{KO}PDGFB GSC was used in this study to establish a model of human proneural-subtype glioblastoma [21]. The cell lines used for *in vitro* experiments are also proneural subtype (GBM14, NCH644) or classical subtype (GBM5av). Thus, the results of DC101 and apelin-F13A treatment in the mouse model hint that targeting VEGFA/VEGFR2 together with apelin/APLNR signaling pathway may be a new strategy to improve the treatment of the proneural and classical glioblastoma subtypes.

5.2 Microglia-derived humanin acts as a protective factor for glioblastoma cells

Another factor important in the communication of GBM cells with microglia might be the microglia expressed gene humanin (HN). We have found the peptide HN to be strongly overexpressed in glioblastoma-associated myeloid cells by comparing the

expression profile of myeloid cells in glioblastoma and the tumor-free brain (unpublished data by our laboratory). In the second part of this thesis, I thus investigated the role of HN in glioblastoma. I first examined the expression of HN in the GBM patient specimens by immunostaining and verified the high expression of HN in GBM. Co-staining of HN and iba1 indicated that microglia may be the main cell type that expresses HN in GBM.

In consideration of the cytoprotective effect of HN reported by previous studies [106, 107, 114], the effect of HNG (a potent HN analogue [106, 133]) on two primary human glioblastoma cell lines was studied *in vitro*. Two types of stress on the cell culture were created by growth factor (hEGF and hFGF) deprivation and temozolomide (TMZ) addition respectively. I found that HNG can rescue glioblastoma cells from growth factor-deprived culture condition in a dose dependent manner and can also protect these cells from the cytotoxicity of TMZ. Hence, these results suggest that the highly expressed HN in GBM could be cytoprotective for tumor cells and support tumor growth. One possibility is that this cytoprotective effect is induced by HN from outside of tumor cells through the activation of receptors on the plasma membrane. Another possibility is that HN exerts anti-apoptotic effects inside the cells by binding to pro-apoptotic protein Bax or IGFBP-3. I tested this by overexpressing HN in GBM cells, and I did not find the rescue effect of intracellular HN under the stress of growth factors deprivation and TMZ, which suggests that HN may not protect the glioblastoma cells through intracellular interactions in our model. One question that needs to be answered for this experiment is the confirmation of the

overexpression of HN in GBM cells by quantitative PCR (qPCR), RNA sequencing or western blot, which could not be finalized within the time-frame of this dissertation project. Even so, HN was probably overexpressed in GBM cells, which were transfected with a plasmid containing HN open reading frame and hygromycin B-resistance gene. Therefore, only the successfully transfected cells in which HN and hygromycin B-resistance gene were expressed would survive after a long period of selection with hygromycin B.

As a preliminary study, the results of *in vitro* experiments are promising. Potential plasma-membrane receptors for HN have been reported in previous studies [114-117]. The first is N-formyl peptide receptors (FPRs) that are related to the activation of ERK1/2 signaling pathway [114]. The second is a tripartite receptor CNTFR/WSX-1/gp130 which activates the STAT3 signaling pathway [117]. As HN acts from outside but not inside of glioblastoma cells, the specific receptor of HN is a crucial aspect for this project and the expression level of HN receptors on GBM cells can be tested by qPCR and western blot. The concentration of the HNG used for *in vitro* experiments was unphysiologically high (20 μM). Therefore, the HN receptor expression level may be exceedingly low when the cells are cultured *in vitro* or the two primary human GBM cell lines used in this study may consistently be low expressing cell lines for HN receptor. Identification of GBM cells with high HN receptor expression level and continuation with pharmacological experiments using HN as an agonist can show if HN receptor expression levels determine HN-sensitivity. Once the HN receptor and HN-activated signaling pathway which underlie the

cytoprotective effect for GBM cells are thoroughly investigated, inhibitors for blocking the HN receptor and associated signaling pathway can be used to establish new pre-clinical GBM treatments and may improve the survival of GBM patients.

In conclusion, I investigated here short peptide signaling molecules like apelin and HN, which have not been given sufficient attention so far. The pro-angiogenic role of apelin in GBM was confirmed, and a previously unknown function of the apelin/APLNR signaling in glioma invasion was uncovered in this study. We also revealed and described for the first time (to the best of my knowledge) a cytoprotective effect of microglia-derived peptide HN on GBM cells. All these findings are conducive to the development of new GBM therapies.

6. Summary

The tumor microenvironment plays an essential role in supporting tumor growth. In this thesis, I focused on the interaction of tumor cells with the newly forming vasculature and the tumor-associated myeloid cells. In this context, I specifically investigated two potential treatment targets in the tumor microenvironment of glioblastoma (GBM). First, I studied the role of apelin/APLNR signaling in GBM. Apelin/APLNR signaling is a pathway that is required for angiogenesis to take place and has been found to be upregulated in GBM. Therefore, I hypothesized that blocking APLNR may improve the effect of anti-angiogenic therapy for GBM. In a survival study using an immunocompetent, orthotopic transgenic glioma model ($p53^{KO}$PDGFB-GBM cells), I found that targeting apelin/APLNR signaling by the mutant APLNR ligand apelin-F13A prolonged the survival of GBM mice. Interestingly, apelin-F13A acted synergistically together with anti-VEFGR2 antibody therapy and prolonged survival of GBM mice even longer when compared to the single compound-treated mice. Here, apelin-F13A significantly reduced tumor angiogenesis and blunted the increased invasiveness caused by anti-VEGFR2 treatment. This demonstrated that there is a previously undiscovered role of apelin/APLNR signaling in controlling glioma invasiveness. Consistent with this, apelin knockdown GBM cells showed a significant increase of invasiveness in an *in vitro* wound healing assay and in *ex vivo* brain slice experiments that I performed next. The pro-invasive effect of the reduction of apelin expression was attenuated by application of exogenous apelin-F13A. All these results suggest that apelin/APLNR

signaling plays dichotomous roles in tumor angiogenesis and GBM invasiveness: apelin promotes GBM angiogenesis and simultaneously blunts GBM invasion. The synthetic APLNR ligand apelin-F13A in turn exerts therapeutic effects by blocking GBM invasion as well as reducing tumor neoangiogenesis.

Glioblastoma-associated myeloid cells are also an important component in the tumor microenvironment promoting tumor growth. In the second part of my thesis, I studied the cytoprotective peptide humanin (HN). HN was found to be more abundantly expressed in glioblastoma-associated microglia/macrophages than in control microglia (from brain tissue of epilepsy patients). In my thesis, I found in addition, that HN expression was higher in GBM specimens than in tumor-free brain tissue as examined by immunostaining. *In vitro*, HNG (a potent HN analogue added to the culture medium) had a protective effect on glioblastoma cells maintained under cell-stress conditions, such as growth factors deprivation. In my experiments, HNG did also protect glioblastoma cells from the GBM chemotherapeutic temozolomide. Overexpression of HN inside the tumor cells, however, failed to induce the cytoprotective effect, suggesting that HN probably acts by receptors on the cell membrane rather than by cell endogenous (cytoplasmic) effects. Hence, microglia-expressed HN could be a tumor-supportive factor in the tumor microenvironment and may play an important role in the resistance to temozolomide in some GBM patients. Thus, blockage of the protumorigenic action of HN could be a possible strategy for adjuvant GBM therapy that deserves further investigations.

Zusammenfassung

Das Mikromilieu des Tumors ist ausschlaggebend für sein Wachstum sowie die Entwicklung von neuen Mikrogefäßen und tumorassoziierten myeloiden Zellen. In dieser Doktorarbeit stelle ich meine wissenschaftliche Arbeit vor welche die Untersuchung von zwei möglichen Behandlungsmethoden im Bereich des Mikromilieus des Glioblastoms (GBM) umfasst. In erster Linie habe ich die Rolle des Apelin/APLNR-Signalweges in Glioblastomen untersucht. Der Apelin/APLNR-Signalweg ist wichtig für die Angiogenese und es hat sich gezeigt, dass Apelin und sein Rezeptor APLNR in Glioblastomen hochreguliert werden. Deshalb stellte ich die Hypothese auf, dass die Blockade des Apelin Rezeptors (APLNR) die Wirkung der anti-angiogenen Therapie verbessern könnte. In einer Überlebenszeitanalyse in der wir immunkompetente, orthotope transgene Gliommodelle ($p53^{KO}$PDGFB-GBM Zellen) verwendet haben, konnte ich herausfinden, dass die Unterdrückung des Apelin/APLNR-Signalweges durch den mutierten APLNR Liganden Apelin-F13A die Überlebenszeit der GBM tragenden Mäuse verlängert. Interessanterweise beobachtete ich einen synergistischen Effekt von Apelin-F13A bei gleichzeitiger Therapie mit dem anti-VEGFR2 Antikörper und zwar verlängerte sich die Überlebenszeit der GBM Mäuse noch mehr im Vergleich zu den Mäusen die nur eine der beiden Behandlungen erhalten hatten. Apelin-F13A reduzierte die Tumorangiogenese signifikant und schwächte den Anstieg der Invasivität des Tumorwachstums ab, der von der anti-VEGFR2 Therapie verursacht wurde. Dies zeigt, dass der Apelin/APLNR-Signalweg in der Kontrolle der Invasivität

der Gliome eine zuvor unentdeckte Rolle spielt. Im Ergänzend dazu habe ich Wundheilungsexperimente in vitro und Experimente mit Hirnschnitten ex vivo durchgeführt, in welchen Apelin knock-down GBM Zellen eine signifikante Steigerung der Invasivität aufwiesen. Der proinvasive Effekt des Verlustes von Apelin wurde durch die Zugabe von exogenem Apelin-F13A abgeschwächt. Diese Ergebnisse weisen darauf hin, dass der Apelin/APLNR-Signalweg in zweierlei Hinsicht eine Rolle für die Tumorangiogenese und die GBM Invasivität spielt: Apelin fördert die Glioblastom-assoziierte Angiogenese und schwächt gleichzeitig das invasive Wachstum des Glioblastoms ab. Der synthetische APLNR Ligand Apelin-F13A wiederum übt seine therapeutische Wirkung aus indem er die GBM Invasivität blockiert und die Neoangiogenese vermindert.

Ein weiterer wichtiger Bestandteil des Mikromilieus des Tumors sind Glioblastom-assoziierte myeloide Zellen die das Tumorwachstum unterstützen. Im zweiten Teil meiner Doktorarbeit habe ich mich mit dem zytoprotektiven Peptid Humanin (HN) befasst. In meinen Untersuchungen konnte ich eine höhere Humanin-Expression in Glioblastom-assoziierten Mikroglia/Makrophagen nachweisen im Vergleich zu Mikrogliazellen die aus dem Hirngewebe von Epilepsie-Patienten stammten und als Negativkontrolle dienten. Zusätzlich konnte ich mit den im Rahmen meiner Doktorarbeit durchgeführten immunhistochemischen Färbungen zeigen, dass die HN-Expression in GBM Gewebeproben höher ist als in tumorfreien Hirngewebeproben. HNG, ein wirksames HN-Analogon welches dem Zellkulturmedium hinzugefügt wurde, zeigte einen zytoprotektiven Effekt bei

Glioblastomzellen die Zellstress ausgesetzt wurden (Entzug der Wachstumsfaktoren). In weiteren Experimenten konnte dieser zytoprotektive Effekt auch bei Glioblastomzellen die mit dem GBM Chemotherapeutikum Temozolomid behandelt wurden beobachtet werden. Weiterhin zeigte sich dieser zytoprotektive Effekt jedoch nicht bei Tumorzellen die eine endogene Überexpression von HN aufwiesen, was darauf hinweisen könnte, dass HN über Zellrezeptoren auf der Zellmembran wirksam wird und nicht über einen endogene zytoplasmatischen Signalweg. Daher scheint es möglich, dass die HN-Expression in den Mikroglia tumorsupportiv wirkt und einer der Gründe für die Temozolomid-Resistenz mancher GBM-Patienten sein könnte. Daraus schließe ich, dass die Blockade dieser protumorigenen Wirkung von HN eine mögliche zusätzliche therapeutische Strategie gegen GBM darstellen könnte und weitere Untersuchungen in diese Richtung wichtig sind.

7. References

[1] Wrensch M, Minn Y, Chew T, Bondy M, Berger MS. Epidemiology of primary brain tumors: current concepts and review of the literature. Neuro-oncology 2002;4:278-99.

[2] Ohgaki H, Kleihues P. Epidemiology and etiology of gliomas. Acta neuropathologica 2005;109:93-108.

[3] Filbin MG, Suva ML. Gliomas Genomics and Epigenomics: Arriving at the Start and Knowing It for the First Time. Annual review of pathology 2016;11:497-521.

[4] Schwartzbaum JA, Fisher JL, Aldape KD, Wrensch M. Epidemiology and molecular pathology of glioma. Nature Clinical Practice Neurology 2006;2:494.

[5] Louis DN, Perry A, Reifenberger G, von Deimling A, Figarella-Branger D, Cavenee WK, et al. The 2016 World Health Organization Classification of Tumors of the Central Nervous System: a summary. Acta neuropathologica 2016;131:803-20.

[6] Gladson CL, Prayson RA, Liu WM. The pathobiology of glioma tumors. Annual review of pathology 2010;5:33-50.

[7] Preusser M, de Ribaupierre S, Wohrer A, Erridge SC, Hegi M, Weller M, et al. Current concepts and management of glioblastoma. Annals of neurology 2011;70:9-21.

[8] Castro MG, Candolfi M, Kroeger K, King GD, Curtin JF, Yagiz K, et al. Gene therapy and targeted toxins for glioma. Current gene therapy 2011;11:155-80.

[9] Lee CY. Strategies of temozolomide in future glioblastoma treatment. OncoTargets and therapy 2017;10:265-70.

[10] Jain KK. A Critical Overview of Targeted Therapies for Glioblastoma. Frontiers in oncology 2018;8:419.

[11] Hegi ME, Diserens AC, Gorlia T, Hamou MF, de Tribolet N, Weller M, et al. MGMT gene silencing and benefit from temozolomide in glioblastoma. The New England journal of medicine 2005;352:997-1003.

[12] Stupp R, Mason WP, van den Bent MJ, Weller M, Fisher B, Taphoorn MJ, et al. Radiotherapy plus concomitant and adjuvant temozolomide for glioblastoma. The New England journal of medicine 2005;352:987-96.

[13] Ronning PA, Helseth E, Meling TR, Johannesen TB. A population-based study on the effect of

temozolomide in the treatment of glioblastoma multiforme. Neuro-oncology 2012;14:1178-84.

[14] Verhaak RG, Hoadley KA, Purdom E, Wang V, Qi Y, Wilkerson MD, et al. Integrated genomic analysis identifies clinically relevant subtypes of glioblastoma characterized by abnormalities in PDGFRA, IDH1, EGFR, and NF1. Cancer cell 2010;17:98-110.

[15] Sidaway P. CNS cancer: Glioblastoma subtypes revisited. Nature reviews Clinical oncology 2017;14:587.

[16] Van Meir EG, Hadjipanayis CG, Norden AD, Shu HK, Wen PY, Olson JJ. Exciting new advances in neuro-oncology: the avenue to a cure for malignant glioma. CA: a cancer journal for clinicians 2010;60:166-93.

[17] Bao S, Wu Q, McLendon RE, Hao Y, Shi Q, Hjelmeland AB, et al. Glioma stem cells promote radioresistance by preferential activation of the DNA damage response. Nature 2006;444:756-60.

[18] Lathia JD, Mack SC, Mulkearns-Hubert EE, Valentim CL, Rich JN. Cancer stem cells in glioblastoma. Genes & development 2015;29:1203-17.

[19] Galli R, Binda E, Orfanelli U, Cipelletti B, Gritti A, De Vitis S, et al. Isolation and characterization of tumorigenic, stem-like neural precursors from human glioblastoma. Cancer research 2004;64:7011-21.

[20] Singh SK, Hawkins C, Clarke ID, Squire JA, Bayani J, Hide T, et al. Identification of human brain tumour initiating cells. Nature 2004;432:396-401.

[21] Simeonova I, Huillard E. In vivo models of brain tumors: roles of genetically engineered mouse models in understanding tumor biology and use in preclinical studies. Cellular and molecular life sciences : CMLS 2014;71:4007-26.

[22] Folkman J. Tumor angiogenesis: therapeutic implications. The New England journal of medicine 1971;285:1182-6.

[23] Hanahan D, Weinberg RA. The hallmarks of cancer. Cell 2000;100:57-70.

[24] Hanahan D, Weinberg RA. Hallmarks of cancer: the next generation. Cell 2011;144:646-74.

[25] Hanahan D, Folkman J. Patterns and emerging mechanisms of the angiogenic switch during tumorigenesis. Cell 1996;86:353-64.

[26] Carmeliet P. Angiogenesis in life, disease and medicine. Nature 2005;438:932-6.

[27] Ronca R, Benkheil M, Mitola S, Struyf S, Liekens S. Tumor angiogenesis revisited: Regulators and clinical implications. 2017;37:1231-74.

[28] Zetter BR. Angiogenesis and tumor metastasis. Annual review of medicine 1998;49:407-24.

[29] Li T, Kang G, Wang T, Huang H. Tumor angiogenesis and anti-angiogenic gene therapy for cancer. Oncology letters 2018;16:687-702.

[30] Dvorak HF. Tumor Stroma, Tumor Blood Vessels, and Antiangiogenesis Therapy. Cancer journal (Sudbury, Mass) 2015;21:237-43.

[31] Jansen M, de Witt Hamer PC, Witmer AN, Troost D, van Noorden CJ. Current perspectives on antiangiogenesis strategies in the treatment of malignant gliomas. Brain research Brain research reviews 2004;45:143-63.

[32] Holmes K, Roberts OL, Thomas AM, Cross MJ. Vascular endothelial growth factor receptor-2: structure, function, intracellular signalling and therapeutic inhibition. Cellular signalling 2007;19:2003-12.

[33] Ferrara N. Vascular endothelial growth factor as a target for anticancer therapy. The oncologist 2004;9 Suppl 1:2-10.

[34] Scappaticci FA. Targeting the VEGF/VEGFR Axis for Cancer Therapy. In: LaRochelle WJ, Shimkets RA, editors. The Oncogenomics Handbook. Totowa, NJ: Humana Press; 2005. p. 429-40.

[35] Ellis LM. Bevacizumab. Nature reviews Drug discovery 2005;Suppl:S8-9.

[36] Linkous AG, Yazlovitskaya EM. Angiogenesis in glioblastoma multiforme: navigating the maze. Anti-cancer agents in medicinal chemistry 2011;11:712-8.

[37] Gerstner ER, Batchelor TT. Antiangiogenic therapy for glioblastoma. Cancer journal (Sudbury, Mass) 2012;18:45-50.

[38] Ameratunga M, Pavlakis N, Wheeler H, Grant R, Simes J, Khasraw M. Anti-angiogenic therapy for high-grade glioma. The Cochrane database of systematic reviews 2018;11:Cd008218.

[39] Specenier P. Bevacizumab in glioblastoma multiforme. Expert review of anticancer therapy 2012;12:9-18.

[40] Gilbert MR. Antiangiogenic Therapy for Glioblastoma: Complex Biology and Complicated Results. Journal of Clinical Oncology 2016;34:1567-9.

[41] Cohen MH, Shen YL, Keegan P, Pazdur R. FDA drug approval summary: bevacizumab (Avastin) as treatment of recurrent glioblastoma multiforme. The oncologist 2009;14:1131-8.

[42] Gil-Gil MJ, Mesia C, Rey M, Bruna J. Bevacizumab for the treatment of glioblastoma. Clinical Medicine Insights Oncology 2013;7:123-35.

[43] Chamberlain MC. Bevacizumab for the treatment of recurrent glioblastoma. Clinical Medicine

Insights Oncology 2011;5:117-29.

[44] Taal W, Oosterkamp HM, Walenkamp AM, Dubbink HJ, Beerepoot LV, Hanse MC, et al. Single-agent bevacizumab or lomustine versus a combination of bevacizumab plus lomustine in patients with recurrent glioblastoma (BELOB trial): a randomised controlled phase 2 trial. The Lancet Oncology 2014;15:943-53.

[45] Dirven L, van den Bent MJ, Bottomley A, van der Meer N, van der Holt B, Vos MJ, et al. The impact of bevacizumab on health-related quality of life in patients treated for recurrent glioblastoma: results of the randomised controlled phase 2 BELOB trial. European journal of cancer (Oxford, England : 1990) 2015;51:1321-30.

[46] Wick W, Gorlia T, Bendszus M, Taphoorn M, Sahm F, Harting I, et al. Lomustine and Bevacizumab in Progressive Glioblastoma. The New England journal of medicine 2017;377:1954-63.

[47] Chinot OL, Wick W, Mason W, Henriksson R, Saran F, Nishikawa R, et al. Bevacizumab plus radiotherapy-temozolomide for newly diagnosed glioblastoma. The New England journal of medicine 2014;370:709-22.

[48] Gilbert MR, Dignam JJ, Armstrong TS, Wefel JS, Blumenthal DT, Vogelbaum MA, et al. A randomized trial of bevacizumab for newly diagnosed glioblastoma. The New England journal of medicine 2014;370:699-708.

[49] Lai A, Tran A, Nghiemphu PL, Pope WB, Solis OE, Selch M, et al. Phase II study of bevacizumab plus temozolomide during and after radiation therapy for patients with newly diagnosed glioblastoma multiforme. Journal of clinical oncology : official journal of the American Society of Clinical Oncology 2011;29:142-8.

[50] Chinot OL, de La Motte Rouge T, Moore N, Zeaiter A, Das A, Phillips H, et al. AVAglio: Phase 3 trial of bevacizumab plus temozolomide and radiotherapy in newly diagnosed glioblastoma multiforme. Advances in therapy 2011;28:334-40.

[51] Batchelor TT, Reardon DA, de Groot JF, Wick W, Weller M. Antiangiogenic therapy for glioblastoma: current status and future prospects. Clinical cancer research : an official journal of the American Association for Cancer Research 2014;20:5612-9.

[52] Mas-Moruno C, Rechenmacher F, Kessler H. Cilengitide: the first anti-angiogenic small molecule drug candidate design, synthesis and clinical evaluation. Anti-cancer agents in medicinal chemistry 2010;10:753-68.

[53] Bergers G, Hanahan D. Modes of resistance to anti-angiogenic therapy. Nature reviews Cancer 2008;8:592-603.

[54] Bottsford-Miller JN, Coleman RL, Sood AK. Resistance and escape from antiangiogenesis therapy: clinical implications and future strategies. Journal of clinical oncology : official journal of the American Society of Clinical Oncology 2012;30:4026-34.

[55] Wang N, Jain RK, Batchelor TT. New Directions in Anti-Angiogenic Therapy for Glioblastoma. Neurotherapeutics : the journal of the American Society for Experimental NeuroTherapeutics 2017;14:321-32.

[56] Kalin RE, Kretz MP, Meyer AM, Kispert A, Heppner FL, Brandli AW. Paracrine and autocrine mechanisms of apelin signaling govern embryonic and tumor angiogenesis. Developmental biology 2007;305:599-614.

[57] Batchelor TT, Sorensen AG, di Tomaso E, Zhang WT, Duda DG, Cohen KS, et al. AZD2171, a pan-VEGF receptor tyrosine kinase inhibitor, normalizes tumor vasculature and alleviates edema in glioblastoma patients. Cancer cell 2007;11:83-95.

[58] Xie Q, Mittal S, Berens ME. Targeting adaptive glioblastoma: an overview of proliferation and invasion. Neuro-oncology 2014;16:1575-84.

[59] Kunkel P, Ulbricht U, Bohlen P, Brockmann MA, Fillbrandt R, Stavrou D, et al. Inhibition of glioma angiogenesis and growth in vivo by systemic treatment with a monoclonal antibody against vascular endothelial growth factor receptor-2. Cancer research 2001;61:6624-8.

[60] Reardon DA, Wen PY. Glioma in 2014: unravelling tumour heterogeneity-implications for therapy. Nature reviews Clinical oncology 2015;12:69-70.

[61] Diamandis P, Aldape KD. Insights From Molecular Profiling of Adult Glioma. Journal of clinical oncology : official journal of the American Society of Clinical Oncology 2017;35:2386-93.

[62] Cloughesy TF, Cavenee WK, Mischel PS. Glioblastoma: from molecular pathology to targeted treatment. Annual review of pathology 2014;9:1-25.

[63] Sandmann T, Bourgon R, Garcia J, Li C, Cloughesy T, Chinot OL, et al. Patients With Proneural Glioblastoma May Derive Overall Survival Benefit From the Addition of Bevacizumab to First-Line Radiotherapy and Temozolomide: Retrospective Analysis of the AVAglio Trial. Journal of clinical oncology : official journal of the American Society of Clinical Oncology 2015;33:2735-44.

[64] Erdem-Eraslan L, van den Bent MJ, Hoogstrate Y, Naz-Khan H, Stubbs A, van der Spek P, et al.

Identification of Patients with Recurrent Glioblastoma Who May Benefit from Combined Bevacizumab and CCNU Therapy: A Report from the BELOB Trial. Cancer research 2016;76:525-34.

[65] O'Dowd BF, Heiber M, Chan A, Heng HH, Tsui LC, Kennedy JL, et al. A human gene that shows identity with the gene encoding the angiotensin receptor is located on chromosome 11. Gene 1993;136:355-60.

[66] Tatemoto K, Hosoya M, Habata Y, Fujii R, Kakegawa T, Zou MX, et al. Isolation and characterization of a novel endogenous peptide ligand for the human APJ receptor. Biochemical and biophysical research communications 1998;251:471-6.

[67] Falcao-Pires I, Ladeiras-Lopes R, Leite-Moreira AF. The apelinergic system: a promising therapeutic target. Expert opinion on therapeutic targets 2010;14:633-45.

[68] Kälin S, Kälin RE. Apelin and Cancer. In: Reizes O, Berger NA, editors. Adipocytokines, Energy Balance, and Cancer. Cham: Springer International Publishing; 2017. p. 137-60.

[69] Mughal A, O'Rourke ST. Vascular effects of apelin: Mechanisms and therapeutic potential. Pharmacology & therapeutics 2018;190:139-47.

[70] Zhen EY, Higgs RE, Gutierrez JA. Pyroglutamyl apelin-13 identified as the major apelin isoform in human plasma. Analytical biochemistry 2013;442:1-9.

[71] Pitkin SL, Maguire JJ, Bonner TI, Davenport AP. International Union of Basic and Clinical Pharmacology. LXXIV. Apelin receptor nomenclature, distribution, pharmacology, and function. Pharmacological reviews 2010;62:331-42.

[72] Medhurst AD, Jennings CA, Robbins MJ, Davis RP, Ellis C, Winborn KY, et al. Pharmacological and immunohistochemical characterization of the APJ receptor and its endogenous ligand apelin. Journal of neurochemistry 2003;84:1162-72.

[73] Fan X, Zhou N, Zhang X, Mukhtar M, Lu Z, Fang J, et al. Structural and functional study of the apelin-13 peptide, an endogenous ligand of the HIV-1 coreceptor, APJ. Biochemistry 2003;42:10163-8.

[74] Yang P, Kuc RE, Brame AL, Dyson A, Singer M, Glen RC, et al. [Pyr(1)]Apelin-13(1-12) Is a Biologically Active ACE2 Metabolite of the Endogenous Cardiovascular Peptide [Pyr(1)]Apelin-13. Frontiers in neuroscience 2017;11:92.

[75] O'Carroll AM, Lolait SJ, Harris LE, Pope GR. The apelin receptor APJ: journey from an orphan to a multifaceted regulator of homeostasis. The Journal of endocrinology 2013;219:R13-35.

[76] Taheri S, Murphy K, Cohen M, Sujkovic E, Kennedy A, Dhillo W, et al. The effects of centrally

administered apelin-13 on food intake, water intake and pituitary hormone release in rats. Biochemical and biophysical research communications 2002;291:1208-12.

[77] Mitra A, Katovich MJ, Mecca A, Rowland NE. Effects of central and peripheral injections of apelin on fluid intake and cardiovascular parameters in rats. Physiology & behavior 2006;89:221-5.

[78] Clarke KJ, Whitaker KW, Reyes TM. Diminished metabolic responses to centrally-administered apelin-13 in diet-induced obese rats fed a high-fat diet. Journal of neuroendocrinology 2009;21:83-9.

[79] Cox CM, D'Agostino SL, Miller MK, Heimark RL, Krieg PA. Apelin, the ligand for the endothelial G-protein-coupled receptor, APJ, is a potent angiogenic factor required for normal vascular development of the frog embryo. Developmental biology 2006;296:177-89.

[80] Kunduzova O, Alet N, Delesque-Touchard N, Millet L, Castan-Laurell I, Muller C, et al. Apelin/APJ signaling system: a potential link between adipose tissue and endothelial angiogenic processes. FASEB journal : official publication of the Federation of American Societies for Experimental Biology 2008;22:4146-53.

[81] Kasai A, Shintani N, Oda M, Kakuda M, Hashimoto H, Matsuda T, et al. Apelin is a novel angiogenic factor in retinal endothelial cells. Biochemical and biophysical research communications 2004;325:395-400.

[82] Kuba K, Zhang L, Imai Y, Arab S, Chen M, Maekawa Y, et al. Impaired heart contractility in Apelin gene-deficient mice associated with aging and pressure overload. Circulation research 2007;101:e32-42.

[83] Chng SC, Ho L, Tian J, Reversade B. ELABELA: a hormone essential for heart development signals via the apelin receptor. Developmental cell 2013;27:672-80.

[84] Pauli A, Norris ML, Valen E, Chew GL, Gagnon JA, Zimmerman S, et al. Toddler: an embryonic signal that promotes cell movement via Apelin receptors. Science (New York, NY) 2014;343:1248636.

[85] Rayalam S, Della-Fera MA, Kasser T, Warren W, Baile CA. Emerging role of apelin as a therapeutic target in cancer: a patent review. Recent patents on anti-cancer drug discovery 2011;6:367-72.

[86] Yang Y, Lv SY, Ye W, Zhang L. Apelin/APJ system and cancer. Clinica chimica acta; international journal of clinical chemistry 2016;457:112-6.

[87] Antushevich H, Wojcik M. Review: Apelin in disease. Clinica chimica acta; international journal of clinical chemistry 2018;483:241-8.

[88] Lacquaniti A, Altavilla G, Picone A, Donato V, Chirico V, Mondello P, et al. Apelin beyond kidney

failure and hyponatremia: a useful biomarker for cancer disease progression evaluation. Clinical and experimental medicine 2015;15:97-105.

[89] Berta J, Kenessey I, Dobos J, Tovari J, Klepetko W, Jan Ankersmit H, et al. Apelin expression in human non-small cell lung cancer: role in angiogenesis and prognosis. Journal of thoracic oncology : official publication of the International Association for the Study of Lung Cancer 2010;5:1120-9.

[90] Sorli SC, Le Gonidec S, Knibiehler B, Audigier Y. Apelin is a potent activator of tumour neoangiogenesis. Oncogene 2007;26:7692-9.

[91] Wu L, Chen L, Li L. Apelin/APJ system: A novel promising therapy target for pathological angiogenesis. Clinica chimica acta; international journal of clinical chemistry 2017;466:78-84.

[92] Glassford AJ, Yue P, Sheikh AY, Chun HJ, Zarafshar S, Chan DA, et al. HIF-1 regulates hypoxia- and insulin-induced expression of apelin in adipocytes. American journal of physiology Endocrinology and metabolism 2007;293:E1590-6.

[93] Heo K, Kim YH, Sung HJ, Li HY, Yoo CW, Kim JY, et al. Hypoxia-induced up-regulation of apelin is associated with a poor prognosis in oral squamous cell carcinoma patients. Oral oncology 2012;48:500-6.

[94] Kasai A, Ishimaru Y, Kinjo T, Satooka T, Matsumoto N, Yoshioka Y, et al. Apelin is a crucial factor for hypoxia-induced retinal angiogenesis. Arteriosclerosis, thrombosis, and vascular biology 2010;30:2182-7.

[95] Seaman S, Stevens J, Yang MY, Logsdon D, Graff-Cherry C, St Croix B. Genes that distinguish physiological and pathological angiogenesis. Cancer cell 2007;11:539-54.

[96] Masiero M, Simoes FC, Han HD, Snell C, Peterkin T, Bridges E, et al. A core human primary tumor angiogenesis signature identifies the endothelial orphan receptor ELTD1 as a key regulator of angiogenesis. Cancer cell 2013;24:229-41.

[97] Muto J, Shirabe K, Yoshizumi T, Ikegami T, Aishima S, Ishigami K, et al. The apelin-APJ system induces tumor arteriogenesis in hepatocellular carcinoma. Anticancer research 2014;34:5313-20.

[98] Hambardzumyan D, Bergers G. Glioblastoma: Defining Tumor Niches. Trends in cancer 2015;1:252-65.

[99] Glass R, Synowitz M. CNS macrophages and peripheral myeloid cells in brain tumours. Acta neuropathologica 2014;128:347-62.

[100] Poon CC, Sarkar S, Yong VW, Kelly JJP. Glioblastoma-associated microglia and macrophages:

targets for therapies to improve prognosis. Brain : a journal of neurology 2017;140:1548-60.

[101] Hambardzumyan D, Gutmann DH, Kettenmann H. The role of microglia and macrophages in glioma maintenance and progression. Nature neuroscience 2016;19:20-7.

[102] Hanisch UK. Microglia as a source and target of cytokines. Glia 2002;40:140-55.

[103] Michell-Robinson MA, Touil H, Healy LM, Owen DR, Durafourt BA, Bar-Or A, et al. Roles of microglia in brain development, tissue maintenance and repair. Brain : a journal of neurology 2015;138:1138-59.

[104] Sierra A, Abiega O, Shahraz A, Neumann H. Janus-faced microglia: beneficial and detrimental consequences of microglial phagocytosis. Frontiers in cellular neuroscience 2013;7:6.

[105] Hu F, Dzaye O, Hahn A, Yu Y, Scavetta RJ, Dittmar G, et al. Glioma-derived versican promotes tumor expansion via glioma-associated microglial/macrophages Toll-like receptor 2 signaling. Neuro-oncology 2015;17:200-10.

[106] Hashimoto Y, Niikura T, Tajima H, Yasukawa T, Sudo H, Ito Y, et al. A rescue factor abolishing neuronal cell death by a wide spectrum of familial Alzheimer's disease genes and Abeta. Proceedings of the National Academy of Sciences of the United States of America 2001;98:6336-41.

[107] Hashimoto Y, Ito Y, Niikura T, Shao Z, Hata M, Oyama F, et al. Mechanisms of neuroprotection by a novel rescue factor humanin from Swedish mutant amyloid precursor protein. Biochemical and biophysical research communications 2001;283:460-8.

[108] Lee C, Yen K, Cohen P. Humanin: a harbinger of mitochondrial-derived peptides? Trends in endocrinology and metabolism: TEM 2013;24:222-8.

[109] Guo B, Zhai D, Cabezas E, Welsh K, Nouraini S, Satterthwait AC, et al. Humanin peptide suppresses apoptosis by interfering with Bax activation. Nature 2003;423:456-61.

[110] Ikonen M, Liu B, Hashimoto Y, Ma L, Lee KW, Niikura T, et al. Interaction between the Alzheimer's survival peptide humanin and insulin-like growth factor-binding protein 3 regulates cell survival and apoptosis. Proceedings of the National Academy of Sciences of the United States of America 2003;100:13042-7.

[111] Xiao J, Kim SJ, Cohen P, Yen K. Humanin: Functional Interfaces with IGF-I. Growth hormone & IGF research : official journal of the Growth Hormone Research Society and the International IGF Research Society 2016;29:21-7.

[112] Nishimoto I, Matsuoka M, niikura T. Unravelling the role of Humanin. Trends in molecular

medicine 2004;10:102-5.

[113] Muzumdar RH, Huffman DM, Atzmon G, Buettner C, Cobb LJ, Fishman S, et al. Humanin: a novel central regulator of peripheral insulin action. PloS one 2009;4:e6334.

[114] Ying G, Iribarren P, Zhou Y, Gong W, Zhang N, Yu ZX, et al. Humanin, a newly identified neuroprotective factor, uses the G protein-coupled formylpeptide receptor-like-1 as a functional receptor. Journal of immunology (Baltimore, Md : 1950) 2004;172:7078-85.

[115] Harada M, Habata Y, Hosoya M, Nishi K, Fujii R, Kobayashi M, et al. N-Formylated humanin activates both formyl peptide receptor-like 1 and 2. Biochemical and biophysical research communications 2004;324:255-61.

[116] Hashimoto Y, Suzuki H, Aiso S, Niikura T, Nishimoto I, Matsuoka M. Involvement of tyrosine kinases and STAT3 in Humanin-mediated neuroprotection. Life sciences 2005;77:3092-104.

[117] Hashimoto Y, Kurita M, Aiso S, Nishimoto I, Matsuoka M. Humanin inhibits neuronal cell death by interacting with a cytokine receptor complex or complexes involving CNTF receptor alpha/WSX-1/gp130. Molecular biology of the cell 2009;20:2864-73.

[118] Mayhew TM, Mwamengele GL, Dantzer V. Comparative morphometry of the mammalian brain: estimates of cerebral volumes and cortical surface areas obtained from macroscopic slices. Journal of anatomy 1990;172:191-200.

[119] Mayhew TM, Mwamengele GL, Dantzer V. Stereological and allometric studies on mammalian cerebral cortex with implications for medical brain imaging. Journal of anatomy 1996;189 (Pt 1):177-84.

[120] Kreczmanski P, Schmidt-Kastner R, Heinsen H, Steinbusch HW, Hof PR, Schmitz C. Stereological studies of capillary length density in the frontal cortex of schizophrenics. Acta neuropathologica 2005;109:510-8.

[121] Franciosi S, Gama Sosa MA, English DF, Oler E, Oung T, Janssen WG, et al. Novel cerebrovascular pathology in mice fed a high cholesterol diet. Molecular neurodegeneration 2009;4:42.

[122] Mastrella G, Hou M, Li M, Stoecklein VM, Zdouc N, Volmar MNM, et al. Targeting APLN/APLNR improves anti-angiogenic efficiency and blunts pro-invasive side effects of VEGFA/VEGFR2-blockade in glioblastoma. Cancer research 2019:canres.0881.2018.

[123] Markovic DS, Glass R, Synowitz M, Rooijen N, Kettenmann H. Microglia stimulate the invasiveness of glioma cells by increasing the activity of metalloprotease-2. Journal of neuropathology

and experimental neurology 2005;64:754-62.

[124] Sliwa M, Markovic D, Gabrusiewicz K, Synowitz M, Glass R, Zawadzka M, et al. The invasion promoting effect of microglia on glioblastoma cells is inhibited by cyclosporin A. Brain : a journal of neurology 2007;130:476-89.

[125] Prewett M, Huber J, Li Y, Santiago A, O'Connor W, King K, et al. Antivascular endothelial growth factor receptor (fetal liver kinase 1) monoclonal antibody inhibits tumor angiogenesis and growth of several mouse and human tumors. Cancer research 1999;59:5209-18.

[126] Imai Y, Ibata I, Ito D, Ohsawa K, Kohsaka S. A novel gene iba1 in the major histocompatibility complex class III region encoding an EF hand protein expressed in a monocytic lineage. Biochemical and biophysical research communications 1996;224:855-62.

[127] Chen Z, Feng X, Herting CJ, Garcia VA, Nie K, Pong WW, et al. Cellular and Molecular Identity of Tumor-Associated Macrophages in Glioblastoma. Cancer research 2017;77:2266-78.

[128] Markovic DS, Vinnakota K, Chirasani S, Synowitz M, Raguet H, Stock K, et al. Gliomas induce and exploit microglial MT1-MMP expression for tumor expansion. Proceedings of the National Academy of Sciences of the United States of America 2009;106:12530-5.

[129] Coniglio SJ, Eugenin E, Dobrenis K, Stanley ER, West BL, Symons MH, et al. Microglial stimulation of glioblastoma invasion involves epidermal growth factor receptor (EGFR) and colony stimulating factor 1 receptor (CSF-1R) signaling. Molecular medicine (Cambridge, Mass) 2012;18:519-27.

[130] Brandenburg S, Muller A, Turkowski K, Radev YT, Rot S, Schmidt C, et al. Resident microglia rather than peripheral macrophages promote vascularization in brain tumors and are source of alternative pro-angiogenic factors. Acta neuropathologica 2016;131:365-78.

[131] Bruno S, Darzynkiewicz Z. Cell cycle dependent expression and stability of the nuclear protein detected by Ki-67 antibody in HL-60 cells. Cell proliferation 1992;25:31-40.

[132] Calebiro D, Godbole A. Internalization of G-protein-coupled receptors: Implication in receptor function, physiology and diseases. Best practice & research Clinical endocrinology & metabolism 2018;32:83-91.

[133] Hashimoto Y, Niikura T, Ito Y, Sudo H, Hata M, Arakawa E, et al. Detailed characterization of neuroprotection by a rescue factor humanin against various Alzheimer's disease-relevant insults. The Journal of neuroscience : the official journal of the Society for Neuroscience 2001;21:9235-45.

[134] Harford-Wright E, Andre-Gregoire G, Jacobs KA, Treps L, Le Gonidec S, Leclair HM, et al.

Pharmacological targeting of apelin impairs glioblastoma growth. Brain : a journal of neurology 2017;140:2939-54.

8. Acknowledgement

Herein I would like to express my sincere gratitude to my supervisor Prof. Rainer Glass and co-supervisor Dr. Roland Kaelin for providing me with the opportunity to pursue this research project and for their guidance in the scientific world. As excellent scientists, their profound knowledge and rigorous attitude towards science have always impressed me. I very much appreciate all their support, encouragement, comments, and suggestions during my doctoral study period. I have learned a lot from them, which will be helpful for my future life and work as well.

I am also very grateful to Ms. Stefanie Lange for her technical assistance during my work at the Neurosurgical Research Laboratory. And for all my colleagues and friends, I would like to express my heartfelt gratitude to them. Without their help and companionship, this journey would be even more difficult and less joyful.

Finally, I want to thank my family for their continued support and concern over the years and also thank the China Scholarship Council (CSC) for offering grants.

9. Publication

Mastrella G*, Hou M*, **Li M***, Stoecklein VM, Zdouc N, Volmar MNM, et al. Targeting APLN/APLNR improves anti-angiogenic efficiency and blunts pro-invasive side effects of VEGFA/VEGFR2-blockade in glioblastoma. Cancer research 2019; 79 (9): 2298-2313 (***Co-first author**).